MICROSCOPY AND SPECTROSCOPY OF WATER UPTAKE IN POLYMER PHOTORESISTS

by

LAURIE A. McDONOUGH

A.B., Bowdoin College, 1998

A thesis submitted to the

Faculty of the Graduate School of the

University of Colorado in partial fulfillment

of the requirements for the degree of

Doctor of Philosophy

Department of Chemistry and Biochemistry

2004

This thesis entitled:

Microscopy and Spectroscopy of Water Uptake in Polymer Photoresists

written by Laurie A. McDonough

Has been approved for the

Department of Chemistry and Biochemistry

_____

Stephen R. Leone

_____

W. Carl Lineberger

Date_____

The final copy of this thesis has been examined by the signatories, and we find that both the content and the form meet acceptable presentation standards of scholarly work in the above mentioned discipline.

McDonough, Laurie A. (Ph.D., Physical Chemistry)

Microscopy and Spectroscopy of Water Uptake in Polymer Photoresists

Thesis Directed by Professor Stephen R. Leone

Water uptake in polymer photoresists is investigated with a combination of methods. An infrared near-field scanning optical microscope (IR-NSOM) is incorporated into an environmental chamber for the measurement of samples composed of alternating lines of poly(t-butylmethacrylate) (PTBMA) and the photochemically modified poly(methacrylic acid) (PMAA) in both low and high water vapor environments. The degree of water vapor sorption is measured using the infrared transmission of 2.85 μm light on a small spatial scale (< 500 nm). The accompanying topographic swelling of the samples is measured using a shear-force feedback loop. Distortion of the topographic structure and variation in transmission contrast indicate that the PMAA zones absorb more water than the PTBMA regions in the water vapor environment.

Atomic Force Microscopy (AFM) is used to measure the same PTBMA/PMAA photoresist along with another sample consisting of poly(t-butylcarbonylstyrene) (tBOC) and its modified counterpart, polyhydroxystyrene (PHOST). Distance sweep measurements show that the tip indents further into PHOST than tBOC regions. The tip-sample interactions do not change when exposed to humidity, thus allowing the measurement of differential swelling. The PTBMA/PMAA photoresist is found to display more differential swelling than the tBOC/PHOST photoresist.

Fourier-Transform Infrared (FTIR) absorption spectroscopy is implemented to measure the infrared spectrum of water absorbed by the ketal-protected poly(hydroxystyrene) (KRS-XE) and tBOC photoresists. The shape and intensity of the OH stretching band of the water spectrum is monitored in a variety of humidity conditions in order to obtain information on the hydrogen-bonding interactions between the water and the polymer chains. The band is deconvoluted into four sub-bands, which represent four types of water molecule environment. A large portion of the sorbed water molecules is believed to be strongly bound to the polar sites of the polymer. The ratios of each type of water are found to be dependent on the humidty conditions to which the sample was exposed. These findings are used to explain the humidity dependence of the deprotection reaction rates, since certain types of water may slow transport of reactive species within the polymer network.

ACKNOWLEDGEMENTS

The completion of this thesis would not have been possible without the contributions of many people. I would like to thank my advisor, Steve Leone, for his moral, financial and scientific support during the course of my graduate school career. He has also contributed by creating a culturally and scientifically diverse group of people with whom I have had the privilege of working. Each member of the Leone group has impacted my life in some way. I can't list them all, but I must mention a few. Tim Barckholtz and Bogdan Dragnea were early mentors who got me started in the lab. Bogdan and Jan Preusser helped tremendously with the conception and realization of the IR-NSOM. I also have to thank the members of the Jila machine and electronic shops for their help in building the apparatus. Postdocs John Husband, Chuck Blackledge and Zee Hwan Kim advised me through some rough patches. Romain Planques helped with the AFM measurements. Juergen Plenge has been a source of wisdom during the writing of this thesis. Fellow graduate students Jodi Szarko (my graduate school twin) and Josh Ballard helped me get through all the highs and lows of graduate school with their support, advice and friendship.

My family has also contributed more support than I ever could have asked for. They have both believed in me and been my inspiration. I wouldn't have even made it to the start of graduate school without my parents, Bill and Sandy McDonough, and their love and care kept me going to the end. My grandparents, Renee and Harold Bonnyman, made sure to teach me that I can do anything I want to in my life. My Auntie Linda Marshall, and my brother Tim and sister Erin have been there for me

and can always make me laugh. I also have amazing friends back on the east coast who have kept in touch, visited me, and cheered me up on many occasions- especially Cyndy Falwell and Caitlin O'Connor. My friends and teammates in Boulder and Berkeley have all helped make graduate school an enjoyable experience. Thanks to everyone, I am very lucky to have all of you in my life.

CONTENTS

List of Tables

List of Figures

Chapter I:

Introduction

1.1 Introduction

The semiconductor industry has a constant drive to make faster and more powerful devices. Manufacturers strive to keep up with Moore's law, which predicts the number of transistors on a chip will double every 18 months. In order to maintain this pace, the processing of the polymer photoresists that provide the patterns for these devices must be understood and controlled with great detail. One factor to consider is the conditions under which the photoresists are processed, because contamination due to exposure to water in the air can affect the fabrication.[1-8] Because of the small size of the features of these patterns, powerful microscopes such as the infrared near-field scanning optical microscope (IR-NSOM) and atomic force microscope (AFM) are used to study water uptake and swelling in the polymers. Additionally, fourier-transform infrared (FTIR) spectroscopy is used to gather information on the interactions between water molecules and polymer chains in the photoresists. Investigations will hopefully provide new insights which can lead to improvements in polymer photoresists that benefit the microelectronics industry.

1.2 Polymer Properties

Polymers are high molecular weight molecules composed of repeating subunits that link together to form long chains. They can be naturally occurring, such as proteins and cellulose, or synthetic, such as polystyrene and Teflon. Molecular

structure and the way a polymer's chains are arranged in a solid are important factors in determining their properties. Polymers are ideal materials for many industrial applications because they have desirable properties such as durability, processability, transparency and electrical and thermal resistance.[9-12] As scientific progress continues, polymers are introduced into every aspect of life, from medicine to food packaging to computers.

When polymers encounter water, the most ubiquitous substance on earth, their properties and functions are affected. Water in liquid or vapor form is absorbed into the polymer; water molecules fill the voids that are formed between polymer chains and then induce relaxation, or swelling of the polymer.[9,11,13-15] The effect is similar to what happens when you wet a sponge. Because of the small size of water molecules, their ease of condensation, and ability to hydrogen bond, water affects polymers in ways that are unique in comparison to any other substance.[14,16]

The presence of water in a polymer film has been shown to affect a variety of physical properties including tensile strength, hardness, net dielectric constant and glass transition temperature.[1,16,17] The swelling of polymer films causes strain and stress, and can induce cracking, degradation and other signs of physical aging.[11,18-21] Plasticization, the softening and increase of flexibility of a polymer material, can occur. In many cases, the sorption of water and its effects are reversible.[13,22]

1.3 Water In Polymers

The amount of water absorbed by a polymer depends on several physical and chemical factors. Water molecules are attracted to a polymer's polar groups. The

number and position of those groups on a polymer chain can affect water sorption.[9,13] Chemical modification by adding particular groups to a polymer can be done to tailor a material's sensitivity. [9,11]

The available volume of film affects the amount of water that can be absorbed. The film's volume can be broken into three elements.[23] The occupied volume is the volume of material without any free space. The interstitial volume is free volume that stems from the vibrational energy of the polymer bonds, and the hole free volume arises from voids formed by polymer chain relaxation. The two types of free volume represent pores that are accessible for water sorption and transport. The pore size and density of pores are major factors in determining water sorption. [18] The orientation of the polymer chains determines whether a polymer is amorphous or crystalline and helps determine the pore size and density. Film thickness is another factor related to volume that affects water uptake. Thin films are shown to behave very differently than bulk materials.[13]

Polymers not only have strong bonds between their monomers to form a chain, but they also have bonds between their chains called cross-links. Hydrogels are three-dimensional polymer networks that are able to absorb extremely large amounts of water. However, they remain insoluble because of their chemical and physical cross-links. The degree of cross-linking determines the hygroscopic properties of the polymer.[14,22] A useful hydrogel is both sensitive and resistant to water. If a polymer is soluble in water, dissolution problems can be overcome by cross-linking or blending with a hydrophobic polymer.[9]

Temperature affects the amount of water that is absorbed.[18] In order to understand this effect, one must understand the principle of glass transition temperature, Tg. This is a characteristic temperature above which the polymer chains are relaxed, mobile and called "rubbery." As the temperature of a polymer drops below T_g, it behaves in an increasingly brittle manner, and can be referred to as "glassy." The glass transition temperature is a property that varies for each individual polymer. Water diffusion above T_g is normally faster than in films that are below the cutoff. Temperatures can be controlled for optimal water uptake, depending on the polymer and the application in use.[18]

In many applications, additives are included in polymer films to produce desired properties. These additives, such as rheology modifiers, pigments, and dispersion agents can influence water absorption.[18,23] This is mainly because of their affect on the available free volume.[24] Processing conditions such as anneal sequence also play a role.[13] Although it is known that many of these factors affect water absorption, it is difficult to determine exactly how the system is affected. Therefore, it is important to study each unique set of conditions in a process to determine the effects of water uptake.

1.4 Water Diffusion in Polymers

A few definitions are pertinent before discussion of water transport in polymers begins. *Absorption* is the uptake of liquids or vapors by a material. *Sorption* is usually a synonym for absorption, but may be used in reference to

equilibrium uptake. *Desorption* is the loss of liquids or vapors by a material. *Permeation* is the transport of liquids or vapors through a material.

Diffusion of water through polymers can follow Fickian or non-Fickian kinetics.[18,24] Fickian transport often occurs in rubbery polymers that possess sufficient chain mobility to allow water penetration.[25] It is an ideal case in which there are no interference of effects such as polymer chain rearrangement. This is because the rate of diffusion of the water is much less than that of the relaxation. It is described by:

$$\frac{dC}{dt} = \frac{d}{dx}\left(D(C)\frac{dC}{dx} \right) , \qquad (1.1)$$

where C is the water concentration, t is time, x is the position in the film in the direction of diffusion, and D is the diffusion coefficient or diffusivity of the water in the polymer. A curve of the mass uptake, M, versus $t^{1/2}$ is linear. The absorption curve eventually smoothly levels off to a saturation level, M_∞. Figure 1.1a shows a theoretical Fickian plot of $M(t)/ M_\infty$ as a function of $t^{1/2}$.

Fickian diffusion is a general description of diffusion through a medium. However, in polymer networks many of the assumptions inherent in the equations break down. The main one is that a polymer exposed to water is often not at equilibrium because its polymer chains are relaxing.[24] This generally occurs in glassy polymers.[24,25]

A case is usually referred to as non-fickian when anomolous plots are obtained. Two-stage, sigmoidal and Case II sorption are well known behaviors also shown in Figure 1.1. Examples of each type of diffusion can be found in the

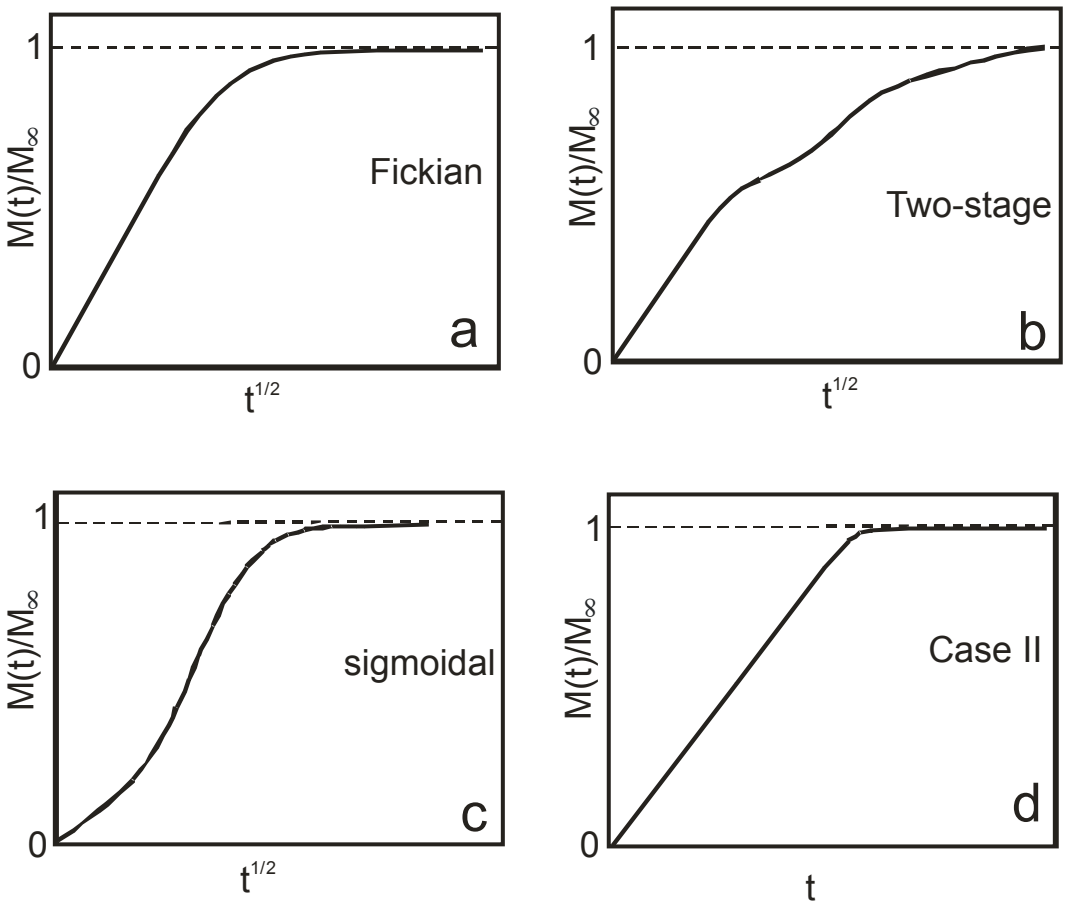

Figure 1.1: Different classes of diffusion. a) Fickian b) Two-stage c) Sigmoidal d) Case II

literature.[18,24] Two-stage diffusion (Figure 1.1b) is characterized by a fast, Fickian absorption followed by slow, non-Fickian behavior after relaxations occur in the polymer matrix. Sigmoidal sorption, shown in Figure 1.1c has an S-shaped curve with an inflection point. In this case, swelling of the polymer creates a strain, which is transient and affects the diffusion.[24] It is also referred to as stress-dependent diffusion.

Case II absorption, shown in Figure 1.1d, is an entirely different type of non-Fickian kinetics. The uptake of water is proportional to time rather than the square root of time, as in other cases. In this case the rate of the polymer chain relaxation is much slower than the rate of diffusion. This creates sharp diffusion fronts or "step-type" concentration profiles in the polymer film.[17,24]

1.5 General Applications of Water Sorption Studies

The study of water sorption in polymers is important for many applications. For example, polymers are used in the coatings industry. Coatings have two main purposes: decoration or aesthetics and protective ability. Polymers can be used as coatings on metal surfaces to protect the metals from the corrosion that occurs when subjected to ambient humidity.[18,23] A hydrophilic coating may be needed to enhance adhesion or wettability of the metal surface. A hydrophobic coating can be used to prevent permeation of water.

Coatings are also important in the food industry.[10,26,27] Water is probably the single most important factor in governing microbial spoilage in foods. Some foods are produced with reduced moisture; these are nonequilibrium systems and can be

very sensitive to changes in moisture content. Therefore polymers that are excellent barriers for water are needed for packaging. Because the cost of packaging material represents an average of 17% of the total cost of goods produced, research on water sorption properties of polymers can be very valuable.

Another area that can gain from knowledge of water uptake in polymers is sensors. Humidity sensors are useful for detection for purposes from comfort in the home to quality control and processing in industries such as food, paper and electronics.[9,12,28] An "electronic nose" is an array of sensors used to characterize complex samples.[29] It consists of various polymers, each sensitive to different chemical vapors. It can perform a complex analysis of chemical vapors, with more reliability than a human nose. Each sensor responds to a particular chemical in a selective way such as a color change, resistance change, production of heat, or by swelling.[11,12,30] There are many industries that require humidity control, such as electronics, food, agriculture and cigars; therefore improved humidity sensors are in great need.

Another major area of research related to water and polymers is drug delivery. A macromolecular drug delivery system includes a drug that is attached to or encapsulated in a carrier molecule such as a synthetic polymer. It is an improvement over oral drugs, which must travel through the entire body before reaching the intended site. The ideal material would be biochemically inert and non-toxic, while protecting the drug until it releases it at the desired site of action.[31]

In the early stages of drug delivery, goals were to achieve a delivery profile that would yield a constant drug level over a long period of time.[32] With traditional

tablets or injections, drug levels rise sharply then tail off over time. The drug is only present in an effective concentration for a short period of time. In a controlled delivery system the drug level in the blood remains constant, at a level between the minimum effective dose and the lethal dose.

Today's drug delivery research is more sophisticated. Scientists look for systems that are inert, biocompatible, mechanically strong, comfortable for the patient, safe from accidental release, simple to administer and remove, and responsive to environmental changes.[32] An effective system would be ideal for treating diabetes. A polymer capsule would deliver insulin upon detection of glucose in the bloodstream. It would also have the ability to stop the delivery when an acceptable level was reached.

Anti-cancer drugs are often problematic because they can cause significant problems in non-diseased areas of the body, leading to non-desirable side-effects for the patient. If a drug were incapsulated in a polymer nanoparticle, it could travel through the blood stream to the tumor, where it would be the correct size to exit the blood stream and enter the tumor. Once inside, the environment in the tumor would cause the polymer to break apart and release the drug. [31,32]

There are three primary mechanisms by which active agents can be released from a polymer drug delivery system. The drug molecules can diffuse out of the polymer pores; the polymer can degrade and fall apart; or the polymer can swell, increase pore size, and then allow diffusion. Because the body is comprised mainly of water, a swelling or dissolving response to water is an important polymer property to understand. An additional mechanism is employed by high molecular weight

polyethylene oxides (PEOs), which swell and form a gel layer upon contact with water.[33] The gel layer erodes slowly, thus modulating the drug delivery rate.

There seems to be an ever-growing number of applications for polymer systems for which understanding water sorption properties is valuable. In the ever-growing weight loss industry, superporous hydrogels could be swallowed by a patient and then swollen to occupy stomach space so there is less room for food and the appetite is suppressed.[34] Water management is a critical problem and design issue for polymer electrolyte fuel cells.[35] In the cosmetics industry, hairsprays with polymers as active ingredients must have stiffness that stands up to humidity.[36]

However, the most important application for this thesis is use of polymers as photoresists for design and patterning of microelectronics such as integrated circuits. The rate of progress in microelectronics is controlled by advances in microlithographic processesing.[37] Therefore, there is abundant research on the relevant tools, methods and materials used. Chemically amplified photoresists are just one class of materials that continues to extend the limits of feature dimensions to squeeze more elements onto a smaller piece of semiconductor material. Details on these photoresists and the importance of understanding their reaction to water exposure will be discussed below.

1.6 Chemically Amplified Photoresists

Chemically Amplified (CA) photoresists were first conceived by Frechet, Willson and Ito.[38,39] They consist of a polymer film with an incorporated photoactive catalyst such as an onium salt photoacid generator (PAG). Figure 1.2 shows a

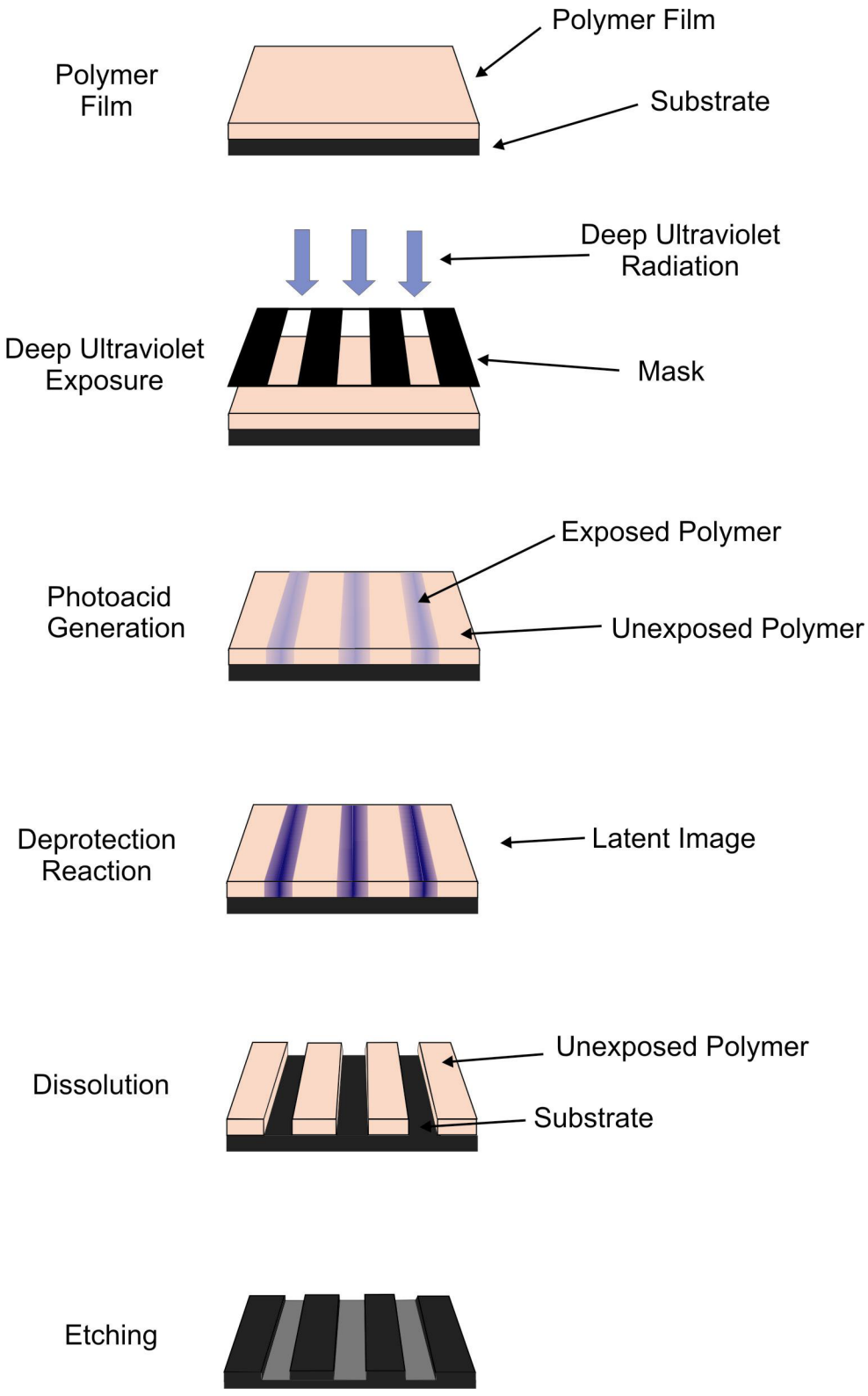

Figure 1.2: Schematic diagram of chemically amplified photoresist processing.

schematic drawing of the processing. The image of light transmitted through a mask is precisely focused onto a resist-coated wafer. A catalytic amount of acid is generated in the regions that are exposed. The acid then participates in a deprotection reaction, often activated by the introduction of heat in a post-exposure bake. The acid fragments the acid labile pendent groups of the polymer and is regenerated. In certain photoresist systems, it has been estimated that each acid molecule cleaves 1000 groups.[2] The result is a latent image of the mask pattern. In a positive tone resist, the exposed polymer is converted from hydrophobic to hydrophilic, so it is soluble in basic developers. (If the radiation renders the polymer less soluble it is called negative tone.) The modified polymer is dissolved, leaving the polymer in the mask pattern on the substrate. Etching, followed by removal of the remaining polymer, provides the desired micropatterned substrate.

There are several factors that affect the resolution and quality of the latent image and therefore the final pattern. These include the mask/illumination system, diffusion, photoacid parameters, volatile products, and airborne contaminants such as water.[2,37,40-43]

The resolution limit of an optical lithography system is set by:

$$w = \frac{k\lambda}{NA}, \tag{1.2}$$

where w is the minimum resolvable feature, k is an empirical constant determined by the individual resist process used, λ is the exposure wavelength, and NA is the numerical aperture of the exposure tool.[2,37] The wavelengths used for exposure have been becoming smaller and smaller over the years. The unfortunate aspect of this method of reducing feature size is that with each new wavelength, a new photoresist

system must be designed. Currently 193 and 157 nm resist materials are at the forefront, and smaller wavelengths, such as 13 nm extreme ultraviolet wavelengths, are being investigated.[2,44]

The light transmitted through the mask is focused onto the resist using a complex system of lenses. Improved resolution may be achieved by increasing the NA of the lens system. However, this results in a decrease in the depth of focus (DOF), represented by:

$$\text{DOF} = k_2 \lambda / (NA)^2 , \qquad (1.3)$$

where k_2 is another process-defined variable and the other variables are the same as above. Because a large DOF is required for best photoresist performance, a balance must be struck between the optimal NA and DOF for achieving the highest resolution.

The photoacid generator is one factor that contributes to the value of k. Widely used onium salts have high quantum yields of acid production, good absorption properties, and good solubility and thermal stability in polymer films.[2,45] The mechanism for photochemical acid generation is complex and currently not fully understood, although it is known that the structure of the PAG influences the generating efficiency. [2,3]

Kinetics of acid transport through the film must also be considered. The acid strength, acid size and acid volatility significantly influence the relationship between deprotection chemistry and diffusion. For example, larger, bulkier photoacids have been employed because they diffuse slower, thus limiting the scope of the diffusion reaction.[2,45] While some diffusion is necessary for catalysis of the photoresist chemistry, the resolution will suffer if the photoacid travels too far into the unexposed

regions. Another way to combat this problem is to employ basic additives to quench the acid if it diffuses out of the desired areas.[2] Also, because the acid diffusion rate increases with heat, post exposure bake temperatures can be tweaked to optimize acid diffusion.

The deprotection reaction causes the evolution of volatile products, which increases the amount of free volume in the polymer film. With more available space to move around, the photoacid becomes more mobile. The rapid loss of volatile products is then followed by a relaxation of the chains in the polymer matrix, causing an effective "shrinking" of the film. The extra free volume is eliminated as the film becomes denser. There is less room for acid transport and the diffusivity decreases.[42] Small molecule products are continuously formed and they can undergo secondary reactions with other components of the film, including the polymer and the acid.[46] Both the reactivity and the diffusivity are constantly changing in the exposed areas of the polymer. This series of events shows a characteristic complexity that makes complete understanding of the acid diffusion very challenging. Investigation into this topic is vigorous and ongoing.[47-51]

1.7 Water in Chemically Amplified Photoresists

Yet another factor that influences the diffusion of the acid in the photoresist and affects the quality and resolution of the latent image is contamination by airborne water. This is an important factor because the humidity conditions present during processing affect the outcome of the latent image. Many studies have found that water influences photoresist processing by decreasing the sensitivity, meaning the

acid molecules are involved in fewer bond cleavages, and therefore the chemical amplification is not as great.[1-3,5-8,52]

For some resist systems, water's presence in the film can alter the absorbance characteristics. Water absorbs much of the 157 nm light, therefore fewer photoacid molecules are generated when water is present in the film. [1,6]

The presence of water causes swelling, which can distort the patterns formed by the photoresist processing. For example, one study found that microbridges formed between adjacent features of the pattern.[53] It was attributed to swelling of the polymer, which caused the features to grow together.

In addition, water can compete with the polymer for the photogenerated acid. The water molecules can react with the acid and create a weaker acid, which is not as effective in the deprotection.[7,8,43] Understanding of the interactions between water and the photoresist is therefore important in order to produce optimal systems.

There is an increasing need for alternatives to photoresists that are currently processed with organic solvents.[54] The use of these solvents is environmentally-unfriendly and can lead to problems and increased costs for fabrication. In response, water-soluble resists are being investigated. Additionally, newly-developed immersion lithography uses water as an index-matching medium, to fill up the air space between the last element of the imaging lens and the surface of the photoresists. Because both of these resist systems use water in their processing, there is a greater interest in the affects of water sorption by polymers.

1.8 Experimental Methods

Techniques used by other researchers to study water sorption in polymers include Fourier Transform Infrared (FTIR) Spectroscopy,[55-57] Quartz Crystal Microbalance (QCM) measurements[58-60] and ellipsometry.[58,61-64] The highly mass-sensitive QCM is ideal for studying extremely thin films. However, the technique requires spinning the polymer films onto quartz crystals. These substrates are normally rough in comparison to the silicon and sapphire substrates used for photoresists. Because each step of the processing affects the outcome of the film, results on quartz crystal substrates may not be relevant. Ellipsometry is very sensitive to both the thickness and the refractive index of a film. It is an important tool in studying polymer swelling by small solvents.

The above mentioned methods lack the ability to study water sorption with high spatial resolution. Because the chemically amplified photoresists are patterned with sub-micron features, a powerful microscope instrument is helpful in elucidating the details of the water uptake. One method that will satisfy this requirement is the Infrared Near-field Scanning Microscope (IR-NSOM). This technique has already been applied to study latent image formation in CA photoresists.[48,65,66] It combines chemical specificity with high spatial resolution. It can be used to map out the water uptake of the photoresist on a sub-micron scale, and simultaneously measure topographical changes due to swelling of the polymer. Modifications to the instrument are needed in order to add water-vapor measurement capabilities. The new IR-NSOM in an environmental chamber is described in detail in Chapter II. The

results of experiments exploring water vapor uptake in CA photoresists using this instrument are discussed in Chapter III.

Another powerful tool for spatially resolved studies on polymer films is Atomic Force Micrscopy (AFM). An AFM provides the ability to measure changes in topography as well interaction forces between a polymer film and a scanning probe that can provide information on vapor uptake. Chapter IV will explore the limitations of this method.

In order to find out how the sorbed water molecules interact with polymer chains in the photoresist, we turned not to a more powerful microscope, but instead to spectroscopy. An FTIR, even without spatial resolution, can teach us about how the water molecules are absorbed by the polymer matrix by looking at the vibrational frequencies of the O-H stretching bands of water and how they are affected by hydrogen bonding. The results of this study will be explained in Chapter V.

The combination of these three methods provides much insight on water vapor uptake in CA photoresists. The data obtained and the discussion presented will help analyze results from previous work on these polymers and eventually help to optimize processing methods.

References for Chapter I

(1) Berger, C. M.; Henderson, C. L. *Polymer* **2003**, *44*, 2101.

(2) Wallraff, G. M.; Hinsberg, W. D. *Chem. Rev.* **1999**, *99*, 1801.

(3) Dentinger, P. M.; Lu, B.; Taylor, J. W.; Bukofsky, S. J.; Feke, G., D.; Hessman, D.; Grober, R. D. *J. Vac. Sci. Technol. B* **1998**, *16*, 3767.

(4) Shibayama, Y.; Saito, M. *Japan. J. Appl. Phys.* **1990**, *29*, 2152.

(5) Padmanaban, M.; Endo, H.; Yoshio, I.; Kinoshita, Y.; Kudo, T.; Masuda, S.; Nakajima, Y. *Proc SPIE* **1992**, *1672*, 141.

(6) Dean, K.; Kishkovich, O. *SPIE, Advances in Resist Technology and Processing* **2000**.

(7) Suga, O.; Yamaguchi, H.; Okazaki, S. *Microelec. Engin.* **1991**, *13*, 65.

(8) MacDonald, S. A.; Clecak, N. J.; Wendt, H. R.; Willson, C. G.; Snyder, C. D.; Knors, C. J.; Deyoe, N. B.; Maltabes, J. G.; Morrow, J. R.; McGuire, A. E.; Holmes, S. J. *Proc. SPIE* **1991**, *1466*, 2.

(9) Adhikari, B.; Majumdar, S. *Prog. Polym. Sci.* **2004**, *29*, 699.

(10) Lange, J.; Wyser, Y. *Packag. Technol. Sci.* **2003**, *16*, 149.

(11) Kondratowicz, B.; Narayanawamy, R.; Persaud, K. C. *Sensors and Actuators B* **2001**, *74*, 138.

(12) Bedoya, M.; Orellana, G.; Morenio-Bondi, M. C. *Helvetica Chimica Acta* **2001**, *84*, 2628.

(13) Buchold, R.; Nakladal, A.; Gerlach, G.; Herold, M.; Gauglitz, G.; Sahre, K.; Eichhorn, K.-J. *Thin Solid Films* **1999**, *350*, 178.

(14) Pradas, M. M.; Ribelles, J. L. G.; Aroca, A. S.; Ferrer, G. G.; Anton, J. S.; Pissis, P. *Colloid Polym. Sci.* **2001**, *279*, 323.

(15) Turner, D. T. *Polymer* **1982**, *23*, 197.

(16) Nogueira, P.; Ramirez, C.; Torres, A.; Abad, M. J.; Cano, J.; Lopez, J.; Lopez-Bueno, I.; Barral, L. *J. Appl. Polym. Sci.* **2000**, *80*, 71.

(17) Chin, J. W.; Nguyen, T.; Aouadi, K. *J. Appl. Polym. Sci.* **1998**, *71*, 483.

(18) van der Wel, G. K.; Adan, O. C. G. *Progress in Organic Coatings* **1999**, *37*, 1.

(19) Perera, D. Y. *Progress in Organic Coatings* **2002**, *44*, 55.

(20) Buchold, R.; Nakladal, A.; Gerlach, G.; Sahre, K.; Eichhorn, K.-J. *Thin Solid Films* **1998**, *312*, 232.

(21) Han, H.; Seo, J.; Ree, M.; Pyo, S. M.; Gryte, C. C. *Polymer* **1998**, *39*, 2963.

(22) Feng, R.; Farris, R. J. *J. Micromech. Microeng.* **2003**, *13*, 80.

(23) Sangaj, N. S.; Malshe, V. C. *Progress in Organic Coatings* **2004**, *50*, 28.

(24) Neogi, P. *Diffusion in Polymers*; Marcel Dekker, Inc: New York, 1996.

(25) Liu, M.; Wu, P.; Ding, Y. D.; Li, S. *Phys. Chem. Chem. Phys.* **2003**, *5*, 1848.

(26) Chirife, J.; Buera, M. D. *Crit. Rev. in Food Sci. and Nutr.* **1996**, *36*, 465.

(27) Arvanitoyannis, I. S. *J.M.S. - Rev. Macromol. Chem. Phys.* **1999**, *C39*, 205.

(28) Costa-Fernandez, J. M.; Sanz-Medel, A. *Analytica Chimica Acta* **2000**, *407*, 61.

(29) Deisingh, A. K.; Stone, D. C.; Thompson, M. *Int. J. Food Sci. Technol.* **2004**, *39*, 587.

(30) Okuzaki, H.; Funasaka, K. *Macromolecules* **2000**, *33*, 8307.

(31) Patri, A. K.; Majoros, I. J.; Barker, J., James R. *Curr. Opin. Chem. Biol.* **2002**, *6*, 466.

(32) Brannon-Pepas, L. Polymers in Controlled Drug Delivery; Medical Plastics and Biomaterials, 1997; Vol. 2004.

(33) Maggi, L.; Segale, L.; Torre, M. L.; Ochoa Machiste, E.; Conte, U. *Biomaterials* **2002**, *23*, 1113.

(34) Park, K. Superporous Hydrogels for Pharmaceutical &Other applications; Akina, Inc, 2004; Vol. 2004.

(35) Weber, A. Z.; Newman, J. *J. Electrochem. Soc.* **2004**, *151*, A311.

(36) Jachowicz, J.; Yao, K. *J. Cosm. Sci.* **2001**, *52*, 281.

(37) Reichmanis, E.; Nalamasu, O. *Science* **2002**, *297*, 349.

(38) Ito, H.; Willson, C. G. *Polym. Eng. Sci* **1982**, *23*, 1021.

(39) Frechet, J. M.; Ito, H.; Willson, C. G. *Proc. Microcirucuit. Eng.* **1982**, *82*, 260.

(40) Ocola, L. E.; Cerrina, F.; May, T. *J. Vac. Sci. Technol. B* **1997**, *15*, 2545.

(41) Houle, F. A.; Hinsberg, W. D.; Sanchez, I. *J. Vac. Sci. Technol. B* **2004**, *22*, 747.

(42) Croffie, E.; Cheng, M.; Neureuther, A. *J. Vac. Sci. Technol. B* **1999**, *17*, 3339.

(43) Burns, S. D.; Medeiros, D. R.; Johnson, H. F.; Wallraff, G. M.; Hinsberg, W. D.; Willson, C. G. *Proc SPIE* **2002**, *4690*, 321.

(44) Sahoo, P. B.; Vyas, R.; Wadhwa, M.; Verma, S. *Bull. Mater. Sci.* **2002**, *25*, 553.

(45) Ablaza, S. L.; Cameron, J. F.; Xu, G.; Yueh, W. *J. Vac. Sci. Technol. B* **2000**, *18*, 2543.

(46) Hinsberg, W. D.; Houle, F. A.; Poliskie, M.; Pearson, D.; Sanchez, M.; Ito, H.; Hoffnagle, J.; Morrison, M.

(47) Preusser, J., personal communication.

(48) Dragnea, B.; Preusser, J.; Szarko, J. M.; McDonough, L. A.; Leone, S. R.; Hinsberg, W. D. *Appl. Surf. Sci* **2001**, *175-176*, 783.

(49) Stewart, M. D.; Tran, H. V.; Schmid, G. M.; Stachowiak, T. B.; Becker, D. J.; Willson, C. G. *J. Vac. Sci. Technol. B* **2002**, *20*, 2946.

(50) Houle, F. A.; Hinsberg, W. D.; Morrison, M.; Sanchez, I.; Wallraff, G.; Larson, C.; Hoffnagle, J. *J. Vac. Sci. Technol. B* **2000**, *18*, 1874.

(51) Lin, E. K.; Soles, C. L.; Goldfarb, D. L.; Trinique, B. C.; Burns, S. D.; Jones, R. L.; Lenhart, J. L.; Angelopoulos, M.; Willson, C. G.; Satija, S. K.; Wu, W.-l. *Science* **2002**, *297*, 372.

(52) Shibayama, Y.; Saito, M. *Jap. J. Appl. Phys.* **1990**, *29*, 2152.

(53) Nakazawa, K.; Shiobara, E.; Asano, M.; Sato, Y.; Tanaka, S.; Oonishi, Y. *Jpn. J. Appl. Phys.* **1999**, *38*, 1569.

(54) Harvard, J. M.; Shim, S.-Y.; Frechet, J. M.; Lin, Q.; Medeiros, D. R.; Willson, C. G.; Byers, J. D. *Chem. Mater.* **1999**, *11*, 719.

(55) Sutandar, P.; Ahn, D. J.; Franses, E. I. *Macromolecules* **1994**, *27*, 7316.

(56) Sammon, C.; Mura, C.; Yarwood, J.; Everall, N.; Swart, R.; Hodge, D. *J. Phys. Chem. B* **1998**, *102*, 3402.

(57) Ichikawa, K.; Mori, T.; Kitano, H.; Kukuda, M.; Mochizuki, A.; Tanaka, M. *J. Polym. Sci. Part B: Polym Phys* **2001**, *39*, 2175.

(58) Chen, W.-L.; Shull, K. R. *Macromolecules* **1999**, *32*, 136.

(59) Kusano, H.; Kimura, S.; Kitagawa, M.; Kobayashi, H. *Thin Solid Films* **1997**, *295*, 53.

(60) Matsuguchi, M.; Sadaoka, Y.; Shinmoto, M.; Sakai, Y. *Bull. Chem. Soc. of Jpn.* **1994**, *67*, 46.

(61) Mikhaylova, Y.; Pigorsch, E.; Grundke, K.; Eichhorn, K.; B/, V. *Macromol. Sym.* **2004**, *210*, 271.

(62) Toomey, R.; Freidank, D.; Ruhe, J. *Macromolecules* **2004**, *37*, 882.

(63) Tang, Y.; Lu, J. R.; Lewis, A. L.; Vick, T. A.; Stratford, P. W. *Macromolecules* **2002**, *35*, 3955.

(64) Golander, C. G.; Rutland, M. W.; Cho, D. L.; Johansson, A.; Ringblom, H.; Jonsson, S.; Yasuda, H. K. *J. Appl. Polym. Sci.* **1993**, *49*, 39.

(65) Dragnea, B.; Preusser, J.; Schade, W.; Leone, S. R.; Hinsberg, W. D. *J. Appl. Phys.* **1999**, *86*, 2795.

(66) Dragnea, B.; Preusser, J.; Szarko, J. M.; Leone, S. R.; Hinsberg, W. D. *J. Vac. Sci. Technol. B* **2001**, *19*, 142.

Chapter II:

Experimental Design of an Infrared Near-field Scanning Optical Microscope (NSOM) in an Environmental Chamber

2.1 Introduction

Classical microscopy has long been a valuable part of scientific research. The technique is non-destructive and easy to use, produces images that can be interpreted by the human eye, and is applicable to samples in their natural environment. However, conventional microscopy is limited by the size of the spot that a light beam can be focused to with normal lens optics. This "diffraction limit" is known to be equal to approximately $\lambda/2$, which is around 250-300 nm for visible light. It is becoming increasingly important to have the ability to image samples with even greater spatial resolution, especially in the biological and materials sciences.[1-4]

The near-field scanning optical microscope (NSOM) is a powerful tool that combines high spatial resolution with the specificity and convenience of optical microscopy. It can be used to simultaneously study the shape and size of samples along with chemical composition, structure and chemical dynamics. The defining characteristic is that it overcomes the diffraction limit by using a sub-wavelength aperture to produce a tiny spot of light on a sample. The obtainable resolution is a function of the probe size and its proximity to the sample.

The accompanying theory was first proposed by Synge in 1928 in a revolutionary series of papers.[5] However, the principle was not realized until 1972, when Ash and Nichols demonstrated imaging using a sub-wavelength aperture for

microwave radiation.[6] This achievement renewed interest in the topic, and in 1984 a microscope like the one proposed by Synge was demonstrated by Pohl's laboratory at IBM Zurich.[7,8] Once several technical difficulties were worked through, such as aperture fabrication and distance regulation, more rapid development of the technique began in the early 1990's.[1,9,10] The NSOM is now a commercially available instrument.

The NSOM technique coupled with visible light allows for high spatial resolution measurement of various processes. Fluorescence imaging of biological samples[1,11], single molecule detection[11-13] and thin polymer film analysis[1,4] are some examples of successful work using this technique.

Coupling an NSOM with infrared light provides a powerful tool to be used in measurement of samples such as polymers and living cells. Vibrational spectroscopy in the "fingerprint region" can be employed as a contrast mechanism. Because of the longer wavelengths involved, infrared microscopy can benefit even more than the visible by overcoming the diffraction limit. However, there are additional technical obstacles that must be hurdled. Finding an optical fiber material for infrared light is one challenge, procuring a tunable, bright IR source is another. The absorptions in the IR are typically weaker, and the sensitivity of IR detectors is usually orders of magnitude smaller than visible counterparts. Despite these challenges, several groups have had success in developing the IR-NSOM.[2,14-17]

The instrument described here is the first example of an IR-NSOM coupled with an environmental chamber. This allows for measurement of the effects of a sample's environment on its topographic and optical properties. In particular, the

absorption of water vapor by patterned chemically amplified photoresist samples can be explored. However, following with the history of the development of the NSOM, there are many technical challenges to be faced. A description of these issues follows.

2.2 Bell Jar Apparatus

A schematic drawing of the bell jar apparatus developed for the experiments is shown in Figure 2.1. A krypton ion laser pumps a color-center laser to produce infrared light tunable from 2.6 – 3.2 μm. This light enters the bell-jar through a calcium fluoride window in the chamber's baseplate. The infrared light is coupled into an optical fiber that ends in a tapered, coated tip. The light emerges from a 200 nm aperture, which is kept close to the sample with a shear-force feedback loop. The transmitted light is measured by a large area PbS detector which sits directly below the sample and is coupled to a lock-in amplifier. Both the sample and the detector rest on a piezo tube scanner, which can move in the x, y and z directions to create 3–dimensional images. The scanning, the feedback loop, and the detected IR signal are all controlled and recorded by a commercial scanning probe microscopy controller. Optical transmission and complementary topographic images are simultaneously measured. The chamber also includes inlets for introduction of gases such as water vapor, and pumping with a mechanical roughing pump. Detailed descriptions of many components of this instrument are given in the following sections.

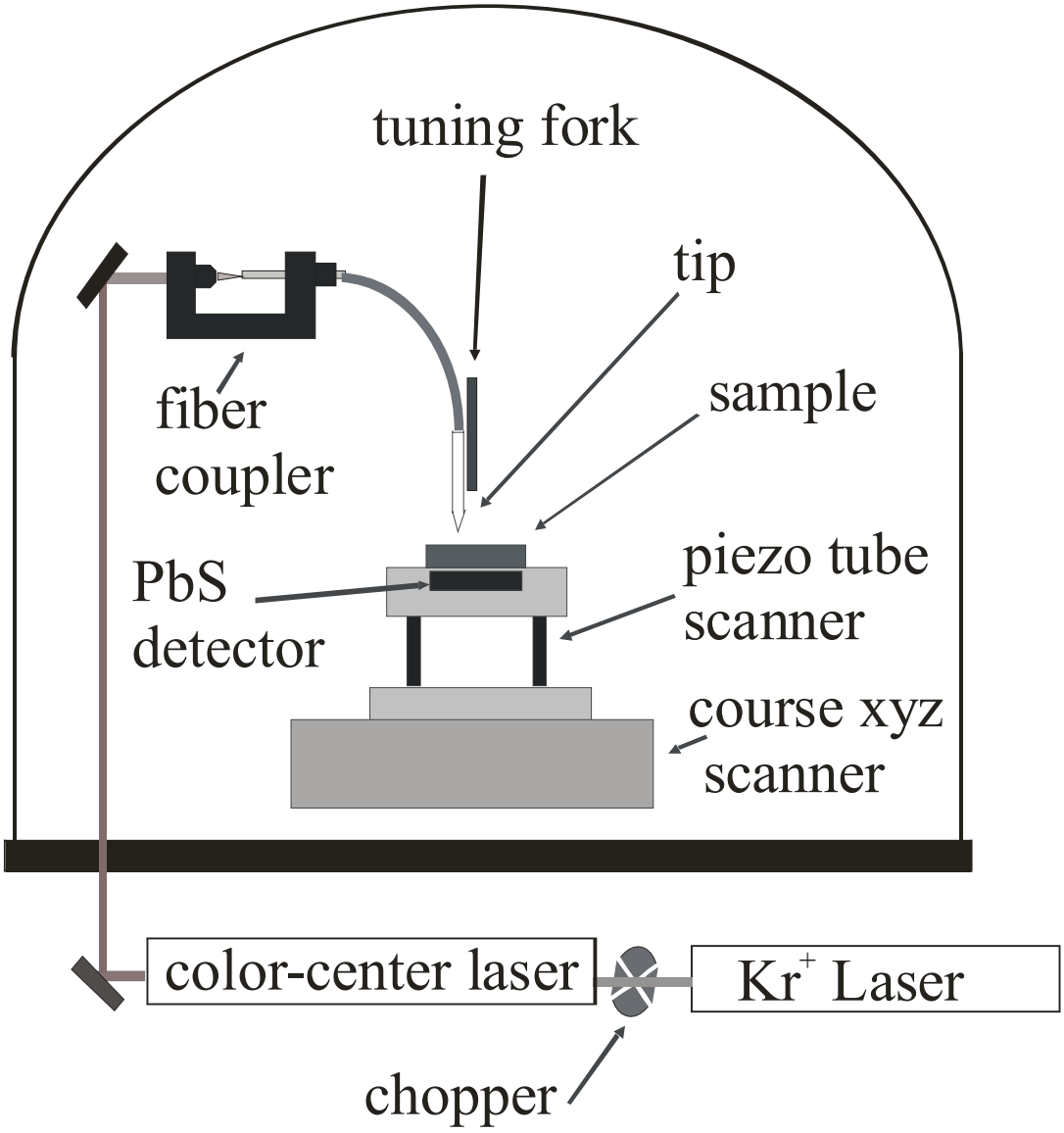

Figure 2.2: Schematic drawing of experimental apparatus

2.3 Water Introduction

Water is prepared in a glass reservoir as shown in Figure 2.2. Distilled water is used to fill the 0.5 L bottom bulb of the glass apparatus approximately 1/3 full. A dewar filled with liquid nitrogen is placed around the bulb so that the water freezes. Once the water is frozen, the valve is opened to the system and the reservoir is pumped down to a pressure of approximately 2×10^{-1} Torr. The valve is closed, and the dewar is removed so the ice melts. This cycle is repeated at least three times, so that air trapped in the ice during rapid freezing is minimized. The end result is 25 L of water vapor available for experiments to be performed in a 60 L bell jar. When the water remains at room temperature for use in experiments, the vapor pressure is 18 Torr. The pressure of water vapor obtainable can be adjusted by changing the temperature of the liquid water. This can be done by placing a bath of cold water or ice water around the bottom of the glass bulb as is done with the liquid nitrogen dewar. Figure 2.3 shows the different vapor pressures of water obtainable vs. the temperature used.[28] Using warm water could produce a partial pressure of water greater than 18 Torr. However, this is undesirable because the bell jar is at room temperature and an excess of water vapor would cause condensation in the experimental chamber.

2.4 Quartz Crystal Microbalance Uptake Measurements

A quartz crystal microbalance is used to measure the kinetics of water uptake in an unpatterned thin film in order to characterize the experimental chamber. Films were prepared using a solution of Poly(methylmethacrylate) polymer purchased from

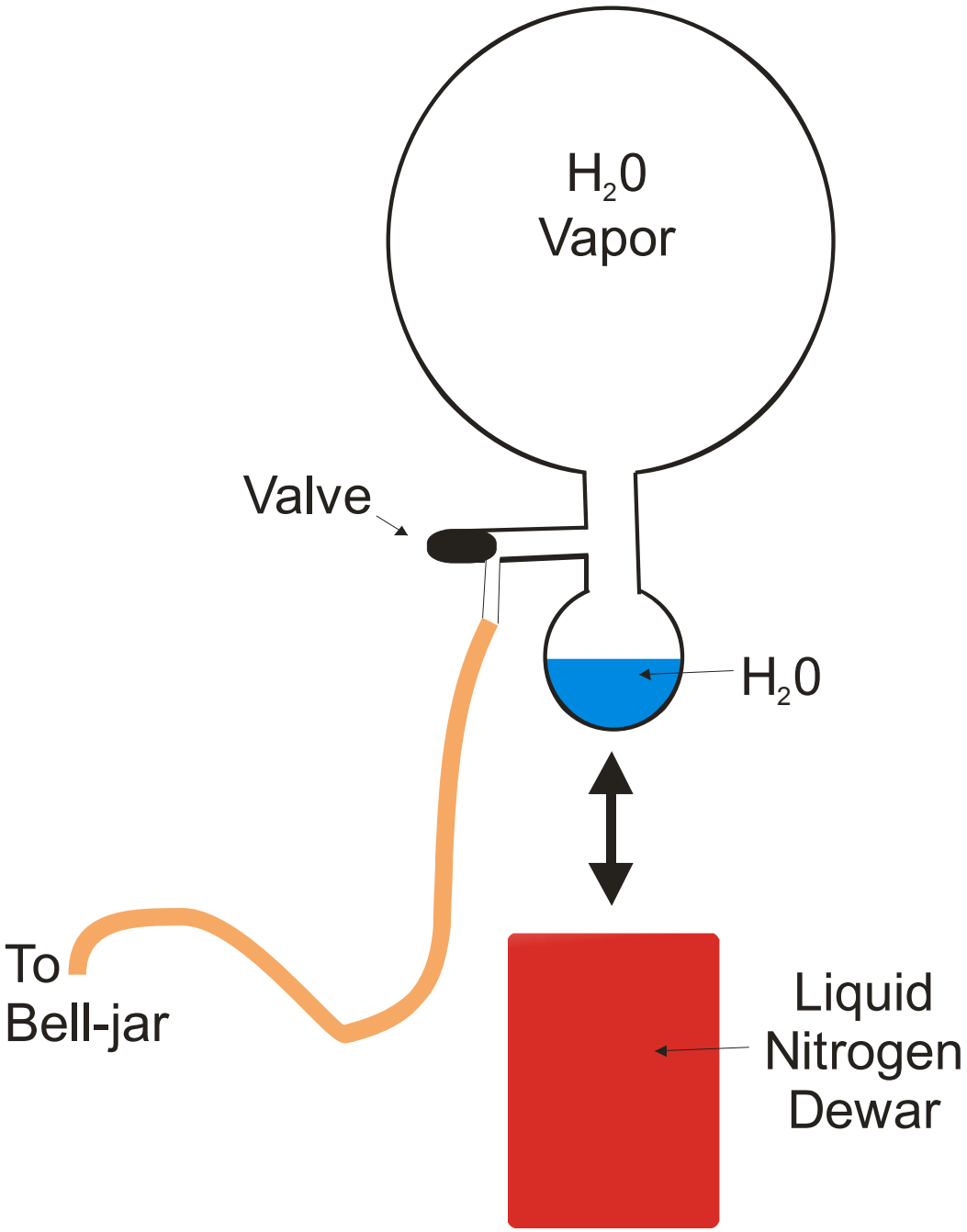

Figure 2.2: Water Vapor Reservoir.

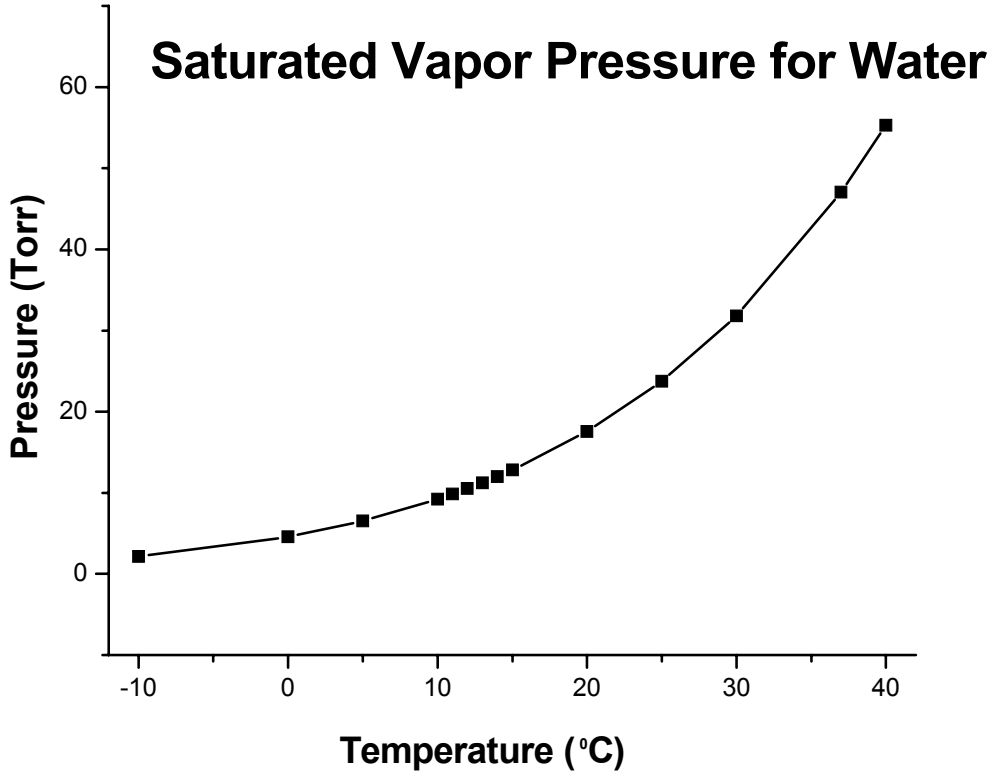

Figure 2.3: Saturated vapor pressure at various temperatures for water.

Aldrich and dissolved in chloroform at a concentration of 10 mg/ml. The solution was spun onto a quartz crystal substrate. A commercial spin coater was used to spin the film for 30 seconds at 5,000 rpm. The result is an approximately one micron thick film on a quartz crystal. Excess polymer is removed from the edges of the film with an acetone-soaked cotton swab in order to ensure good contact with the microbalance.

The polymer-coated quartz crystal is loaded into the quartz crystal microbalance (QCM) apparatus, which is installed in the bell jar. The crystal oscillates at a certain frequency, and when the polymer absorbs water, mass is gained and the oscillation frequency changes.[29] The change in frequency can be converted to change in mass, and the mass of water absorbed by the polymer can be determined using the following equation:

$$\Delta f = -C_f \bullet \Delta m, \qquad (2.1)$$

where Δf is the observed frequency change, Δm is the change in mass per unit area, and C_f is the sensitivity constant for the crystal used.

Figure 2.4 shows what happens during the introduction of water vapor into the chamber. The clock is started and at 15 seconds the valve to the water reservoir is opened, and vapor is allowed into the chamber. The pressure is recorded once every second using a MKS Baratron gauge, and the mass gained by the polymer film is measured simultaneously by the QCM. Figure 2.4 shows the normalized pressure and mass vs. time curves; 2.4a shows the evolution over one hour, while figure 2.4b shows just the first 250 seconds.

The pressure in the chamber rises very quickly over the first 50 seconds, then continues to increase at a slower rate over the entire hour. The first, fast part occurs

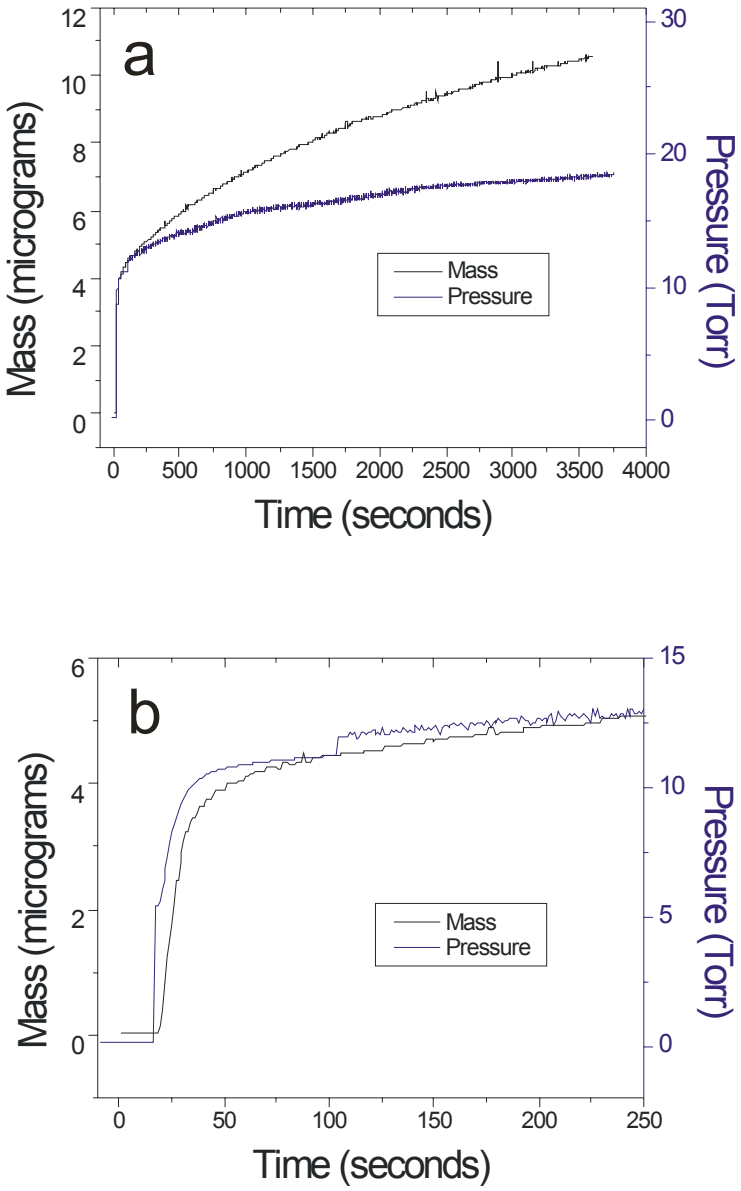

Figure 2.4: Water vapor introduction into bell jar chamber and accompanying mass uptake by polymer. a) Pressure of water vapor (blue) and mass of polymer-absorbed water (black) vs. time. b) Enlargement of first 250 seconds of the same vapor introduction shown in part a.

when the vapor available in the water reservoir flows into the bell jar. The second, slower part occurs as more vapor is created by the liquid water at the bottom of the reservoir. The mass taken up by the polymer follows the same pattern. Figure 2.4b shows that in the first 40 seconds, the slope of the pressure and mass uptake curves are the same. This means that the mass uptake may be limited by available water vapor, and therefore, kinetic studies in this chamber are probably not possible. A smaller chamber would fill more quickly, and therefore may give a better indication of the rate of water uptake by the polymer. This factor should be considered in future real-time experiments.

2.5 Infrared Laser

The laser used to produce infrared light is a Burleigh FCL color-center laser pumped by a Coherent Krypton ion laser. This type of laser is a four-level system that operates with a solid-state crystal. The alkali halide crystal is doped with impurities during growth to create anionic vacancies filled with electrons called F-centers. Processing of the crystal with white light at temperatures near -20 °C makes the F-centers capable of producing stimulated emission. As shown in Figure 2.5, the electrons absorb the light from the pump laser and are transferred to an excited level. They undergo fast, radiationless transitions, as well as transitions that produce emission of infrared light. The crystal will not lase at room temperature, however. It must be constantly cooled with liquid nitrogen because the fluorescence quantum efficiency decreases with increasing temperatures.

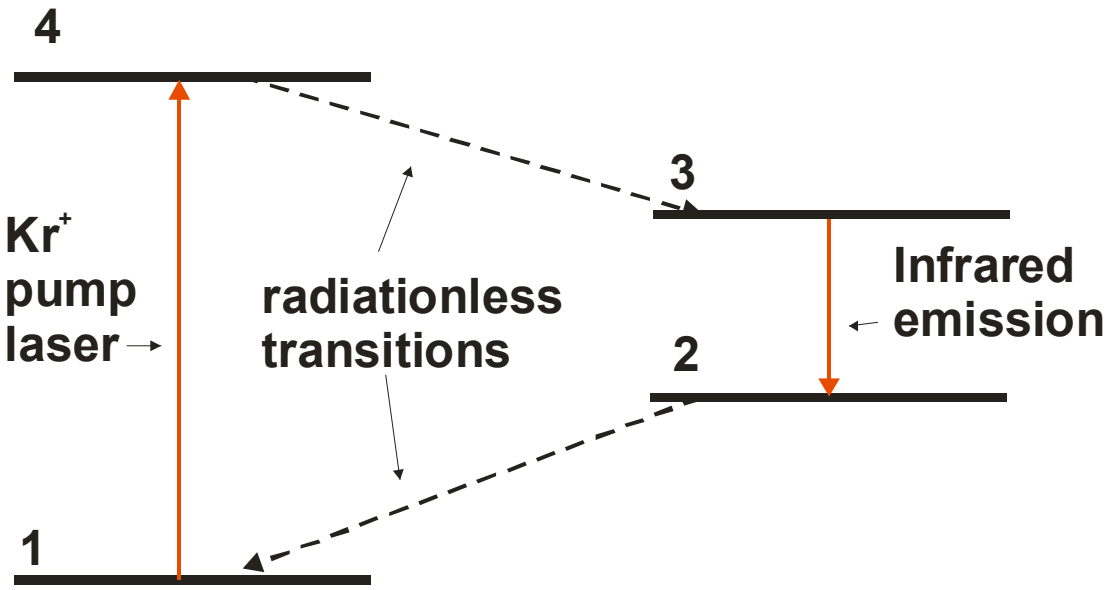

Figure 2.5: Lasing cycle for color-center laser.

The result is a continuously tunable, narrow linewidth, high power output in the 2.6 – 3.2 μm region. The FCL has advantages over other infrared sources because it has a narrow linewidth. It produces a higher output than diode lasers, and is easier to use than an OPO.

One drawback of the FCL laser is the higher level of intensity fluctuations, due to the pump laser. The noise in the FCL is compared to that of an infrared diode laser in Figure 2.6. A fast-fourier transform (FFT) signal analyzer was used to show the power of each laser at different frequencies. The FCL has a large amount of noise at a variety of frequencies, while the laser diode shows a relatively small amount of noise. This can limit the experiment if the signal intensity is small, because the signal-to-noise ratio will not be high enough to measure a clear image. Use of a lock-in amplifier to measure signal at a specific chopped frequency can eliminate much, but not all, of the noise.

2.6 Infrared Fiber Tips

The microscopic aperture needed for overcoming the diffraction limit in the NSOM experiment is provided by the creation of a coated, tapered fiber tip. The infrared fiber used for these experiments is SG fiber purchased from Infrared Fiber Systems, Inc. with an optimal transmission range of 0.45 – 5.0 μm. The fiber has a 200 μm diameter core made up of 53% ZrF_4, 20% BaF_2, 4%LaF_3, 3% AlF_3 and 20% NaF. The core is surrounded by a glass clad, and then covered with a polymeric buffer coating. The polymer coating keeps the brittle core from breaking upon bending.

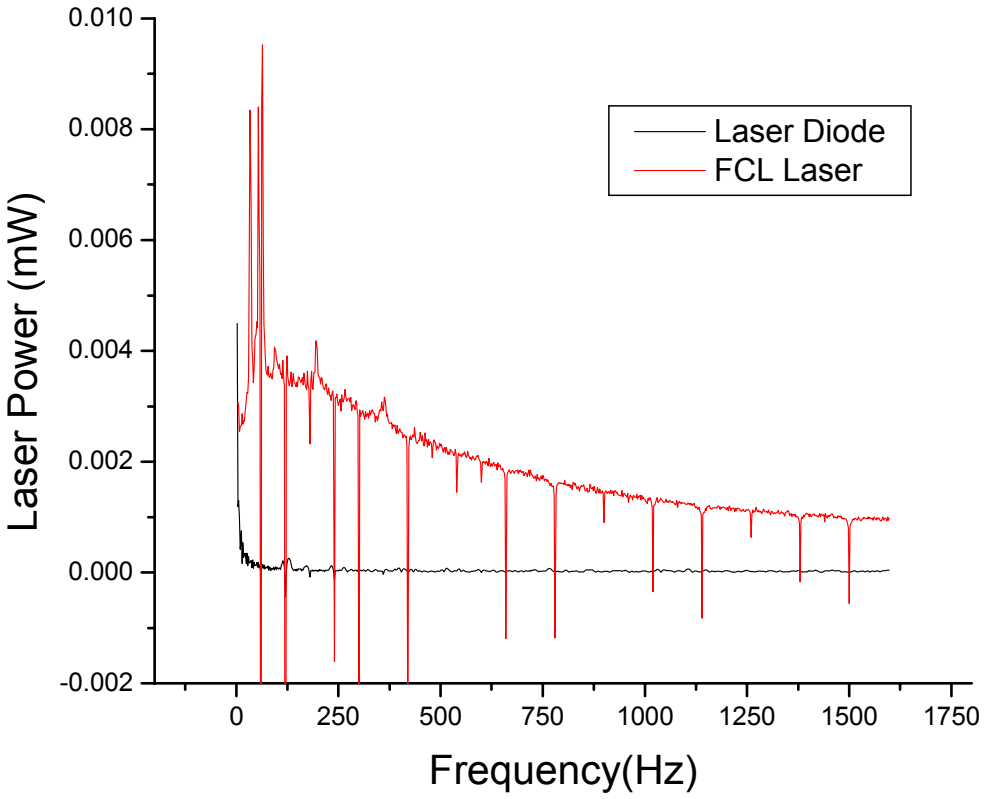

Figure 2.6: Graph of Laser power vs. Frequency for two different infrared lasers. The FCL laser has more noise and fluctuation than an infrared diode laser.

Approximately 5 cm of the coating and cladding is removed from end of the fiber, so that the glass core is completely exposed. The fiber is dipped in a heated solvent, such as 1-methyl-2-pyrrolidinone, for one minute; then dipped in methanol for several minutes and wiped with a tissue to remove any remaining coating. It is mounted on a commercial micro-pipette puller.

The apparatus used to pull the fibers is shown in figure 2.7. A standard procedure is followed.[18] When the shutter is opened, the fiber is heated by a CO_2 laser which is focused in the plane of the fiber to a diameter of ~ 1 mm, giving a power density of 10 W/cm^2. The micropipette puller uses a set program of controlled force and velocity to pull the fiber into a tapered tip while providing control over taper length and tip size. A constant, weak force is applied to the fiber during heating until a certain velocity is reached, and then a stronger force is applied until the fiber breaks. This two step-process produces the best shaped tip for maximum throughput.[15,18] The slow pull results in a taper to a diameter slightly larger than the wavelength of light, and the faster pull allows for a sharp tip.

Examples of Scanning Electron Microscope (SEM) images of aluminum coated tips produced by this pulling method are shown in Figure 2.8. Part (a) shows the long taper, part (b) shows the short taper, and part (c) shows the tip. A tip with this shape should have a transmittance of around 10^{-4} in comparison to a cleaved end fiber.[15] It is necessary to use the SEM to check for proper taper length and shape because the commercial fibers purchased do not always have a consistent composition. A slight change in the material makeup can require a different laser power. If the heat is too high for a particular fiber, the taper produced can be too

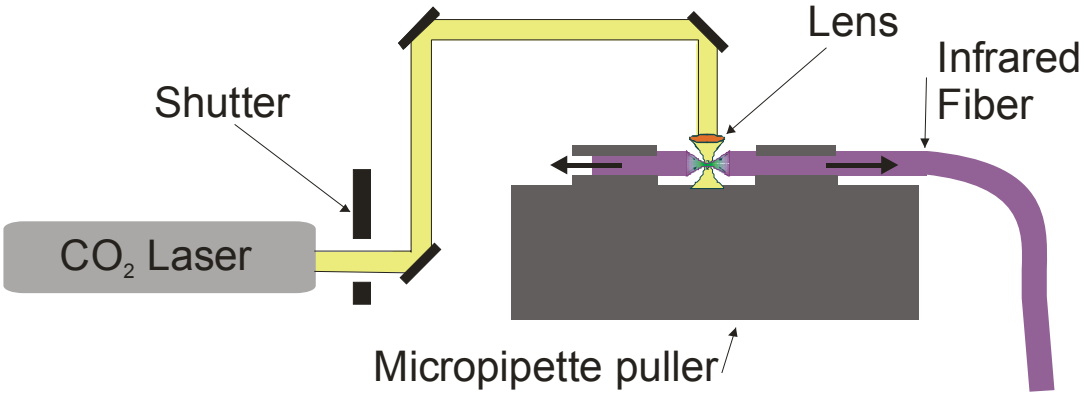

Figure 2.7: A schematic diagram of the fiber pulling apparatus.

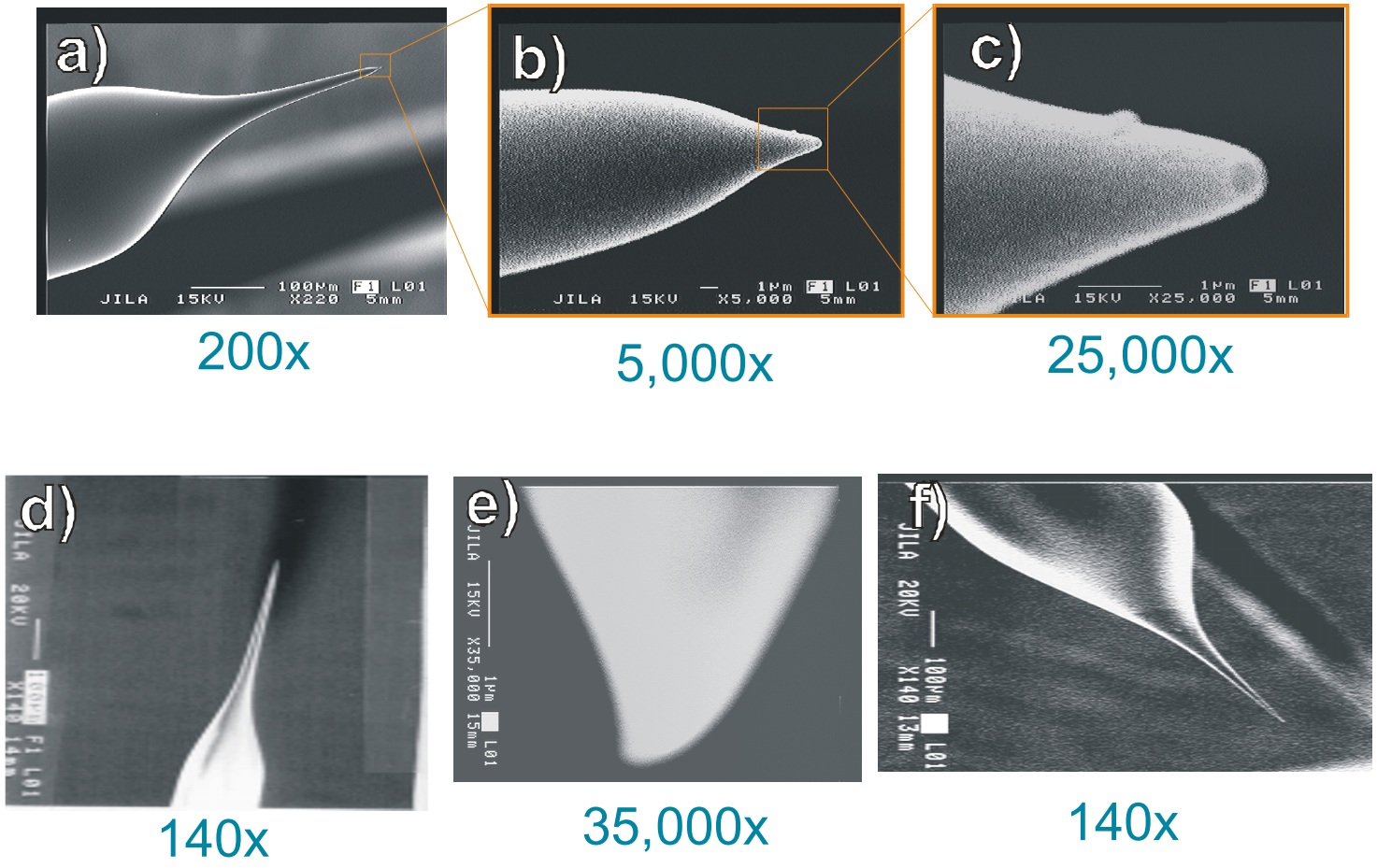

Figure 2.8 Examples of Scanning Electron Microscopy (SEM) images of pulled infrared fiber tips. a) The first, longer taper. b) The second, shorter taper. c) The sharp tip end. d) A tip with a longer taper than optimal for maximum transmittance. e) A tip with a curved "hook." f) A tip that has been etched to remove a hook.

long, and transmittance is decreased. An example of this is shown in Figure 2.8d. On the other hand, if the laser power is too low, and the fiber is not heated enough, it can break in a jagged fashion, without creating a sharp tip.

Another parameter to monitor is the alignment of the focused laser beam onto the fiber. If the laser is not aligned properly, the fiber can be heated non-uniformly, and this can cause the tip to "hook" when pulled. An example of this type of tip is shown in Figure 2.8e. However, because some of the fiber purchased has its own non-uniformity, it is sometimes not possible to eliminate the hook. In this case, it is possible to remove the hook via a variation on an etching technique described by Michaels, et al. A 0.6 M HCl and 0.04 M $ZrOCl_2$ etchant solution is prepared and placed in a small vial. Then 2,2,4-trimethylpentane is dropped over the etchant solution until a distinct layer can be seen. The hooked tip is lowered so that the end of the tip just penetrates the lower level (by the human eye). After 10 – 20 seconds the tip is removed and rinsed with acetone for 3-5 minutes. An example of a resulting tip is shown in Figure 2.8f. Although the hook is removed, the taper is a little longer than ideal, so the preference is to pull tips that do not have a hook.

Once the pulling parameters are optimized, the pulled fibers are coated in an evaporative bell jar coater, shown in figure 2.9. The fibers are mounted in the bell jar

on chucks which are rotated via an external stepper motor. A chromium rod and a tungsten boat holding balled up aluminum wire are mounted on electrodes. The bell jar chamber is pumped down to a pressure on the order of 10^{-6} Torr. The metals are resistively heated and evaporate. When the shutter is open, the evaporated metal

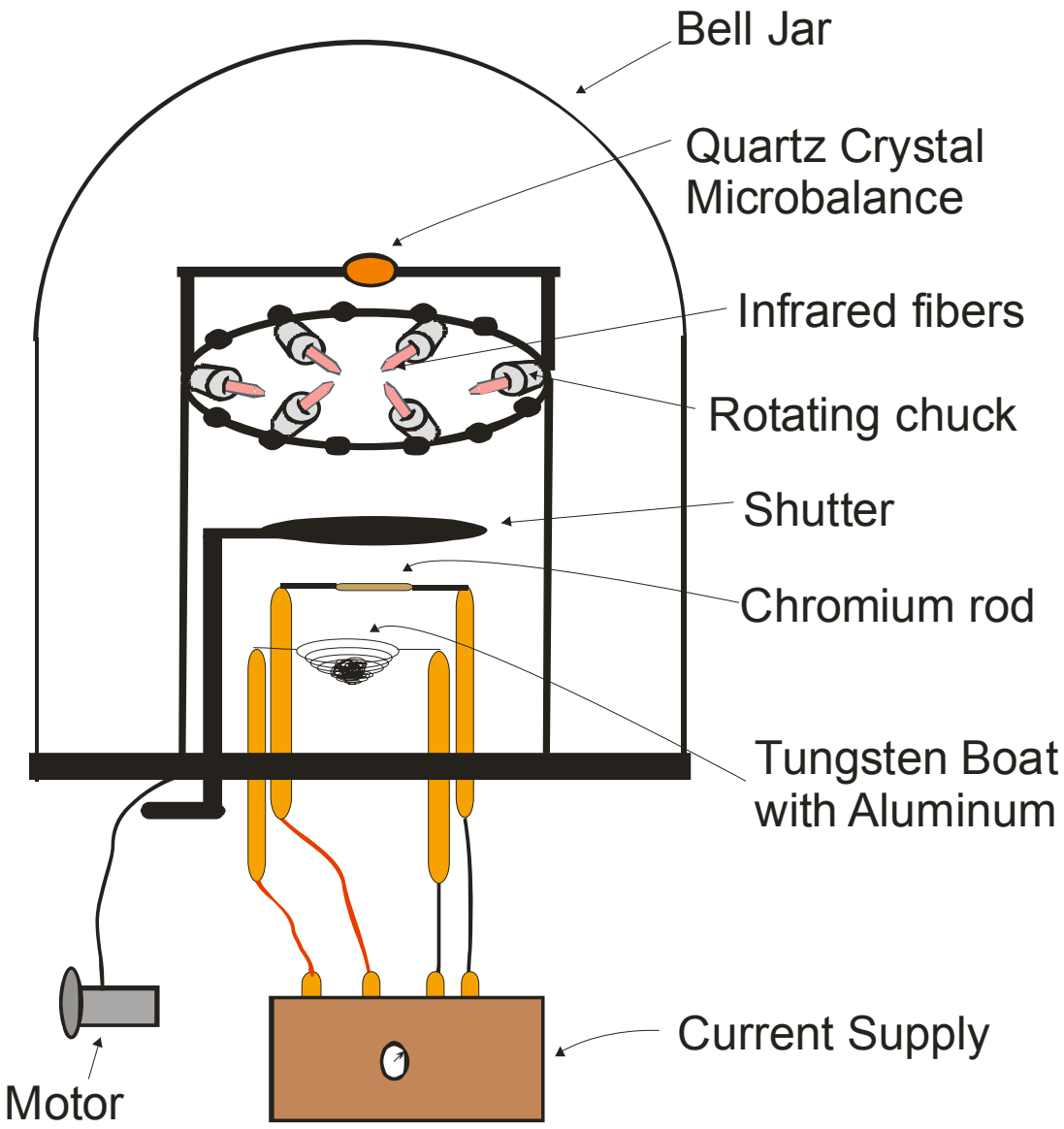

Figure 2.9: Schematic diagram of coating apparatus.

coats the infrared fibers. Due to the 40° angle at which they are mounted, the fibers are coated everywhere except at the tip, creating an aperture with a 200 nm diameter. (See Figure 2.8c) A 30 nm thin layer of chromium covers the fibers first to improve the adhesion of the aluminum, then a 120 nm layer of aluminum is coated over the chromium. The thicknesses are measured by an upside-down mounted quartz crystal microbalance inside the bell jar. A thinner coating could cause light to leak through the coating and diminish the resolution of the microscope, while a thicker coating may make the probe too large to image small topographic changes or prevent light from emerging from the aperture. With this aperture, a resolution of 300 nm is obtainable.[2] The "diffraction limit" of 3 μm light is approximately 1.5 μm, so the NSOM configuration provides a large improvement.

One major difficulty in the pulling and coating process is the brittle nature of the infrared fiber. If the tip should touch any surface it will break instantly. If the tip is only slightly broken, it may still be used for imaging, but will provide a poorer resolution. However, a large break will cause too large an aperture to image any of the sample features. Also, if the tip is broken before coating, the coating process may not form a proper aperture. It is impossible to see with the human eye, or even a classical microscope, if the tip has been broken. The SEM can be used to check for breakage and reproducibility, however, it is not convenient or practical to check every tip.

2.7 Shear-Force Microscopy

The high resolution of an NSOM is derived not only from a small sub-wavelength aperture, but also from the tip-sample distance regulation that is provided by shear-force microscopy. Keeping the tip close to the sample allows for a small spot size of light on the sample. Maintaining a constant gap between tip and sample eliminates optical artifacts and allows for measurement of the topography of a sample. It also reduces accidental tip-sample contact and therefore decreases tip breakage. The main components of the shear-force feedback system are a probe, a tuning fork, a piezoelectric tube scanner, and a feedback system. They are displayed in a schematic diagram in figure 2.10.

The optical fiber described in section 2.6 is glued along the side of one prong of a quartz crystal tuning fork with a resonant frequency of around 32 kHz. The tapered, coated fiber tip is aligned so that it is hanging just below the end of the fork. The fork is glued to a macor fiber holder. A piezoelectric transducer is also mounted to the macor and is used to excite the mechanical resonance of the fork. A signal is sent to the piezo from the driver circuit, which vibrates the fork and causes the tip to dither parallel to the sample surface. The prongs of the fork are electrically coupled, which allows for amplitude measurement with a lock-in amplifier.

The sample is placed on a home-built scanner, which is mounted on a base with a picomotor controller. This allows the sample to be moved in the z direction with a remote control. When the sample and tip come within near-field range of each other, the amplitude of the tip dither is damped by shear forces. A feedback loop, controlled by a scanning probe microscope controller, allows the tip to be locked in at

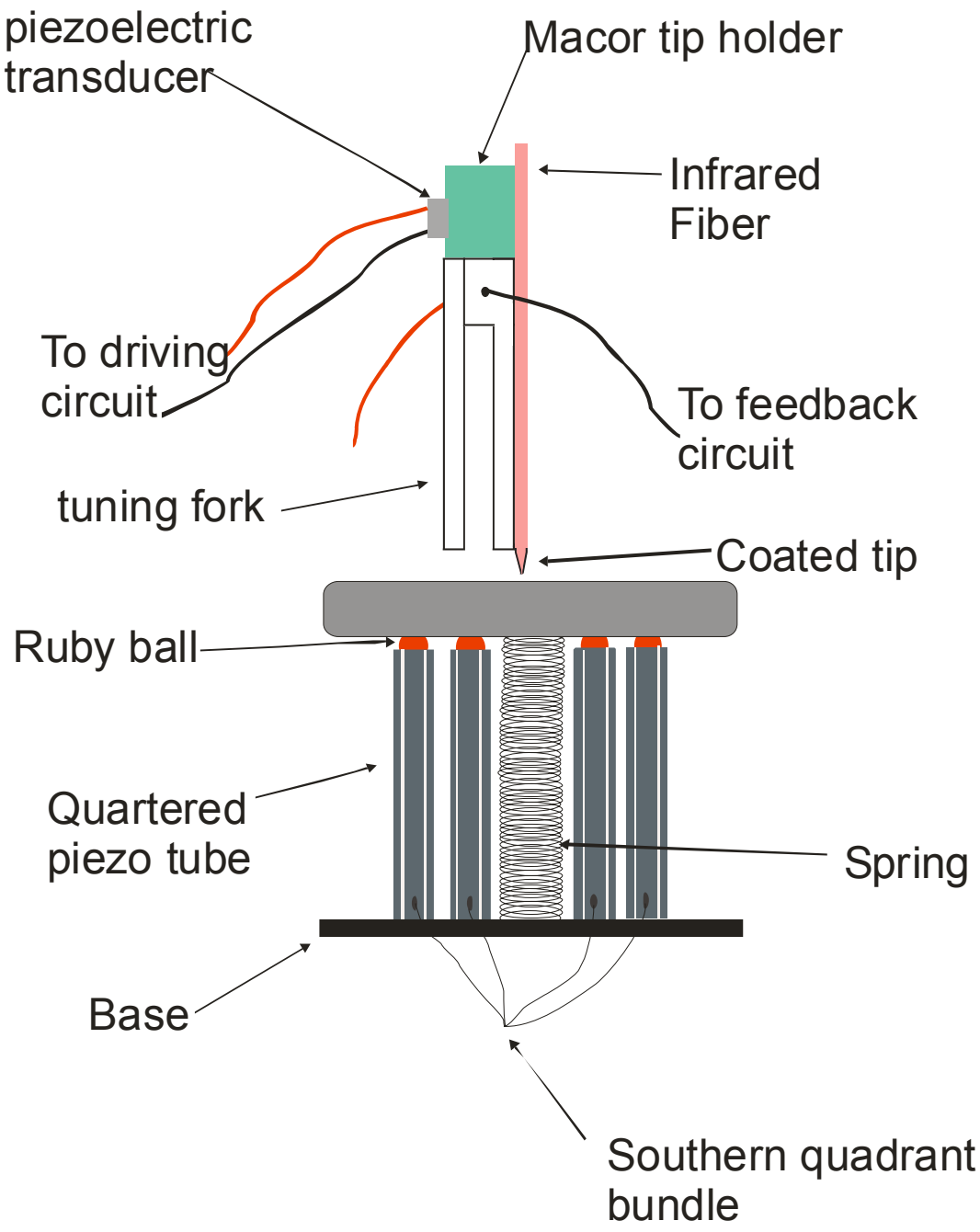

Figure 2.10: Schematic diagram of shear-force system.

a constant gap of approximately 10 – 20 nm above the surface. The controller signals the scanner to retract or extend its legs to maintain the constant gap.

The scanner is made from an aluminum base, to which four ceramic piezoelectric tube "legs" have been glued. The piezotubes, purchased from Boston Piezo-Optics Inc. are made of PZT-5H material, and coated with electroless nickel electrodes. The outside coating of the tubes is divided into four quadrants and the inside of the tube is negatively poled. Wires are soldered to each electrode and are collected into bundles of north-facing quadrants, southern quadrants, eastern quadrants, western quadrants and insides. These wire bundles are connected to the shear-force feedback loop and allow the scanner to scan in the xy-direction and maintain a constant gap in the z-direction. The scanner head rests on ruby spheres, which are placed on the tops of the piezo legs, to allow for smooth scanning.

The feedback loop must be set to a certain dithering amplitude in order to start the scan. First the tip is dithered while the tip is far from the surface of the sample. Then the sample is moved up towards the tip using a picomotor controller. This has remote operation capabilities so that it may be used while the system is under vacuum. Once the tip gets into the near-field range, the amplitude is damped. The amplitude is set to a value of approximately 70 percent of its free oscillation for the feedback loop. The picomotor contoller may also be used to make adjustments during a scan when the feedback loop cannot keep up with topographic changes due to limitations of the piezo tube scanner.

A sample with known features is imaged to test the performance of the scanner. The result is shown in Figure 2.11. The aluminum-on-glass sample was created with electron beam lithography and contains aligned lines, circles and triangles. The image taken with the home built scanner shows curved lines, indicating a hysteresis. The circles look flattened and are not as uniform as they should look. The outline of circle number 5, which is the roundest-looking of the features, is superimposed onto all the circles to clearly demonstrate the variety in the appearance of the shapes. This test indicates that topography measured with this apparatus should not be taken as absolute. A high performance, commercial scanner should be purchased for better analysis of sample topography. However, most of the experiments performed with this apparatus are done on simple, well known patterns. For example, chemically- amplified photoresists contain uniform stripes. Another point to consider is that most commercially available scanners can not be guaranteed for use in water vapor environments.

The shear forces that damp the tip dithering have been measured but are still not well understood.[1,19-23] Depending on several factors, the forces are comprised of some mixture of electrostatic, van der Waals, and capillary forces.[24,25] The environment surrounding the microscope, including the pressure, humidity and temperature, can affect the behavior of the shear-force feedback system. Experiments were performed in the bell jar apparatus to quantify and demonstrate the environmental influences.

Figure 2.12 shows two shear-force images of a patterned polymer photoresist. Figure 2.12a was measured in ambient conditions. Arrows point out horizontal lines,

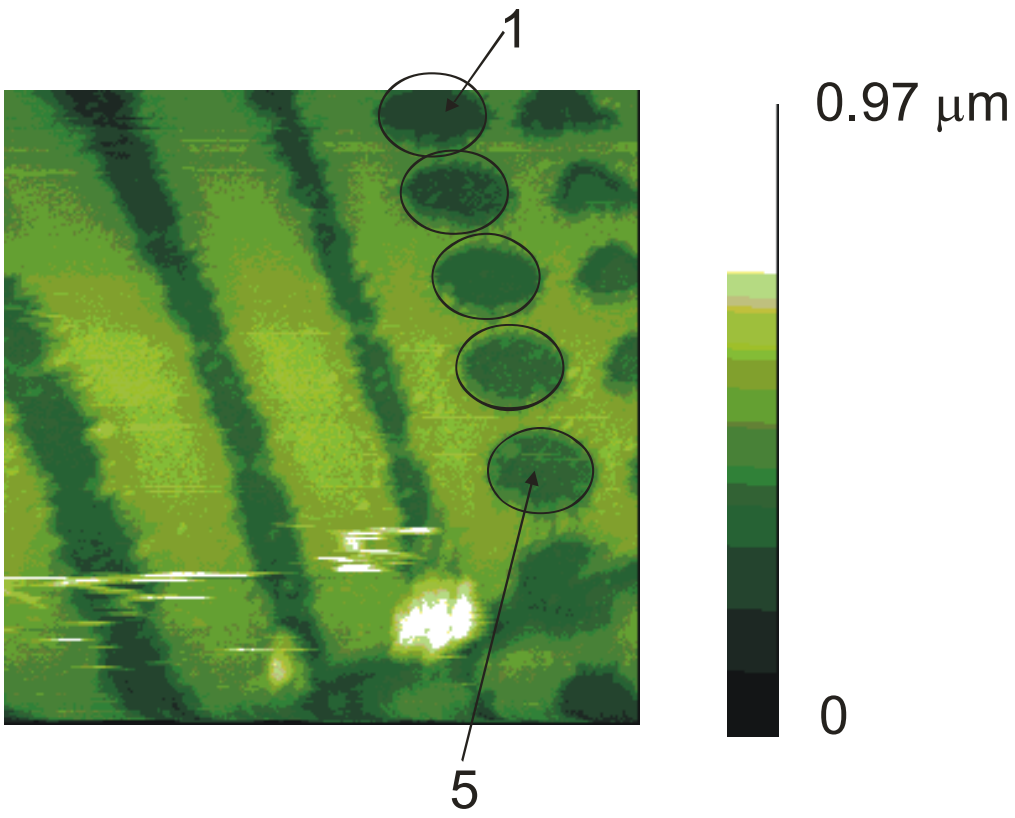

Figure 2.11: A 12 μm x 12 μm shear-force image of a patterned aluminum on gold sample. The outline of circle five is superimposed on all the circles to demonstrate the hysteresis of the scanner.

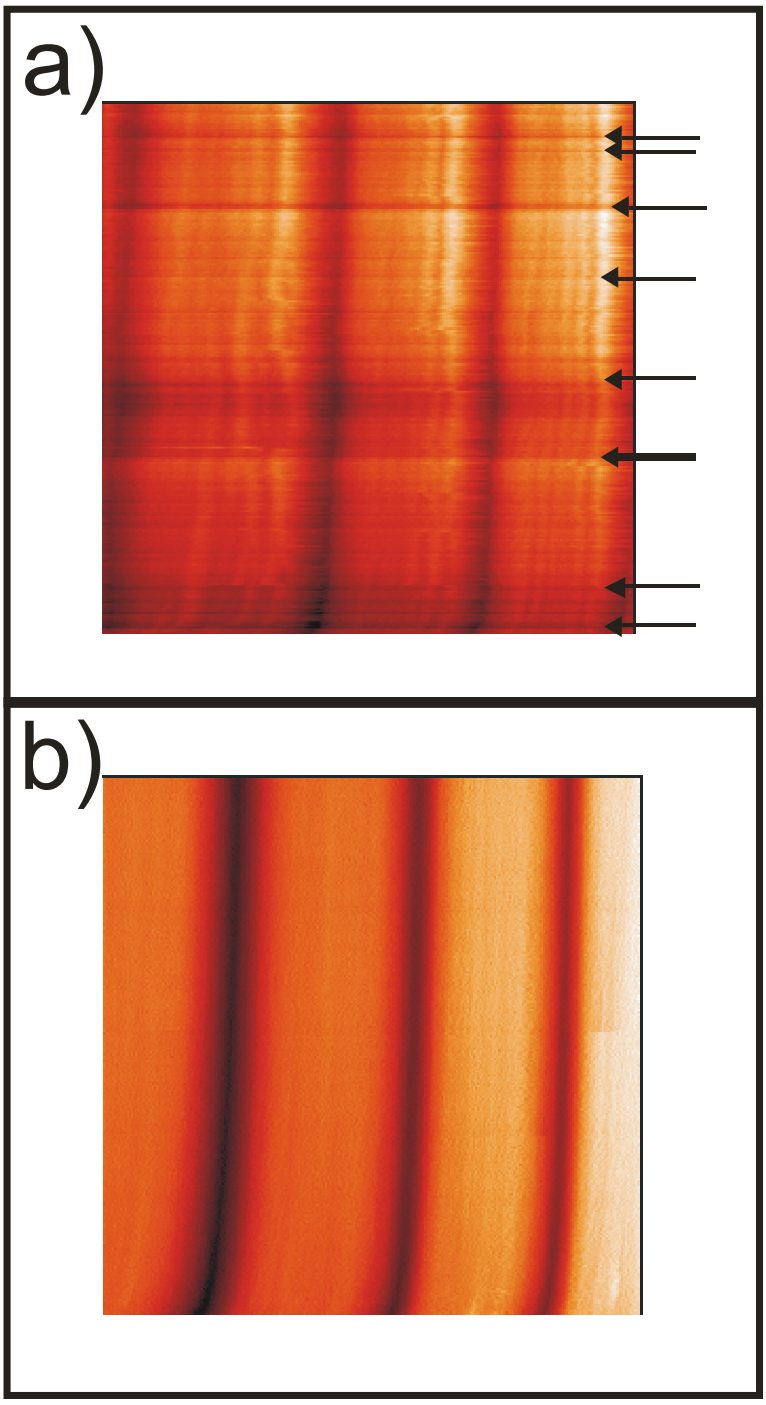

Figure 2.12: Shear force image of patterned polymer photoresist. a) image measured in ambient conditions. b) image measured in 10^{-1} Torr.

or "streaks," which are not part of the topography of the sample. These types of lines are often present in topography-type scanning probe microscope images, including shear-force and atomic force microscope (AFM) images. Figure 2.12b shows an image of the same sample, taken on roughly the same spot on the sample as Figure 2.12a, measured in the bell jar at a pressure of 10^{-1} Torr. This image does not show any of the streak artifacts present in the ambient measurement. This comparison of two images in different atmospheric conditions shows a common result.

Because the streaks are present in the ambient image but not the vacuum image, it is possible that they are caused by the thin water layer present on all surfaces. This water layer strongly affects the interaction between the tip and sample.[4,24,26,27] As the tip approaches the sample, not only is the damping perturbed, but a "liquid neck" can form.[26] The neck can be stretched as the tip and sample pull apart, and the neck can also break and re-form. The formation and/or breakage of the liquid neck is one possible cause of the streaks in the image.

Performing the imaging experiments in vacuum can provide an impressive improvement in the data quality. Not only are streaks eliminated, but higher spatial resolution can also be obtained.[23] The feedback system is also far more stable in vacuum when water is not present. Various experiments were performed to try to understand the instability that is introduced when water is present in the chamber.

The results of one such experiment are shown in Figure 2.13. The graph shows amplitude vs. frequency for the tuning fork with a tip mounted on the macor. Amplitude is measured by a FFT signal analyzer. The tip is far away from the sample surface, therefore, humidity effects are not a result of tip-sample interactions. The

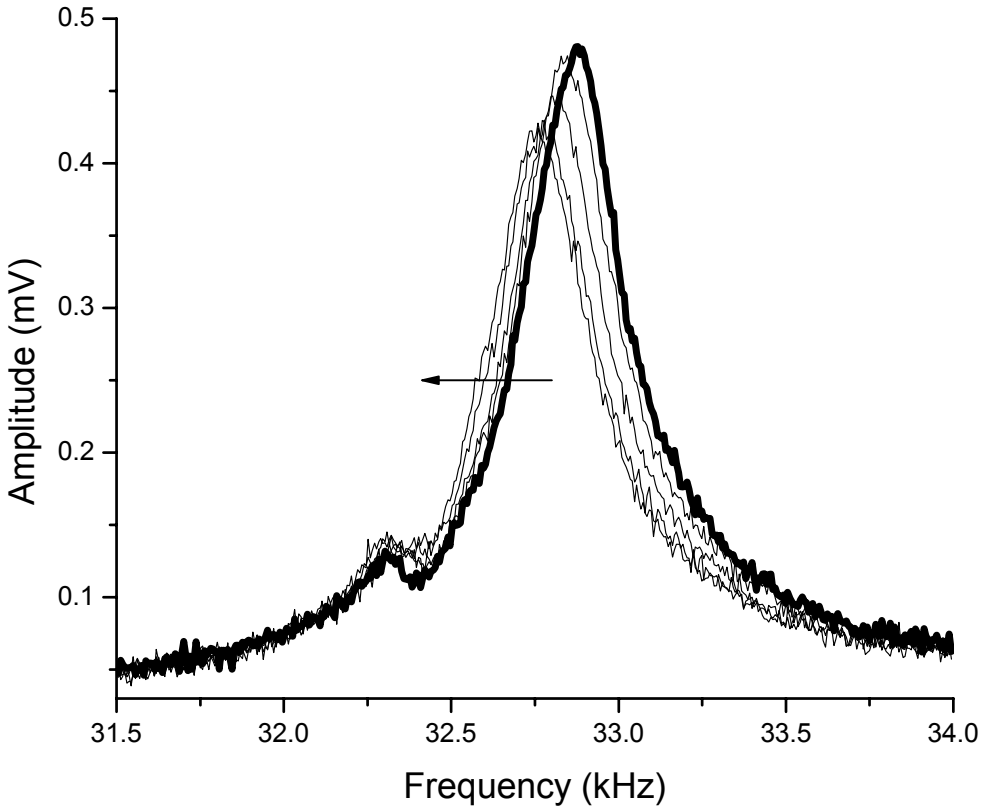

Figure 2.13: Frequency vs. amplitude for the tuning fork. The bold trace was measured in 250 mTorr. The thin traces were taken every 5 minutes after the addition of 18 Torr water vapor. The arrow points in direction of progressing time.

bold trace was measured at a vacuum pressure of 250 mTorr. The peak amplitude is found at 32.88 kHz, which is considered the resonant frequency of the fork. Water vapor was introduced into the chamber to a pressure of 18 Torr. New traces, taken every five minutes, are represented by the thin lines. The arrow points in the direction of passing time. As the system is exposed to humidity for a longer period of time, both the resonant frequency and the amplitude at the resonant frequency decrease.

The exact cause of this is unknown. One hypothesis is that a film of water on the tuning fork formed by condensation affects the resonance. However, the growth of such a film would be fast at these water vapor pressures, and the effect in question evolves over 20 minutes or more. Another theory is that the glue holding the tip on the macor holder absorbs water. Different types of glue were tried, but were either unsuccessful in remedying the problem or did not dry quickly enough to hold the fork in place. This change in resonance causes instability in the shear force measurements and makes it difficult to measure "real-time" topography changes induced by the introduction of water vapor.

An attempt to make a real time measurement of topography is shown in Figure 2.14. This experiment shows linescans, which are images created by a single line scanned back and forth repeatedly. The x axis represents distance, because the tip moves back and forth over the same 10 μm long line. The y axis represents time, so the image shows any changes that occur in the topography over the time it takes to record the data. The z axis, represented by the color bar to the right of the image, represents height. Figure 2.14a was recorded in the bell jar chamber at a vacuum

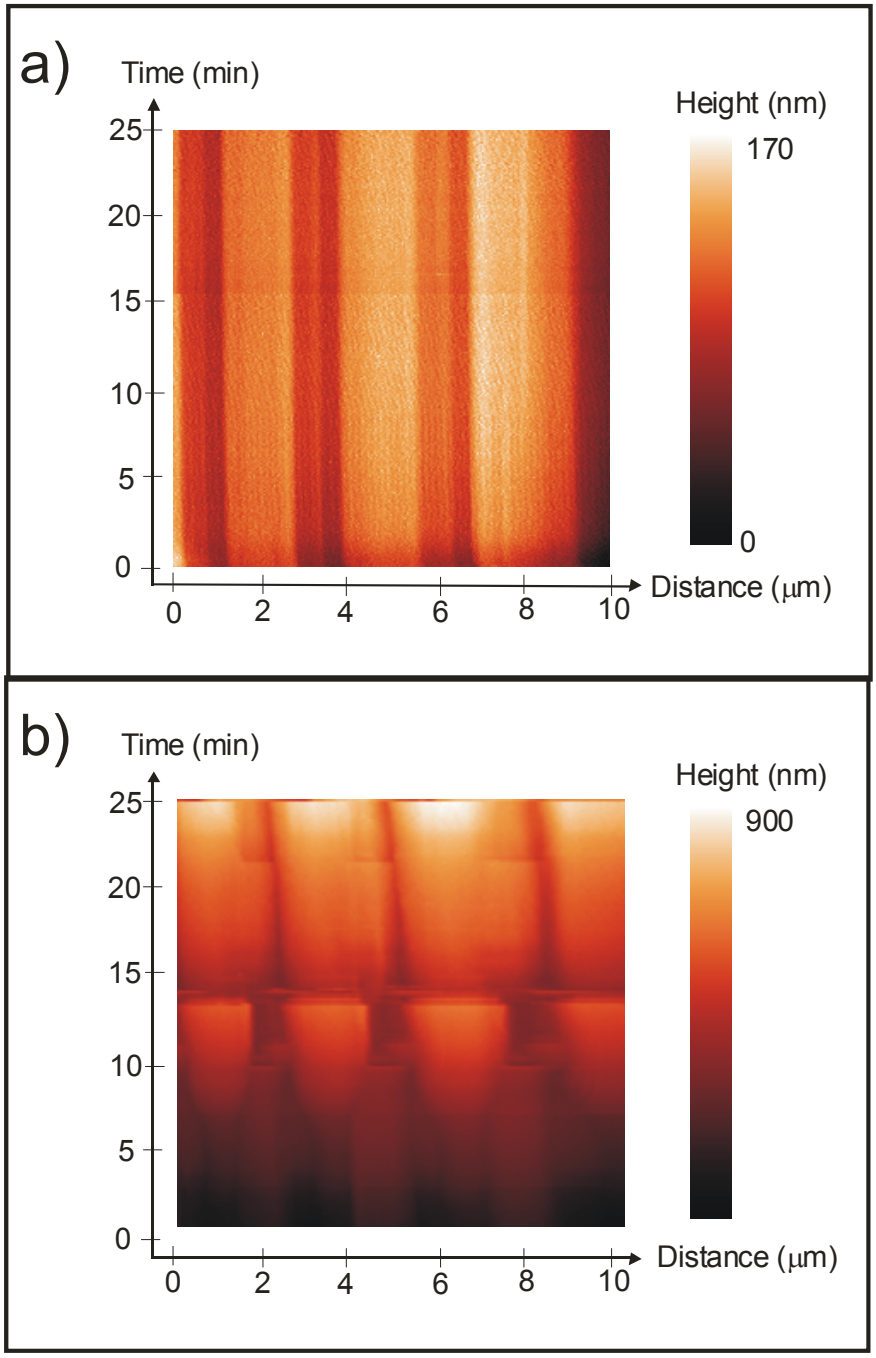

Figure 2.14: Linescans of polymer photoresist versus time. a) Linescan measured in bell jar chamber at a pressure of 200 mTorr. b) Linescan measured with 18 Torr water vapor introduced to chamber.

pressure of 200 mTorr. The sample studied is a patterned polymer photoresist. The darker areas represent a thinner polymer material which is hydrophilic. The lighter areas are made of a thicker, more hydrophobic material. There were no changes in the atmosphere, as the same pressure was held during the scan, and therefore no changes in the topography. As a result, the image looks uniform over time.

Figure 2.14b is a linescan measured in the belljar chamber after 18 Torr of water vapor is introduced and already allowed to equilibrate for 45 minutes. The equilibration is necessary to reliably set the initial tip-sample distance. Otherwise, the changes in tip behavior and topography are too rapid and great. The resonance and amplitude of the dithering are changing initially as shown in Figure 2.13, therefore the feedback loop is not reliable enough to measure topography. At the same time, the polymer is swelling. Both of these changes not only make measurements difficult, but can also cause the tip to be broken by contact with the sample. The equilibration period helps overcome these issues. Over the first five minutes it appears that the thinner, more hydrophilic polymer swells more than the thick polymer. Between five and 10 minutes it appears that the hydrophilic polymer swells even further, to the point that it is now the thicker polymer. From ten minutes on, it appears that this hydrophilic polymer is swelling in the x direction as well as the z direction. Around 14 minutes the piezotubes in the scanner reached their maximum retraction and needed to be re-set, causing a distruption in the image. The picomotor controller allowed for external control of the z-stage over distances not obtainable solely with the piezo-tube scanner.

Although it would be a very interesting result, to be able to watch a polymer swelling using a shear force microscope, it seems that this image may be due to artifacts. One reason being, at time zero the polymer looks very similar to the vacuum linescan shown in Figure 2.14a. Yet the sample had time to equilibrate after the introduction of water, so it seems unlikely that there would be almost no change for 45 minutes, and then it would undergo such a drastic change in 25 minutes.

The change in the appearance of the linescan in time could be due to ongoing changes in tip-sample interaction. The interaction distance between the tip and sample may be increased when the tip is positioned over a very wet surface. This effect may be exaggerated by the confined nature of the polymer pattern. More work is needed to understand the factors contributing to this result.

2.8 Visible NSOM

Images were first measured using a 690 nm visible laser diode in order to test and optimize the apparatus. Figure 2.15 shows examples of complementary topography and optical linescans of a one micron thick, uniform poly(methylmethacrylate) (PMMA) film. In order to create this image, a single line was scanned repeatedly in the x-direction. Therefore, the y-axis represents time. After the linescan is started the valve to the water was opened slightly and water was allowed in at a very slow rate, to a partial pressure of 10 Torr. This point is denoted in figure 2.15a by the line corresponding to "water in." After approximately 8 minutes the valve to the water vapor supply was closed and the chamber was opened

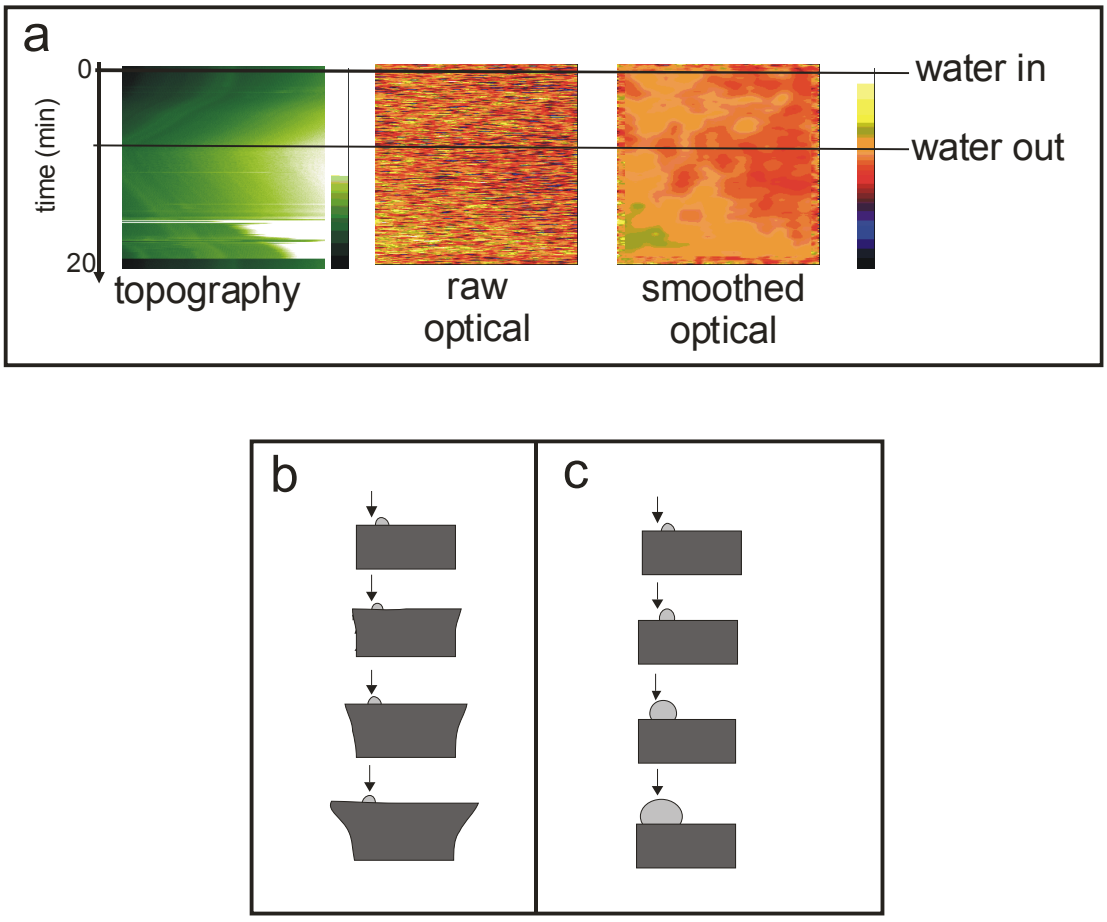

Figure 2.15: Characterization experiment with visible NSOM. a) Corresponding Topography and Optical transmission linescans. The microscope scanned in the x direction, the y direction shows time. b) Cartoon of swelling scenario where the polymer film swells vertically and horizontally to reveal a feature on the sample. c) Cartoon of swelling scenario where one feature on the film swells in all directions. Both b and c are possible explanations for the change in the linescan images shown in a.

to the vacuum pump. This point is denoted, "water out." The chamber pressure at the end of the scan was 0.8 Torr. Because of the very slow rate of water introduction and removal, it was possible to maintain the feedback loop. If the tip was about to crash in to the sample, it was possible to use the picomotor controller to adjust the distance further than the piezotube scanner could.

The topography image shows a change in the sample occurring with humidity. A feature appears to be growing in on the right side of the image, shown by the white color, which indicates an increase in height. There are at least two possible scenarios for this change, shown in figures 2.15b and 2.15c. Figure 2.15b shows the entire film swelling upward and outward. The feature being imaged, perhaps a grain of polymer, or even a grain of dust, is out of range at the beginning of the scan. The arrow in the figure points to the location of the tip as it scans. As the film swells laterally, the feature comes into view of the microscope. The tip starts to scan more and more of the feature with each line. When the water is removed, the process is reversed. Figure 2.15c shows a single feature on the sample swelling. The feature starts out of view of the microscope and a larger area of it gets scanned as it swells.

The corresponding transmission optical image is taken simultaneously with the topographic image. Water has a very small overtone absorption at 690nm, so the contrast could either be due to the presence of water or simply to a change in sample thickness, and therefore a change in transmission of light. It is very difficult to obtain any information from the raw optical image. However, with the imaging programs available, the data can be processed to help with the analysis. In this case, the optical image was smoothed by the adjacent averaging of the nearest 10 points. Now we can

see a darker area in transmission corresponding to the bright area in topography. Where the sample is thicker, less light is allowed through. Perhaps the more swollen area contains more water, and therefore allows less transmission of 690 nm light.

2.9 Conclusions

An IR-NSOM with environmental chamber has been achieved. The microscope incorporates a color-center laser, which has a narrow linewidth optimal for spectroscopic use. However, performance of the NSOM is limited by the low signal-to-noise ratio produced when a noisy laser is emitted from a tiny aperture. A ratio of at least 3 to 1 is necessary to obtain recognizable images; this is possible when all components of the NSOM system are optimized.

The laser light is coupled to an optical fiber with a tapered, coated tip. Fabrication of the tip is challenging, and special care must be taken not to break the tip during set-up of the experiment. It is estimated that only 1 in 10 tips produced is not broken during production.[30]

The tip-sample distance is regulated with a shear-force microscopy feedback loop. This is based on a home-built piezo tube scanner and is controlled by a commercial controller. It allows for the production of 3-dimensional images. The scanner has a hysteresis, therefore the topographic data must be used to recognize shapes and changes in shapes, but not to quantify an absolute measurement.

The microscope is incorporated into an environmental bell jar chamber. Images can be measured in vacuum, which improves their quality. Water vapor can be introduced to the experimental chamber. The water affects the shear-forces, and

care must be taken in analysis of these images. Due to the large volume of the bell jar, the vapor may be absorbed by the polymer faster than it fills the chamber, so adjustments are necessary for true kinetic studies.

Despite the challenges presented by IR-NSOM in an environmental chamber, it successfully produces images that provide information on the properties and functions of polymer samples. Chapter 3 provides a detailed account of experiments on water vapor uptake by chemically amplified photoresists.

References for Chapter II

(1) Dunn, R. C. *Chem. Rev.* **1999**, *99*, 2891.

(2) Dragnea, B.; Leone, S. R. *Int. Rev. Phys. Chem.* **2001**, *20*, 59.

(3) Hecht, B.; Sick, B.; Wild, U. P.; Deckert, V.; Zenobi, R.; Martin, O. J. F.; Pohl, D. W. *J. Chem. Phys* **2000**, *112*, 7761.

(4) Barbara, P. F.; Adams, D. M.; O'Connor, D. B. *Annu. Rev. Mater. Sci.* **1999**, *29*, 433.

(5) Synge, E. *Philos. Mag.* **1928**, *6*, 356.

(6) Ash, E. A.; Nicholls, G. *Nature* **1972**, *237*, 510.

(7) Durig, U.; Pohl, D. W.; Rohner, F. J. *J. Appl. Phys.* **1986**, *59*, 3318.

(8) Pohl, D. W.; Denk, W.; Lanz, M.; Rohner, F. J. *J. Appl. Phys.* **1984**, *44*, 651.

(9) Betzig, E.; Trautman, J. K.; Harris, T. D. *Science* **1991**, *251*, 1468.

(10) Isaacson, M.; Cline, J. A.; Barshatzky, H. *J. Vac. Sci. Technol. B* **1991**, *9*, 3103.

(11) van Hulst, N. F.; Veerman, J.-A.; Garcìa-Parajò, M. F.; Kulpers, L. K. *J. Chem. Phys* **2000**, *112*, 7799.

(12) Garcìa-Parajò, M. F.; Veerman, J.-A.; van Noort, S. J. T.; de Grooth, B. G.; van Hulst, N. F. *Bioimaging* **1998**, *6*, 43.

(13) Betzig, E.; Chichester, R. J. *Science* **1993**, *262*, 1422.

(14) Michaels, C. A.; Gu, X.; Chase, B.; Stranick, S. J. *Appl. Spectrosc.* **2004**, *58*, 257.

(15) Dragnea, B.; Preusser, J.; Schade, W.; Leone, S. R. *J. Appl. Phys.* **1999**, *86*, 2795.

(16) Keilmann, F. *Vibrational Spectroscopy* **2002**, *29*, 109.

(17) Schaller, R. D.; Johnson, J. C.; Wilson, K. R.; Lee, L. F.; Haber, L. H.; Saykally, R. J. *J. Phys. Chem. B* **2002**, *106*.

(18) Valaskovic, G. A.; Holton, M.; Morrison, G. H. *Applied Optics* **1995**, *34*, 1215.

(19) Karrai, K.; Grober, R. D. *Appl. Phys. Lett.* **1995**, *66*, 1842.

(20) Burns, A. R.; Carpick, R. W. *Appl. Phys. Lett.* **2001**, *78*, 317.

(21) Brunner, R.; Marti, O.; Hollricher, O. *J. Appl. Phys.* **1999**, *86*, 7100.

(22) Chuang, Y.-H.; Wang, C.-J.; Pan, C.-L. *Appl. Phys. Lett.* **1996**, *69*, 3312.

(23) Polonski, V. V.; Yamamoto, Y.; White, J. D.; Kourogi, M.; Ohtsu, M. *Jpn. J. Appl. Phys.* **1999**, *38*, L826.

(24) Davy, S.; Spajer, M.; Courjon, D. *Appl. Phys. Lett.* **1998**, *73*, 2594.

(25) Lapshin, D. A.; Letokhov, V. S.; Shubeita, G. T.; Sekatskii, S. K.; Dietler, G. *Ultramicroscopy* **2004**, *99*.

(26) Colchero, J.; Storch, A.; Luna, M.; Gòmez Herrero, J.; Barò, A. M. *Langmuir* **1998**, *14*, 2230.

(27) Wei, P. K.; Fann, W. S. *J. Appl. Phys.* **2000**, *87*, 2561.

(28) *CRC Handbook Of Chemistry and Physics*; 84 ed.; Lide, D. R., Ed.; CRC Press, 2003.

(29) Czaderna, A. W.; Thomas, T. M. *J. Vac. Sci. Technol. A* **1987**, *5*, 2412.

(30) Dragnea, B., personal communication.

Chapter III:

Water Vapor Uptake in Photolithographic Polymers Observed by Infrared Near-field Scanning Optical Microscopy in a Controlled Environment

3.1 Introduction

Transmission near-field scanning optical microscopy (NSOM) uses a sub-wavelength aperture probe that is scanned in close proximity to the surface of a sample to overcome the diffraction limit on spatial resolution. Infrared-NSOM (IR-NSOM) provides the possibility of vibrational spectroscopy and band specificity with this high spatial resolution. Although visible light is more frequently used with NSOM, IR-NSOM has been used to study systems from semiconductors to polymers to human cells.[1-11] This work further develops the IR-NSOM by integrating it into a controlled environment chamber so that samples can be explored in select vapor environments. Previous work with a visible NSOM in vacuum explored the effect of varying temperatures on semiconductor samples.[12,13] Now, additionally, samples can be exposed to various gases, and the changes they undergo can be monitored.[14]

An infrared NSOM has been developed in our group to study chemically amplified photoresists.[11] The method has been successful in probing the photoresists spatially and chemically. Chemical subgroup specificity allows for determining the locations of regions of various chemical compounds in polymer films with high spatial resolution. Figure 3.1 shows images of a patterned photoresist consisting of stripes of poly(t-butylmethacrylate) (PTBMA) and poly(methacrylic acid) (PMAA). Infrared optical transmission images were taken at 2 different wavelengths with a

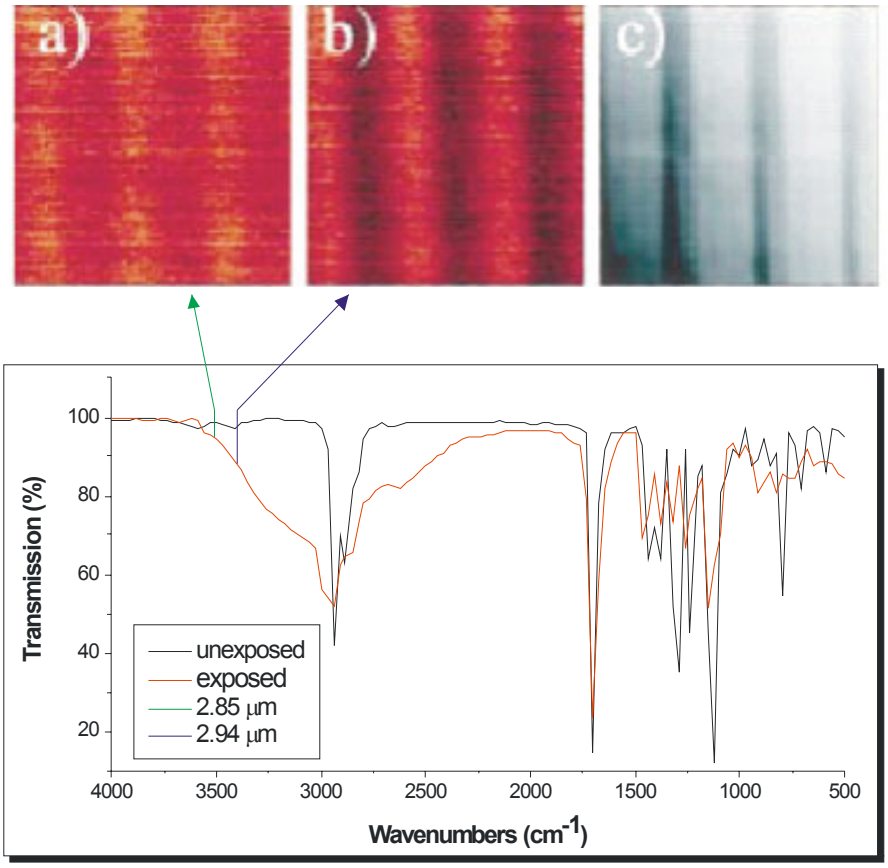

Figure 3.1: Infrared near-field and topographic images (upper panels, 12.5 μm x12.5 μm) of deep ultraviolet patterned and post-exposure baked poly(t-butylmethacrylate) (PTBMA), and corresponding spectral changes (lower panel) as acquired by an FTIR on non-patterned exposed and unexposed samples. The chemical specificity of the set-up is demonstrated by the difference in contrast when using (a) 2.85 μm wavelength or (b) 2.94 μm. Topographic changes visible in the shear-force image (c) occur due to shrinkage of the exposed areas of the film.

corresponding topographic image. The image in figure 3.1a[11] was measured at 2.85 μm, a wavelength at which there is very little absorption by either the modified or unmodified polymer. In a separate experiment, the image in figure 3.1b was measured at 2.94 μm. At this wavelength there is absorption by the exposed polymer, but not by the unexposed. Therefore, there is more contrast in figure 3.1b, indicating the differences in the exposed and unexposed regions of the photoresist. The change in contrast from one IR image to another (~2%) corresponds to the expected absorption contribution from the hydroxyl groups of PMAA. Refractive index contributions to the optical contrast are minimized with narrow field of view collection optics, but still produce a small effect. The success of this IR-NSOM led to the development of the microscope in an environmental chamber described in Chapter II.

Here we study how polymer samples react when exposed to water vapor. This topic has importance for many polymer industries, including packaging, chemical sensors, drug delivery, artificial organs, and electronics. It is particularly important in patterned chemically amplified photoresists, which are used in the fabrication of micro and nanocircuits in the electronics industry.[15,16] Many polymers swell and change shape when they absorb enough water vapor. The degree of vapor uptake and swelling depends on factors such as film processing and quality, polymer composition and density, molecular orientation of the chains, size and density of pores, and film thickness.[17-21] Because photochemically modified areas have a different affinity for water than the unexposed areas, swelling of the polymer can cause distortions of

patterns. This can lead to problems with reproducibility and transfer of the desired mask for subsequent etching.

Until now, some of the better methods used to study vapor uptake in polymer films were Fourier transform infrared spectroscopy[17,22-24] and gravimetric analysis.[18-21] However, these methods do not provide the spatial resolution that IR-NSOM can; 300 nm spatial resolution has been achieved with transmission IR-NSOM at a wavelength of 3 μm.[9-11] This paper describes the results of an IR-NSOM implemented in a controlled environment chamber to measure vapor uptake and swelling in polymers on a small spatial scale.

3.2 Experimental Materials

Samples used are patterned, acid catalyzed, photolithographic polymers similar to those studied by Dragnea et al.[9-11] A 1.0 μm thick poly(t-butylmethacrylate) (PTBMA) film containing the photoacid generator triphenylsulfonium hexafluoroantimonate was covered by a quartz/chrome mask and exposed to UV light in the range of 200-300 nm. The film was then baked at 130 °C for 5 minutes to activate the acid-catalyzed thermal deprotection chemistry. In the post-exposure bake, the ester groups are converted to a hydrogen bonded carboxylic acid, poly(methacrylic acid) (PMAA), and the volatile product isobutylene is produced, thus shrinking the film substantially in the UV exposed regions. The resulting pattern used here has alternating 2 μm wide lines of approximately 1 μm thick PTBMA and 0.5 μm thick PMAA.

3.3 Experimental Apparatus

The infrared microscope is a variant based on the IR-NSOM apparatus developed by Dragnea et al.[9-11] It is described in detail in Chapter II. A schematic diagram of the set-up is shown in Figure 2.1. The NSOM was built inside a bell jar environmental chamber capable of obtaining pressures down to 0.10 Torr. A Kr^+ laser pumps a color-center laser, giving 2.6-3.2 μm infrared light, which is absorbed by the O-H stretching vibration of water vapor. For experiments described here, the laser was tuned to a wavelength of 2.85 μm. Figure 3.2 shows that this is a wavelength at which there is low absorption by either the exposed (PMAA) or unexposed (PTBMA) polymer. There should be very little contrast due to the difference in absorbance by these two polymers in the infrared images. However, water is strongly absorbed at 2.85 μm. Therefore, contrast in the optical transmission image can be used to determine regions of the polymer sample with greater amounts of sorbed water. A "map" of the water sorption can be created.

The beam of infrared light enters the bell jar through a CaF_2 window in the chamber's base plate. The light is coupled into an infrared fiber composed of zirconium aluminum fluoride, which is transparent from 0.45 – 5.0 μm. The fiber is pulled into a tip at one end using a variable-pulling method.[9,10] The tip is coated with aluminum, typically leaving a 200 nm aperture. Due to the brittleness of the material, some of the tips used in this work may have fractured to sizes larger than 200 nm. The tip is suspended above the sample, which sits on an x-y scanning stage moved by three piezoceramic tube legs. Directly below the sample is a large area, room

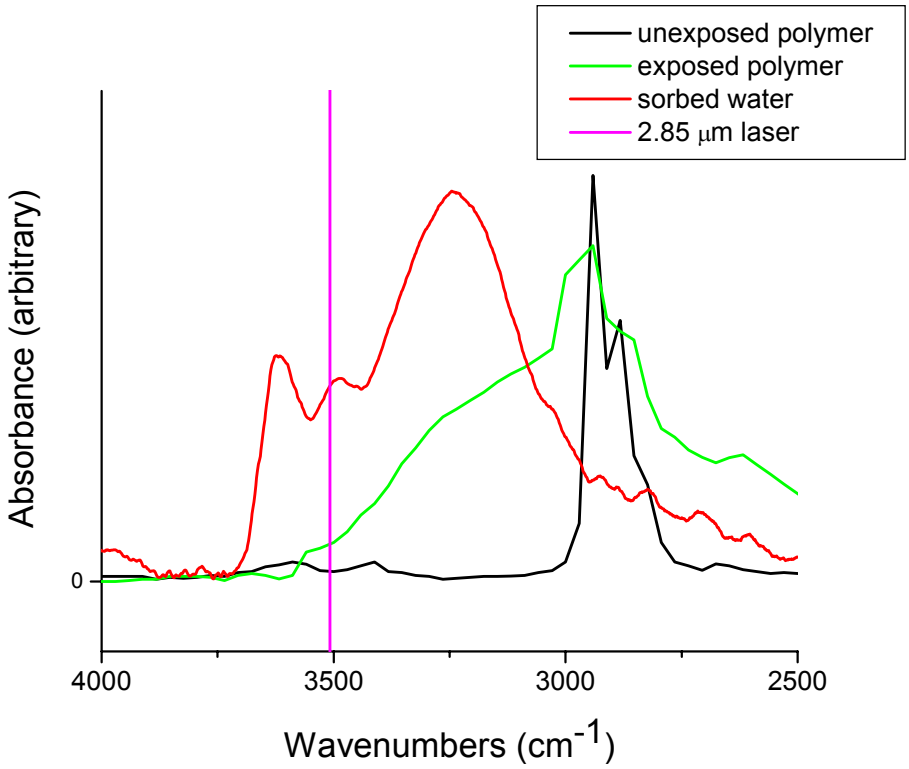

Figure 3.2: FTIR spectra of unexposed polymer (black), exposed polymer (green), water absorbed by the exposed polymer (red); and a line denoting the wavenumber to which the FCL laser is tuned for the IR-NSOM experiement.

temperature, PbS detector, which measures the transmission of the infrared light. The fiber tip is glued to a small tuning fork, which allows the topography to be measured via the shear-force feedback method.[25] The scanning and data acquisition are controlled by a scanning probe microscope controller.

All the necessary alignment procedures are carried out before the chamber is evacuated. The IR beam is coupled into the fiber and the tip is positioned above the sample in the near-field. Once the alignment is established, the glass bell-jar is placed on the base plate and the chamber is pumped down. A picomotor screw allows for external control of the tip-sample distance in the z direction when the NSOM is enclosed. Up to 18 Torr of water vapor can be introduced to the chamber and is allowed to equilibrate for at least 45 minutes before a scan begins. In future work, real time measurements of uptake may be possible. Evident problems are the need to follow the changes in distances due to the polymer swelling and to adjust for changes in shear force feedback signals due to the water vapor environment.

3.4 Experimental Procedures

Images shown here are produced by scanning a line 256 times in the x direction, while disabling the scanning in the y direction. Each line scan also consists of 256 points. The transmission of light through the sample and the height of the tip above the sample are simultaneously recorded. The lines can be averaged and plotted to obtain a profile of the topography and transmission of the sample. The averaging produces an improvement in the signal-to-noise ratio. This work shows two sets of

measurements that compare the topography and optical properties of the sample in vacuum conditions and in a water vapor environment.

3.5 Two Micron Features

Topographic images of the sample are shown in Figure 3.3. Figure 3.3a was recorded in a vacuum of 0.10 Torr pressure, while Figure 3.3b was measured in 16 Torr water vapor. Their average line profiles are plotted together in Figure 3.4a to show that when exposed to a water vapor environment the gap between the highest point in the topography image and the lowest point is diminished. Figure 3.4a shows that the depth of the topographical valley is 0.4 μm in vacuum; however, it is actually deeper. Because the fiber tip is too wide, the tip cannot reach the bottom of the valley. Therefore, it cannot produce an accurately scaled topographic image. We know from atomic force microscopy (AFM) experiments done on the sample that the valley is actually 0.5 μm deep. Note also that the region containing PTBMA, the thicker polymer, is not flat. This structure is discussed in detail in previous work,[11] and it may be due to some combination of UV irradiation, edge enhancement and shrinkage. A schematic diagram of how the tip might follow the sample's topography is shown in Figure 3.4b.

Figure 3.4a shows that the depth of the valley for the sample exposed to water vapor is only 220 nm. This indicates that the PMAA swells 280 nm more than PTBMA when exposed to 16 Torr water vapor. It is possible that the PTBMA also swells slightly, but we can only measure the relative change. The measured swelling suggests that the PMAA has absorbed more water than the PTBMA.

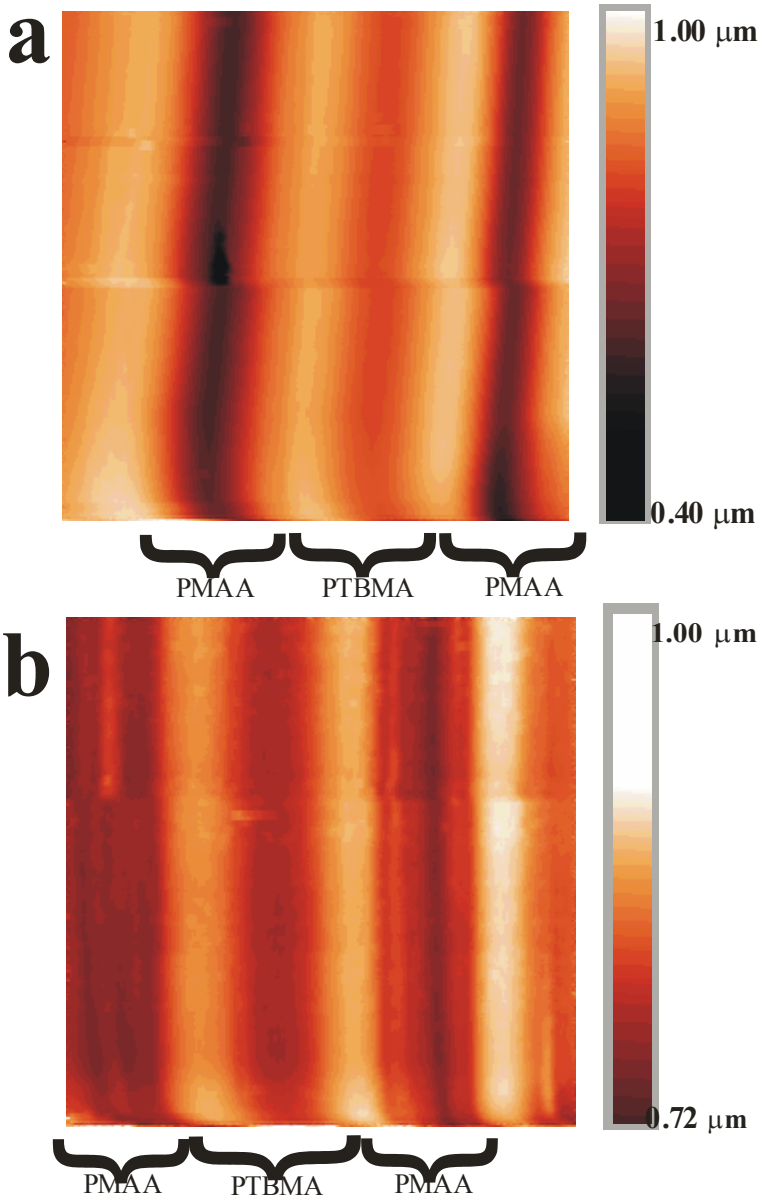

Figure 3.3: Topographic images of photolithographic polymers with 2 μm wide lines. Each image represents a single line scanned 256 times. (a) Topographic linescan of sample in vacuum. (b) Topographic linescan of sample in 16 Torr water vapor environment.

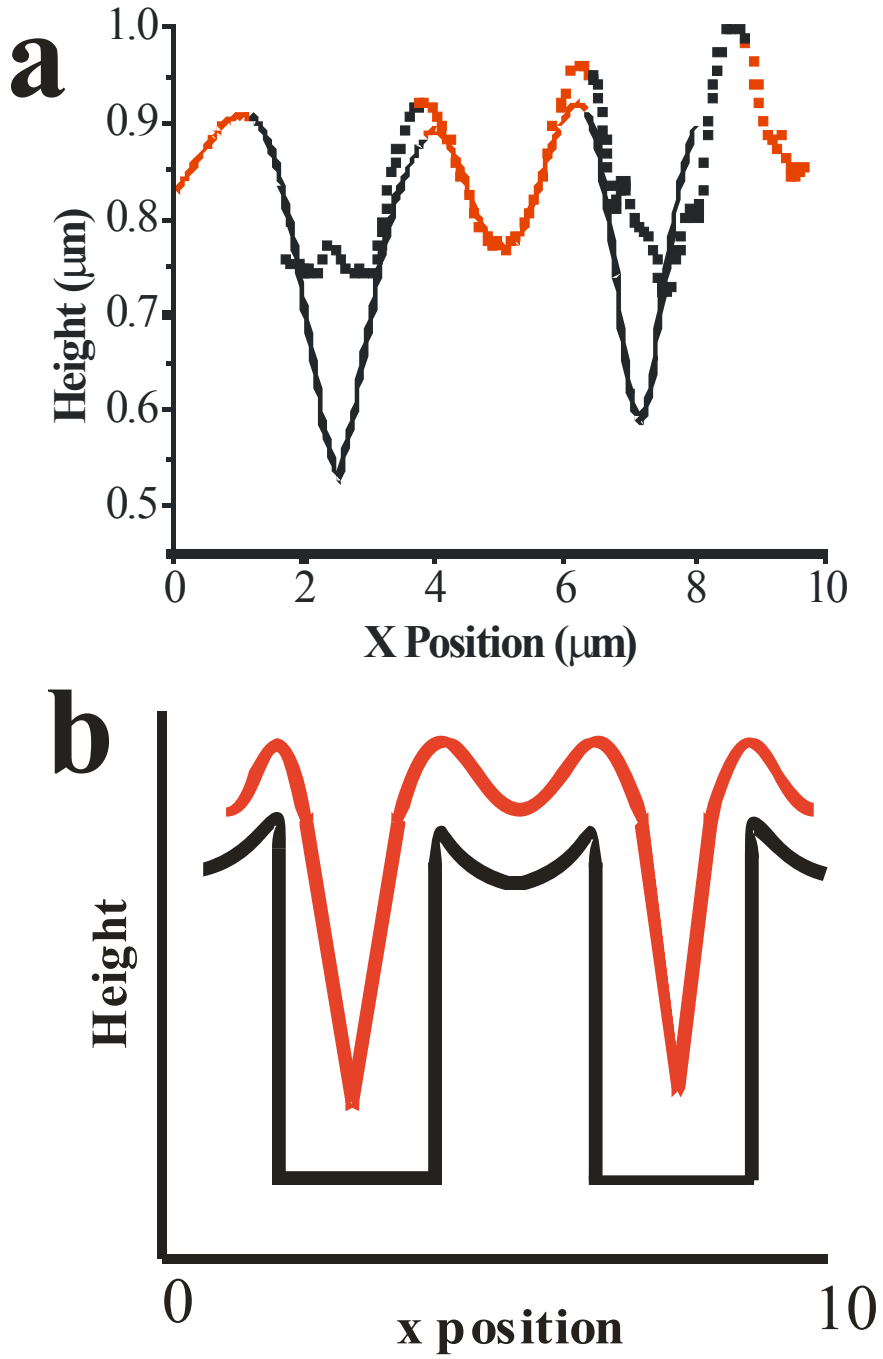

Figure 3.4: (a) Average line profiles. The solid line is an average profile of Figure 3.3a and the dashed line is an average profile of Figure 3.3b. The red line portions represent PTBMA and the black lines represent PMAA. (b) A schematic drawing of the tip following the sample surface. The black line is a profile of the sample's topography, and the red line shows how the tip follows that surface to produce the topography image.

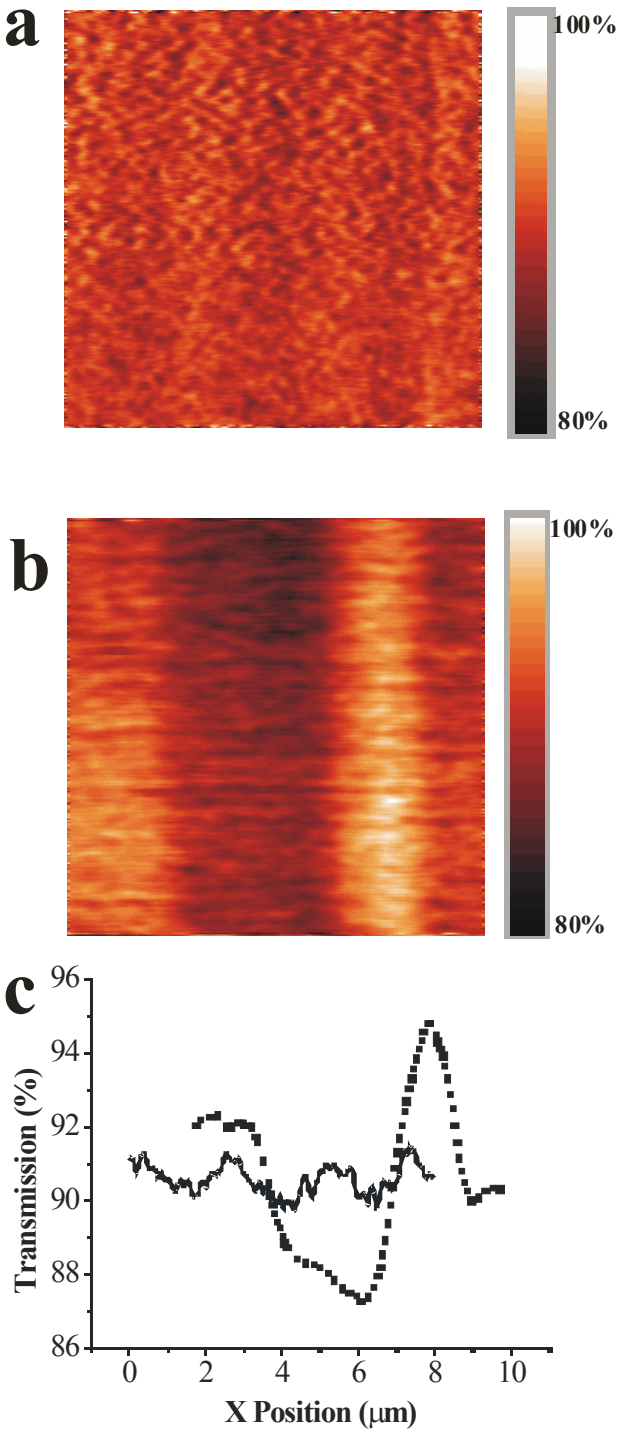

Figure 3.5: Transmission images of 2.85 μm light through photolithographic polymers with 2 μm wide lines. Each image represents a single line scanned 256 times. (a) Transmission linescan recorded in vacuum conditions. Darker regions represent smaller transmission intensity. (b) Transmission linescan recorded in 16 Torr water vapor environment. (c) Average line profiles of parts a and b. The solid line represents the average of the image in part a, the dashed line represents the average of b.

Figures 3.5a and 3.5b show the infrared transmission images recorded simultaneously with the topography images in Figures 3.3a and 3.3b, respectively. Figure 3.5a, recorded under vacuum conditions, shows an image that is almost completely featureless, while Figure 3.5b shows large oscillations in the intensity of light reaching the detector. The reason is that one polymer absorbs more water than the other, thus allowing through less light. Again, the lines were averaged and profiles of these images are plotted in Figure 3.5c. This graph shows a 6 ± 1% difference between the greatest and the smallest detected intensities. This number was obtained by taking the average of the two local maxima, subtracting the average of the two local minima, then computing error bars using their standard deviations. It is obvious that this contrast is not due to a topographic artifact, since the transmission contrast increases while the topographic contrast decreases. However, the difference is not pure absorption contrast. There are several other contributing factors, which are discussed below.

The modified and unmodified polymers have different indices of refraction. This effect is explained by Dragnea et al.[9] as a change in cone angle of detection for our particular set-up, and it is expected to produce a variation of 0.5%. It is this effect that causes a slight oscillation of the transmission signal in the vacuum case. Another contrast mechanism can be the change in index of refraction with concentration of water. During vapor uptake, a polymer's index will first increase as void-spaces are filled, and then the index can decrease as the film swells.[26] The changes in index of refraction will cause a further change in the amount of light transmitted to the PbS

detector. Depending on the concentration of water in the film, this process can either enhance or diminish the transmission contrast.

Figure 3.6 shows an experiment which was carried out in order to demonstrate this process. A broken tip with an aperture on the order of a few microns is suspended over the sample at a distance which is out of range of the near-field. Therefore, the size of the spot of light that hits the sample is fairly large. The light travels through both modified and unmodified regions of the photoresist before reaching the PbS detector. Under vacuum, the transmission of light through the sample is around 63-64%. Water is slowly introduced into the chamber. At first, this causes an increase in the transmission of infrared light into the sample. This is the opposite of what would normally be expected, because water absorbs infrared light. The result can be explained by index of refraction changes. The introduction of the water causes the void-spaces in the polymer to be filled, and the polymer's index of refraction increases. This causes light to be bent in a different manner as it travels through the sample, and less if reflected off of the interfaces. Therefore, more light arrives at the detector. As more water is added to the chamber, and thus to the polymer, the film swells and causes a decrease in the index of refraction. Now the light rays are bent in such a way that more is reflected at the interfaces. Coupled with the increase in absorption of infrared light by the water, the effect results in a decrease of transmission of infrared light to the detector.

The OH stretching band of water can also change shape depending on the concentration of water. Several examples are cited in the literature.[22-24] Therefore, an increase in transmission at one laser wavelength does not always correlate linearly to

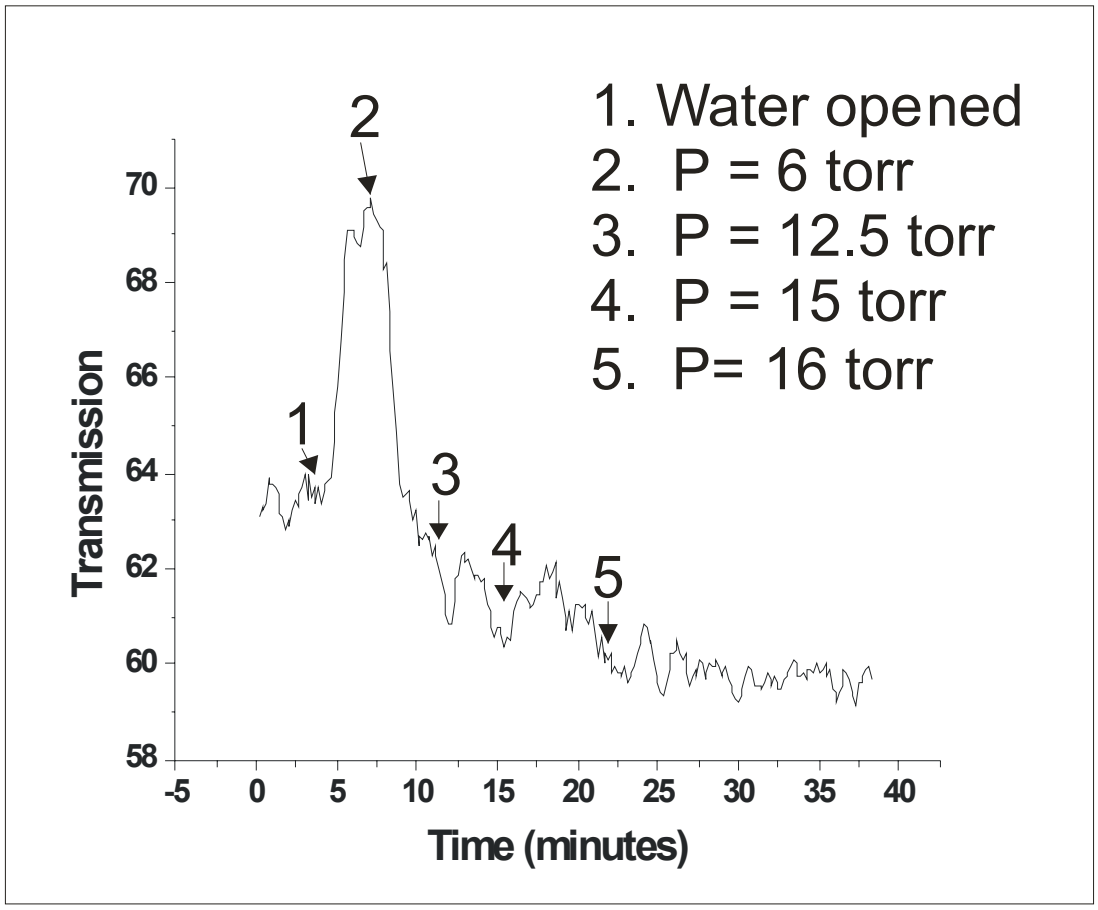

Figure 3.6: Transmission of 2.85 μm laser light through a polymer photoresist sample. The laser is emitting from a large aperture fiber tip and is far from the sample, therefore a large spot size of light hits the sample. A valve is opened slightly to introduce water at a time indicated by the number 1. The partial pressure of water rises slowly and is indicated on the graph until it reaches a pressure of 16 Torr and remains constant.

the amount of water present. This topic will be explored further in Chapter V. In addition, the absorption of light by the gas phase water vapor in the controlled environment chamber will create a baseline that must be subtracted.

Another factor that could decrease the transmission contrast is the size of the NSOM aperture tip. When the tip's aperture is broken or too large, the transmission contrast is not as sharp or as great as it should be.

All of these factors combined make it difficult to determine the concentration of water in the film. In the future, experiments with a quartz crystal microbalance will be performed simultaneously to quantitatively correlate the water concentration in the NSOM signals by more traditional gravimetric methods. Also, use of a tunable laser source with a wider range of available wavelengths will make more experiments accessible. For example, if an image was recorded using a laser tuned to 3750 cm^{-1}, a measurement could be taken that has no contrast contributions from either the OH stretch of the modified polymer or the water. (see Figure 3.2) The percent contrast found in such an image could be subtracted from the contrast in an image measured at 3500 cm^{-1} to minimize index of refraction effects. FTIR experiments should also be carried out to investigate band shifts and give access to information on water molecule interactions.

Optical and topographic images should be spatially consistent. The area that transmits less light should correspond to the region that swells more, because these are the regions with a greater amount of water present. However, in these particular experiments, the optical images are shifted by 2 microns from the topographic images. This is shown in figure 3.7. This is clearly an artifact because similar

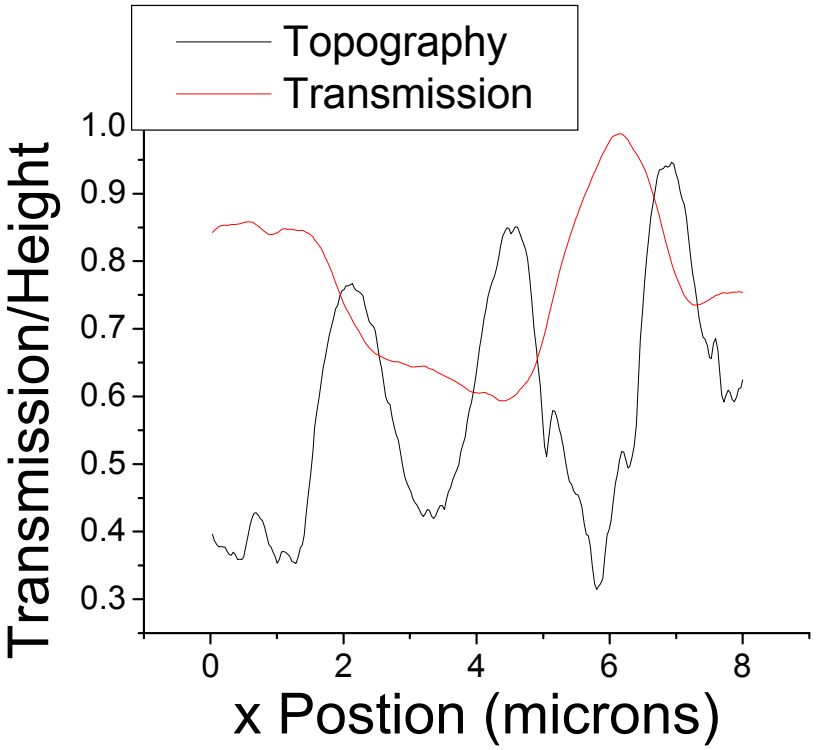

Figure 3.7: Corresponding topography and transmission linescans in a 16 Torr water vapor environment. The topography line (black) is the same as the dotted line shown in Figure 3.4a. The transmission line (red) is the same as the dotted line in Figure 3.5c.

experiments on samples with 4 micron thick lines were also shifted by 2 microns. We do not know why the optical images were shifted but hypothesize that it may be image displacement due to the relatively large probe used. The point on the tip that is interacting with the sample to form the shear force image may be different from the optically transparent region for the transmission intensity. For example, a sharp grain of aluminum coating can protrude from the side of the tip and interact with the sample to form the topographic image, while light emerges from the center of the tip to form the optical image. Future work will correlate the transmission zones with the topographic images more rigorously.

3.6 Four Micron Features

Figure 3.8 shows an example of average linescans on four micron features. The same procedure is carried out as for the above two micron features, but a different area of the sample was probed where four micron features are present. The fiber tip used for these experiments is different from the one used in the previous experiments. This new fiber tip made it possible to better correlate the transmission and topography images. They match up well, with the topographic valleys (PMAA regions) overlapping the areas with lower transmission. This image was measured in an atmosphere of 18 Torr water vapor. The water, which is present in a higher concentration in the PMAA, absorbs the infrared light and decreases the transmission.

The measurements were repeated several times in various environments. The results are summarized in table 3.1. For each environment, we report the depth of the valley (Δ H) and the transmission contrast (Δ T). In an 18 Torr water vapor

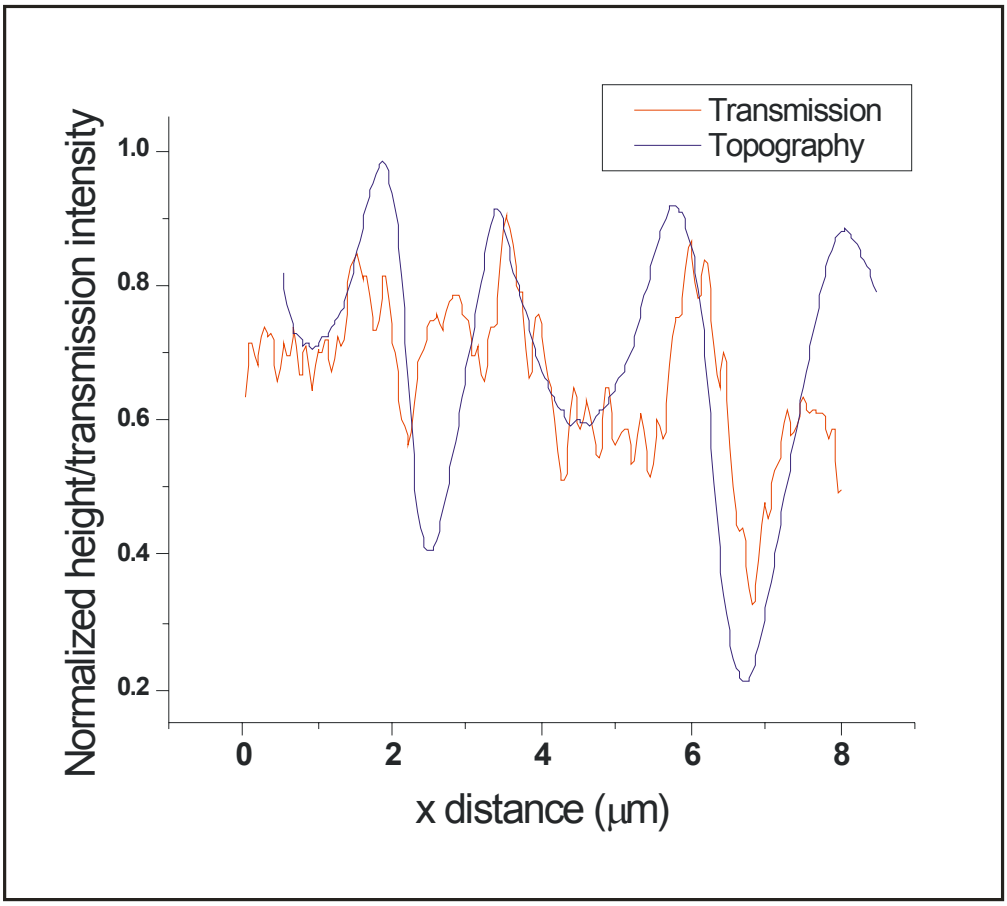

Figure 3.8: Average linescans in transmission and topography for 4 micron features of a polymer photoresist in 18 Torr water vapor.

environment, the PMAA swells 0.20 ± 0.09 microns more than the PTBMA. The error bars were determined by multiple runs with the same tip. This matches well with the result of 0.28 microns swelling found on the 2 micron feature experiments in the above section.

Table 3.1: Height and Transmission data in various experimental conditions

Environment	Δ H (μm)	Δ T (%)
Vacuum (0.20 Torr)	0.56 ± 0.05	0.35% ± 0.02 %
10 Torr Water Vapor	-	0.40% ± 0.02%
18 Torr Water Vapor	0.36 ± 0.04	0.45% ± 0.02%

The change in transmission shows that there is a 0.10% difference in transmission contrast in going from a dry to a water vapor environment. This result is quite different from the result on two micron images, which was 6 ± 1 %. The difference could be due to differences in the tip used and its aperture. The aperture on the tip used for these experiments could be larger in size, or even slightly broken, thus reducing the contrast. This result highlights the need for consistent tips in order to make comparisons between experiments.

On the positive side, the result also shows the sensitivity of the IR-NSOM. It was able to determine a range of transmission contrast for three different environments (vacuum, 10 Torr, 18 Torr).

3.7 Conclusions

In order to increase the quality of the images and the information obtained from the IR-NSOM described here, several changes to the experimental set-up are required. First, detection should be improved by replacing the large area, room temperature PbS detector with a liquid nitrogen cooled, small area, photovoltaic InSb detector.[10] Use of varying numerical aperture collection optics would assist in reducing the contrast due to the cone angle effect.[9] Efforts can also be made to facilitate real-time measurements of vapor uptake. One way to achieve this would be to operate in constant height mode, rather than constant gap mode, so that the probe would not interact with the sample. It will also help to determine the source of the changes in the shear-force feedback signals with change in water vapor pressure. Perhaps the use of a non-absorptive glue to stick the fiber on the tuning fork will solve this problem and allow for time-resolved measurements.

This work demonstrates a new method for exploring the vapor uptake of polymers. The shear-force topographic method produces a value for the swelling of a polymer in a vapor environment and, with calibration of a known system, can become a precise measure of the amount of water absorbed in the sample. The transmission data complements the topographic images, and the results can be used to quantify the amount of water in a sample if more work is completed to separate the various contributing effects. Infrared NSOM under environmental control is an excellent potential new tool for determining where water vapor uptake occurs in a polymer sample on a small spatial scale.

References for Chapter III

(1) Dragnea, B.; Leone, S. R. *Int. Rev. Phys. Chem.* **2001**, *20*, 59.

(2) Schaller, R. D.; Saykally, R. J. *Langmuir* **2001**, *17*, 2055.

(3) Stranick, S. J.; Chase, B.; Michaels, C. A. *Abstracts of ACS* **2001**, *221*, 173.

(4) Cricenti, A. *J. Alloys Cmpds* **2001**, *328*, 2.

(5) Hong, M. K.; Jeung, A. G.; Dokholyan, N. V.; Smith, T. I.; Schwettman, H. A.; Huie, P.; Erramilli, S. *Nuc. Inst. Mths. Phys. Res.* **1998**, *144*, 246.

(6) Knoll, B.; Keilmann, F. *Appl. Phys. A* **1998**, *66*, 477.

(7) Sahlin, J. J.; Peppas, N. A. *J. Appl. Polym. Sci.* **1997**, *63*, 103.

(8) La Rosa, A. H.; Yakobson, B. I.; Hallen, H. D. *Appl. Phys. Lett.* **1997**, *70*, 1656.

(9) Dragnea, B.; Preusser, J.; Schade, W.; Leone, S. R.; Hinsberg, W. D. *J. Appl. Phys.* **1999**, *86*, 2795.

(10) Dragnea, B.; Preusser, J.; Szarko, J. M.; Leone, S. R.; Hinsberg, W. *J. Vac. Sci. Technol. B* **2001**, *19*, 142.

(11) Dragnea, B.; Preusser, J.; Szarko, J. M.; McDonough, L. A.; Leone, S. R.; Hinsberg, W. *Appl. Surf. Sci.* **2001**, *175-176*, 783.

(12) Gray, M. H.; Hsu, J. W. P. *Rev. Sci. Inst.* **1999**, *70*, 3355.

(13) Gray, M. H.; Hsu, J. W. P. *Appl. Phys. Lett.* **2000**, *76*, 1294.

(14) Elbs, H.; Fukunaga, K.; Stadler, R.; Sauer, G.; Magerle, R.; Krausch, G. *Macromolecules* **1999**, *32*, 1204.

(15) Padmanaban, M.; Endo, H.; Inoguchi, Y.; Kinoshita, Y.; Kudo, T.; Masuda, S.; Nakajima, Y.; Pawlowski, G. *Proc. SPIE* **1992**, *1672*, 141.

(16) MacDonald, S. A.; Cleacak, N. J.; Wendt, H. R.; Willson, C. G.; Snyder, C. D.; Knors, C. J.; Deyoe, N. B.; Maltabes, J. G.; Morrow, J. R.; McGuire, A. E.; Holmes, S. J. *Proc. SPIE* **1991**, *1466*, 2.

(17) Sutandar, P.; Ahn, D. J.; Franses, E. I. *Macromolecules* **1994**, *27*, 7316.

(18) Buchold, R.; Nakladal, A.; Gerlach, G.; Herold, M.; Gauglitz, G.; Sahre, K.; Eichhorn, K. J. *Thin Solid Films* **1999**, *350*, 178.

(19) Chen, W. L.; Shull, K. R.; Papatheodorou, T.; Styrkas, D. A.; Keddi, J. L. *Macromolecules* **1999**, *32*, 136.

(20) Hutcheon, G. A.; Messiou, C.; Wyre, R. M.; Davies, M. C.; Downes, S. *Biomaterials* **2001**, *22*, 667.

(21) Neogi, P. *Diffusion in Polymers*; Marcel Dekker, Inc.: New York, 1996.

(22) Ping, Z. H.; Nguyen, Q. T.; Chen, S. M.; Zhou, J. Q.; D., D. Y. *Polymer* **2001**, *42*, 8461.

(23) Yarwood, J.; Sammon, C.; Mura, C.; Pereira, M. *J. Mol. Liq.* **1999**, *80*, 93.

(24) Linossier, I.; Gaillard, F.; Romand, M.; Feller, J. F.; Sci., J. A. P. *J. Appl. Polym. Sci.* **1997**, *66*, 2465.

(25) Karrai, K.; Grober, R. D. *Appl. Phys. Lett.* **1995**, *66*, 1842.

(26) Cross, G. H.; Ren, Y.; Swann, M. J. *Analyst* **2000**, *125*, 2173.

Chapter IV:

Atomic Force Microscopy Measurements of Humidity Effects on Polymer Films

4.1 Introduction

Atomic Force Microscopy (AFM) is used to study a variety of properties of polymer films, including surface morphology, structure, mechanical stability, local elastic response, friction and adhesive forces.[1-6] The ability to make these measurements has led to advances in polymer nanotechnology and microfabrication processes.[1,7]

The AFM measures the attractive and repulsive forces between a sample and a tip. In "contact mode," a probe consisting of a cantilever with a sharp tip is scanned across the surface of a sample. The tip is in continuous contact with the surface, and the bending of the cantilever due to surface topography is measured. High spatial resolution images are produced. However, the forces applied to the sample surface in these measurements can cause damage to a soft polymer film. Therefore, a reduced force mode with intermittent contact between the tip and sample called "tapping mode" is used to image polymer surfaces. [1,2,4]

In tapping mode AFM, the cantilever with tip is driven to oscillate at its resonance frequency with a certain amplitude, A_0. The cantilever is brought close to a sample surface and "taps" the surface with a set point amplitude, A_{sp}. As the probe scans the sample, damping of its oscillation due to repulsive or attractive forces between the sample and the tip is monitored. A laser beam is focused on the cantilever and

reflected onto a four-quadrant photodetector that measures the amplitude. The vertical position is controlled by a feedback mechanism, much like the shear-force feedback system described in Chapter II. It works to keep the amplitude of the oscillating probe constant, and it produces an image of the sample topography.

In order to understand images produced by tapping mode AFM, the tip-sample interaction must be studied. This can be achieved by experiments carried out in the distance-sweep mode. The amplitude of a tapping cantilever is measured as a function of the distance between the tip and sample, while the lateral position of the cantilever remains constant. Local mechanical properties of the polymer surface, which influence the topographic image produced in tapping mode AFM, can be investigated.[8]

This work will use AFM to measure changes in polymer photoresist film properties with humidity. Polymer films tend to absorb water and swell when exposed to humidity. The extent of this swelling will be investigated with tapping mode AFM imaging. The changes in polymer film properties will be explored in order to interpret these images.

4.2 Materials

Polymer solutions of poly(t-butylcarbonylstyrene) (tBOC) with photoacid generator are prepared by IBM using a previously described method[9] and spun onto 25 mm silicon wafers. The resulting tBOC film is 193 nm thick. The resist is exposed to a line-space pattern using a contact mask and a dose of 10 mJ/cm^2

ultraviolet light at 254 nm. The post-exposure bake at 100°C for 90 seconds results in a conversion of exposed areas to polyhydroxystyrene (PHOST). The resulting lines and spaces are nominally 4 microns in width.

4.3 Instrument

The instrument used for experiments is a Digital Instruments Multimode AFM operated in tapping mode. Probes used are standard silicon tips with a resonant frequency around 300 Hz and a tip diameter of 5 – 10 nm. A 60 liter bell jar is placed over the entire AFM apparatus, with a space in the base allowing a nitrogen stream to purge the experiment. The nitrogen is passed through a reservoir containing water to produce wet nitrogen. Wet and dry nitrogen are mixed to produce the desired humidity. Care is taken not to aim the stream towards the tip, so the flow of gas will not affect measurements. For all experiments, equilibration of one hour at the chosen humidity is allowed.

Distance sweep measurements were carried out on both exposed and unexposed regions of the polymer. In order to locate these regions, the sample was scanned in tapping mode. Once the line-space pattern was identified, the tip could be positioned either over the raised lines (tBOC) or the thinner areas (PHOST). Then the distance sweep could be carried out over that particular polymer.

4.4 Distance Sweep Measurements

Figure 4.1a shows a schematic drawing of a distance sweep measurement. A cantilever with a tip oscillates at a given amplitude, A, that depends on the distance

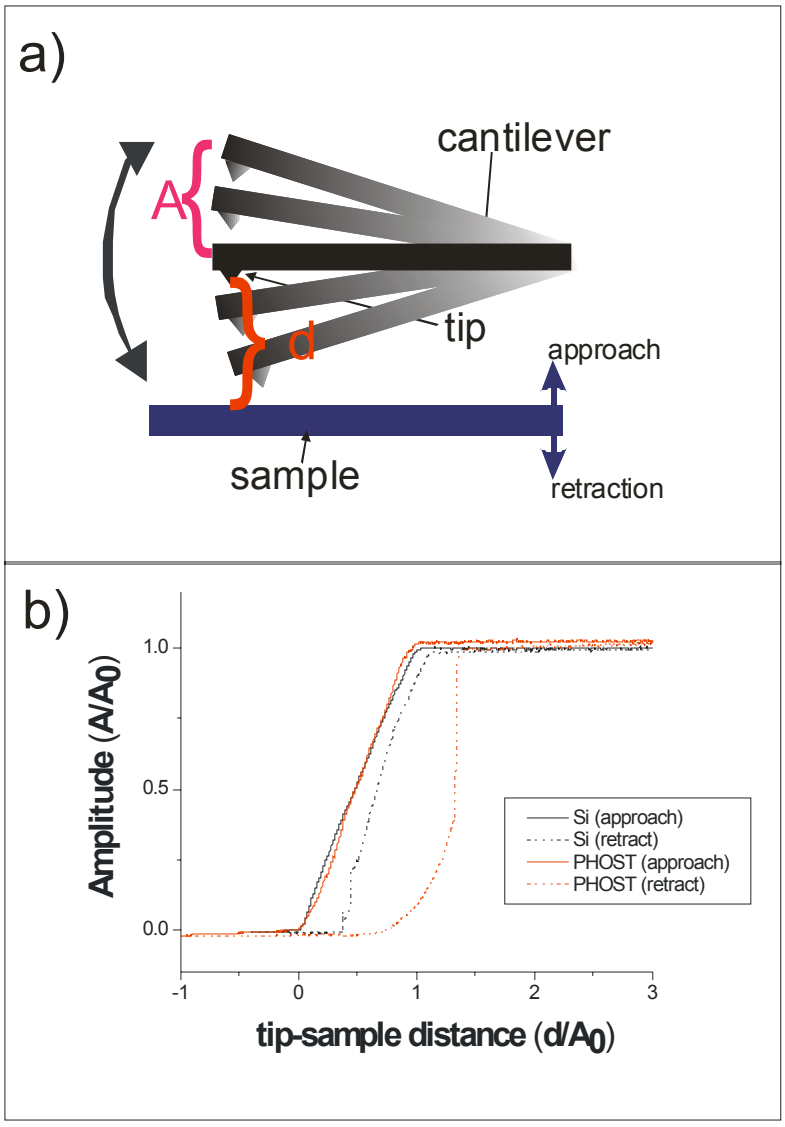

Figure 4.1: Distance sweep measurements. a) Schematic drawing of a distance sweep experiment. B) Curves from measurements on a silicon wafer (black lines) and the modified photoresist polymer PHOST (red lines). The solid lines indicate the approach of the tip to the sample, the dashed lines represent the retraction of the tip from the sample.

between the tip and the sample, d. The amplitude is measured as the distance is decreased (approach) and increased (retraction). The result is a plot called a distance sweep curve. Figure 4.1b shows the results of distance sweep measurements performed on the PHOST polymer (red lines) as well as a plain silicon wafer (black lines). These experiments were performed in a nitrogen purge environment of 11% relative humidity (RH). The solid lines indicate measurements where the tip was approaching the surface from far away. The dashed lines represent retractions, where the tip started at zero distance and was moved away from the sample. The silicon curves are used to highlight the characteristic properties of the amplitude vs. distance curves for stiff samples as opposed to polymers.

When the tip is very far from the surface, the cantilever oscillates freely at an amplitude of A_0. The amplitude is not dependent on distance in this regime. The value of A_0 is determined by the driving force applied to the cantilever, and is constant for each curve. In order to compare various experiments conducted with a variety of driving forces, it is standard practice to normalize the amplitude and the distance by dividing by A_0, the freely oscillating value. All figures shown in this section have sweeps performed at similar values of A_0, unless otherwise specified. A value of around 30 nm would be typical.

As the tip reaches the interaction region, the amplitude is damped as it moves closer to the sample surface. The interaction begins roughly where the distance between tip and sample is equal to the free oscillation amplitude of the cantilever ($d/A_0 = 1$). As the amplitude first begins to decrease, the slope of the silicon curve is greater than that of the PHOST curve. The amplitude decreases more slowly when

approaching softer, more rubbery samples in comparison to stiff samples when the same value of A_0 is set.[2,8] When the tip – sample distance is equal to zero, the tip ceases oscillation on both curves. Normal tapping mode images typically set the feedback loop to an amplitude equal to 90% of A_0.

A feature in need of highlighting is the difference in the retraction curves. The PHOST retraction curve has a much larger hysteresis than the silicon curve. This is because the tip indents into the polymer due to its softness and becomes "stuck." More force is needed to pull it out of the polymer film than to retract from a hard silicon substrate.[6]

Another set of experiments was performed to measure differences in local tip-sample interaction for the exposed and unexposed regions of the polymer. Results of experiments done in an 11% RH atmosphere are shown in Figure 4.2a. Distance sweeps for PHOST are red; TBOC are blue. Again, solid lines represent approaches and dashed lines mean retractions. Results for the approach curves on each polymer are very similar. However, there is a slight difference in the retractions. PHOST has a larger hysteresis, meaning it is a softer, more rubbery polymer and the tip may indent further or have more difficulty pulling out of the film. This is somewhat expected because during the deprotection reaction the modified polymer loses volatile products and "shrinks." Thus its polymer chains have relaxed and the film is more rubbery as a result. In tapping mode AFM, the tips tend to indent further into rubbery films over glassy films.[10]

The distance sweeps are repeated after 1 hour in a high humidity (80% RH) environment, and the results are shown in Figure 4.2b. The results are surprising,

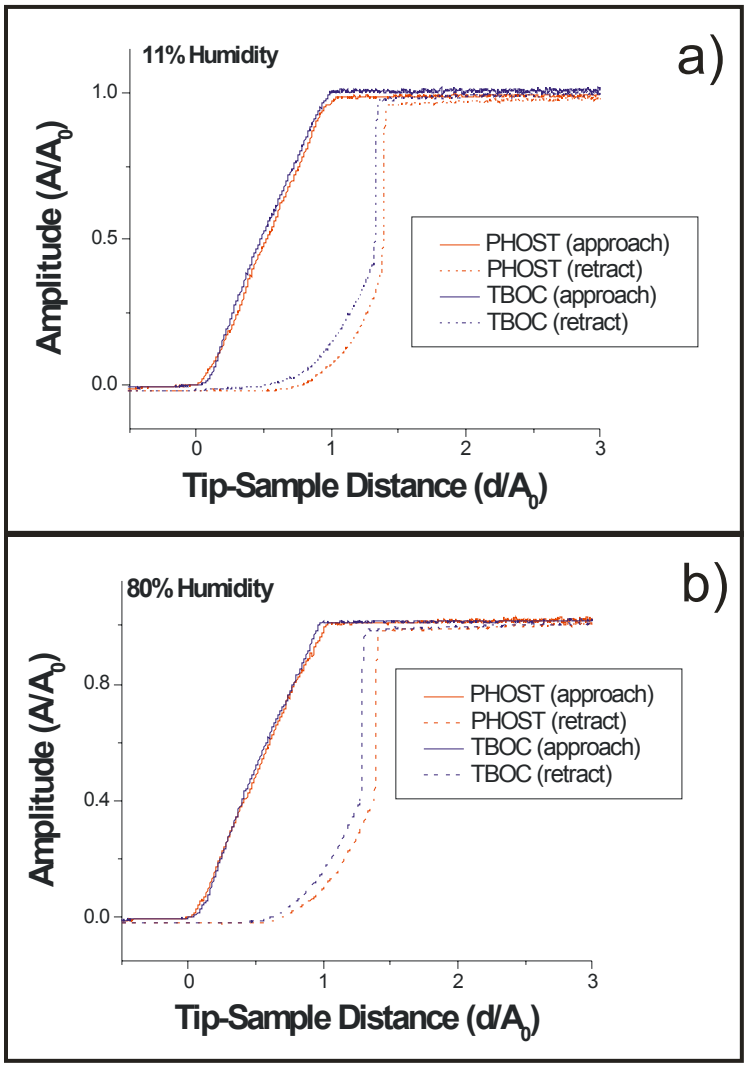

Figure 4.2: Distance sweeps measured for PHOST (red lines) and TBOC (blue lines). Solid lines are approach curves, dashed lines are retraction curves. a) Measured with nitrogen purge in an atmosphere of 11% RH. B) Measured at 80% humidity.

because they look very similar to the dry sweeps. The absorption of water has not seemed to change the mechanical properties of the polymer enough to alter the tip-sample interaction. It was also expected that because the PHOST polymer absorbs more water, its mechanical properties would change, and therefore the tip-sample interaction would change more drastically than the TBOC interaction. However, this was not the case.

Because the tip-sample interactions do not change noticeably with humidity, height images recorded under a variety of humidity environments can all be interpreted the same way. Therefore, the differential swelling can be measured. Differential swelling means the swelling amount of one polymer compared to another. The absolute swelling cannot be determined using AFM. In other words, if both the TBOC and the PHOST lines swell by the same amount, the differential swelling is zero.

4.5 Differential Swelling Measurements

Tapping mode images of the patterned polymer resists were measured at 11%, 23%, 43% and 56% RH. A typical 15 μm x 15 μm image is shown in Figure 4.3a. In order to measure the swelling of the sample at each humidity, it is necessary to determine ΔH, the change in height between the exposed and unexposed regions. Figure 4.3b shows a profile of the topographic image which clearly shows the peaks and valleys. The value of ΔH is quantified by first taking a histogram of the height values represented in the image, shown in Figure 4.3c. Two peaks are evident. The one at a positive height value corresponds to the height of the unexposed, TBOC

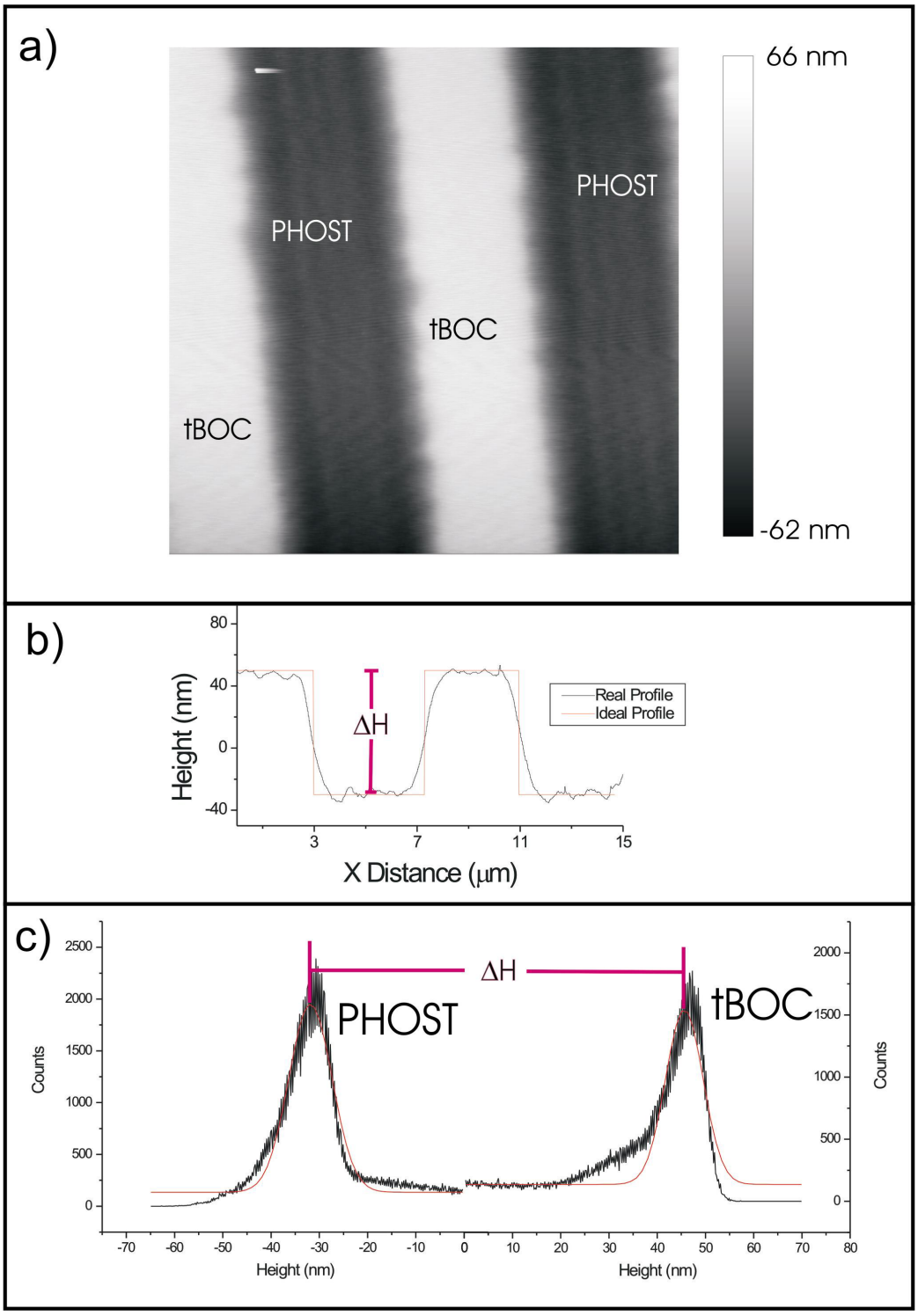

Figure 4.3: Differential swelling measurements of a TBOC/PHOST photoresist. a) 15 μm x 15 μm tapping mode AFM image measured at 23% RH. b) Profile of height vs. distance for one line across the photoresist. c) Histogram of number of data points for each height represented in the image fitted with Gaussian curves.

polymer, the other corresponds to the height of the exposed, thinner, PHOST polymer. In order to systematically choose a value for the peak, the histogram was fitted with a Gaussian curve for each polymer. The photoresists are not intended to produce Gaussian histograms. In fact, if they were ideal, there would only be two height values represented on the histogram. Half of the counts would represent the height of tBOC, the other half would be the height of PHOST. However, the photoresists are not ideal and therefore many height values are represented. The difference between the heights represented at the peaks of these two curves is ΔH.

This procedure was carried out on an image taken at each humidity. The results are shown in Table 4.1. Error bars are a result of the Gaussian fit. The value of ΔH decreases with increasing humidity, meaning the exposed, PHOST region of the polymer swells more than the unexposed areas. This result is expected because PHOST is the more hydrophilic polymer and would naturally absorb more water. The percent differential swelling, ΔS, at a given humidity, x, is calculated by:

$$\Delta S_x = \frac{(\Delta H_{11} - \Delta H_x)}{\Delta H_{11}}, \qquad (4.1)$$

where ΔH_{11} is the change in height between exposed and unexposed regions at 11% RH, the lowest achievable humidity with this experimental set-up.

What is unexpected is how small the differential swelling is. In Chapter III, a photoresist made of PTBMA/PMAA is found to have 36% differential swelling. However, that photoresist is composed of a different polymer material. In order to have experiments that could be compared, AFM images of the PTBMA/PMAA sample with 4 micron lines were carried out in both a nitrogen purge environment

Table 4.1: Differential Swelling in patterned, TBOC photoresists.

Relative Humidity (%)	ΔH (nm)	Differential Swelling (% decrease in ΔH from dry film)
11	79.5 ± 0.1	-
23	77.5 ± 0.1	2.5 ± 0.3%
43	76.2 ± 0.1	4.2 ± 0.3 %
56	75.2 ± 0.1	5.4 ± 0.3 %

(13% RH) and a humid environment (70% RH). The histograms for these two images are shown in Figure 4.4.

As explained in Chapter III, the region containing PTBMA, the thicker, unexposed polymer, is not flat. This causes a double peak in the histogram. Figure 4.4c shows horizontal line profiles of the image, which clearly illustrate the reason for the double peak in the histogram. This profile looks odd in comparison to the profile of the tBOC/PHOST photoresist shown in 4.3b. The oscillation makes it difficult to decide how to determine ΔH. Ultimately, an average of the two highest peaks was used as the height for PTBMA. Choosing the maximum height value for the height of PTBMA was also considered. The final result is a differential swelling of $37 \pm 3\%$ in going from a dry environment to a humid one. This matches well with the value of 36% that can be calculated from measurements done in Chapter III on 4 micron samples. Distance sweep measurements could not be reliably obtained on these samples because of the oscillating profile. It appeared that the approach curves had no humidity dependence, but it could not be guaranteed that the approaches took place on the intended polymer.

Although the results match up well, the experiments described here and in Chapter III have key differences which may make them difficult to compare. The experiments in Chapter III were performed in a vacuum bell jar chamber, so change in pressure could have played a role. It is also important to consider the two types of microscopy used to measure topography. In shear-force microscopy, employed in the experiments described in Chapter III, the tip is dithered laterally, or somewhat parallel to the surface. If there are contributions to the height measurements from

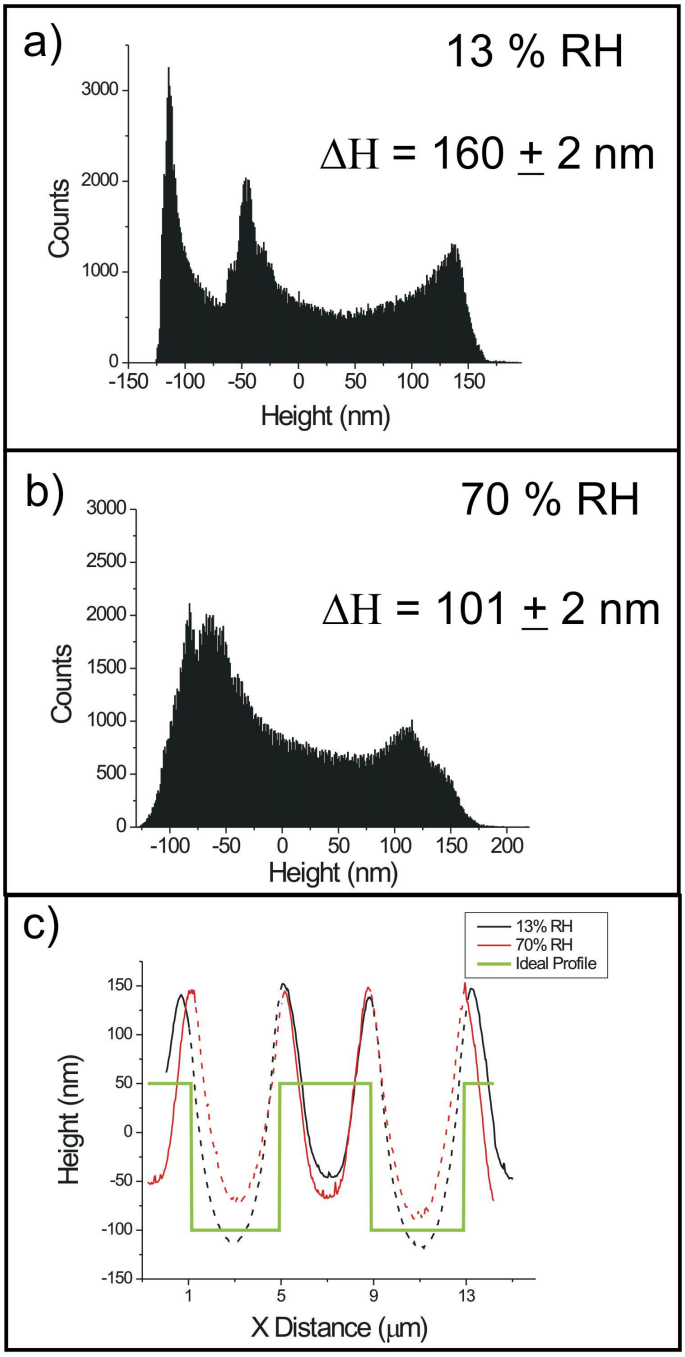

Figure 4.4: Height histograms of 15 μm x 15 μm tapping mode AFM images measured on PTBMA/PMAA photoresists. a) Histogram for image measured under nitrogen purge (13% RH). b) Histogram for image measured in 77% RH humid environment. c) Profiles of one horizontal line in the image. Solid lines represent PTBMA regions, dashed lines represent PMAA regions.

differences in tip-sample interaction for the two different polymers, it may be magnified by prolonged interaction. If the tip-sample interaction changes when a polymer becomes saturated with water, the differential swelling could be exaggerated. The AFM tip dithers perpendicular to the surface, so effects from a hydrophilic surface are not as strong.

4.6 Humidity Effect on Distance Sweep Curves

Models of the three possible types of distance sweep curve described in the literature are shown in Figure 4.5. The type of curve observed depends on the sample material, the free amplitude of the cantilever and the tip-sample interaction.[11] Part a shows a Type I curve, where the amplitude decreases linearly with tip-sample distance. In Figure 4.5b, a Type II curve depicts a step-like transition. The transition is an observation of the formation of a "liquid neck" due to capillary forces between the tip and a film of water on the sample surface. A Type III curve, shown in Figure 4.5c, is similar to Type II, but has a smooth transition.

There have been many distance sweep studies performed on stiff materials, but there is still a lot to learn about polymers. A study by Zitzler, et al. looked at amplitude vs. distance curves as a function of humidity for both hydrophilic and hydrophobic stiff surfaces.[3] They found that when the free oscillation amplitude A_0 is greater than a critical amplitude A_c, the distance sweep curve is type II. Below A_c the curve is type I. This doesn't mean that no capillary is formed at lower amplitudes, just that it cannot be observed. For hydrophilic surfaces, the value of A_c increases with humidity, but there is no trend for hydrophobic surfaces. The critical amplitude

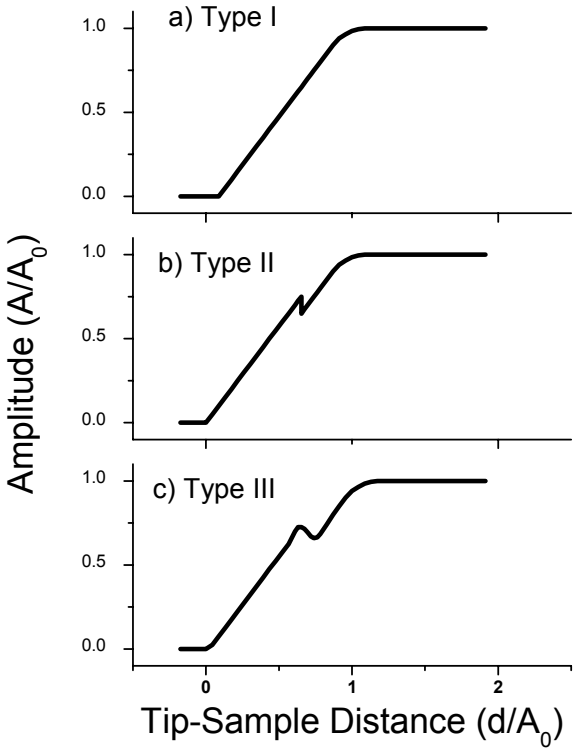

Figure 4.5: Three different theoretical amplitude vs. distance curves.

is simply a measurement of the A_0 value at which distance sweep curves change from Type I to Type II. It has no other significance other than the fact that a hydrophilic surface has a humidity dependent A_c while a hydrophobic surface has a humidity independent A_c value.

The work done by Zitzler and colleagues was carried out with silicon tip and mica sample, which is considered a stiff material. Both surfaces were chemically processed to obtain hydrophilic or hydrophobic properties as desired. The work shows that the distance sweeps could be used as a probe of local hydrophilicity at different points on a sample surface.

It would be interesting to probe the local hydrophilicity of the polymers in a photoresist using a similar experiment to Zitzler's. Attempts were made to carry out such measurements on TBOC and PHOST samples at a variety of humidities and amplitudes. Figure 4.6 shows an example of one set of sweeps performed on TBOC at 13% RH. Each curve is measured at a different value of A_0, but the curves are normalized so they may all be viewed on the same scale and compared. The A_0 value ranges from as small as possible to still achieve a curve, and as large as possible without damaging the cantilever or tip. The shape of the curve appears to be dependent on the free oscillation amplitude. At lower values of A_0, the amplitude decreases at a slower rate at normalized tip-sample distance (d/A_0) values near one. The curves are also noisier. However, all of the curves appear to be Type I, with no transition to Type II occurring. This is consistent at each humidity explored, which included a range between 13% and 80% RH. Because no transition is detected, there is no A_c.

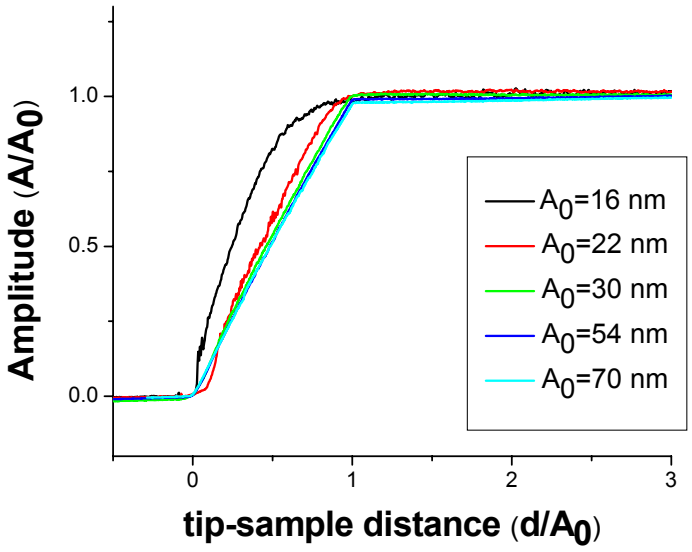

Figure 4.6: Distance sweep curves on TBOC measured at a variety of A_0 values.

Because the literature does not include many distance sweep studies on polymers, it is not known if the type II curve has been measured on soft surfaces. There may be a physical reason why the transition cannot be detected on softer samples. On the other hand, perhaps more careful control of experimental parameters such as tip surface preparation may produce type II curves.

4.7 Conclusions

Tapping mode AFM can be used to measure polymer photoresists. Differential swelling at can be quantified by capture of tapping mode images at a variety of humidities. These images can be carefully analyzed by consideration of distance sweep curves, which measure local mechanical properties of the polymer sample. Amplitude vs. distance curves performed on exposed and unexposed regions of a TBOC/PHOST polymer photoresist do not show a humidity dependence. Therefore, tip-sample interaction was determined to have little effect on differential swelling measurements.

Attempts to measure A_c, the critical amplitude of free oscillation above which Type II curves exist, were unsuccessful. Therefore, it was not possible to measure humidity dependence of A_c when approaching photoresist samples, which would have been a way to quantify hydrophilicity.

References for Chapter IV

(1) Ratner, B. D.; Tsukruk, V. V. *Scanning Probe Microscopy of Polymers*; American Chemical Society: Washington, DC, 1996; Vol. 694.

(2) Bar, G.; Delineau, L.; Brandsch, R.; Ganter, M.; Whangbo, M.-H. *Surface Science* **2000**, *457*, L404.

(3) Zitzler, L.; Herminghaus, S.; Mugele, F. *Phys. Rev. B.* **2002**, *66*, 155436.

(4) Chen, X.; Davies, M. C.; Roberts, C. J.; Tendler, S. J. B.; Williams, P. M.; Davies, J.; Dawkes, A. C.; Edwards, J. C. *Ultramicroscopy* **1998**, *75*, 171.

(5) Opdahl, A.; Hoffer, S.; Mailhot, B.; Somorjai, G. A. *The Chemical Record* **2001**, *1*, 101.

(6) Magonov, S., N.; Reneker, D. H. *Annu. Rev. Mater. Sci.* **1997**, *27*, 175.

(7) Sheiko, S. S. *Adv. Polym. Sci.* **2000**, *151*, 61.

(8) Kopp-Marsaudon, S.; Leclere, P.; Dubourg, F.; Lazzaroni, R.; Aimè, J. P. *Langmuir* **2000**, *16*, 8432.

(9) Burns, S. D.; Medeiros, D. R.; Johnson, H. F.; Wallraff, G. M.; Hinsberg, W. D.; Willson, C. G. *Proc. SPIE* **2002**, *4690*, 321.

(10) Leclere, P.; Dubourg, F.; Kopp-Marsaudon, S.; Bredas, J. L.; Lazzaroni, R.; Aimè, J. P. *Appl. Surf. Sci.* **2002**, *188*, 524.

(11) Garcia, R.; San Paulo, A. *Ultramicroscopy* **2000**, *82*, 79.

Chapter V:

Fourier Transform Infrared Spectroscopy Studies of Water-Polymer Interactions in Chemically Amplified Photoresists

5.1 Introduction

Water sorption is an interesting process that can affect the physical, mechanical and chemical properties of a polymer. It is important to many polymer industries, including packaging, chemical sensors, drug delivery, artificial organs, and electronics. The rate and extent of the water uptake are determined by a variety of factors, such as temperature, humidity, polymer chemistry, film thickness, pore size and density, and material processing.[1-6] The structure of the sorbed water is of particular importance, as it can give insight into the interactions between the water and the polymer substrate. Water is a unique penetrant because it interacts strongly with polar groups of the polymer and can form clusters that are confined by the polymer chains. Among the physical changes that water can induce are plasticization, hygrothermal degradation, swelling, alteration of tensile strength and hardness, and change in net dielectric constant of a film.[3-5,7,8] Water can also affect chemical processes in polymers such as the deprotection reaction in photoresists used in the fabrication of electronic circuits.[3,9-11]

Poly(t-butoxycarbonylstyrene) (tBOC)[12] and ketal-protected Poly(hydroxystyrene) (KRS-XE)[13] are two important chemically amplified photoresist systems. The tBOC polymer, shown in Figure 5.1a, is a thin film cast

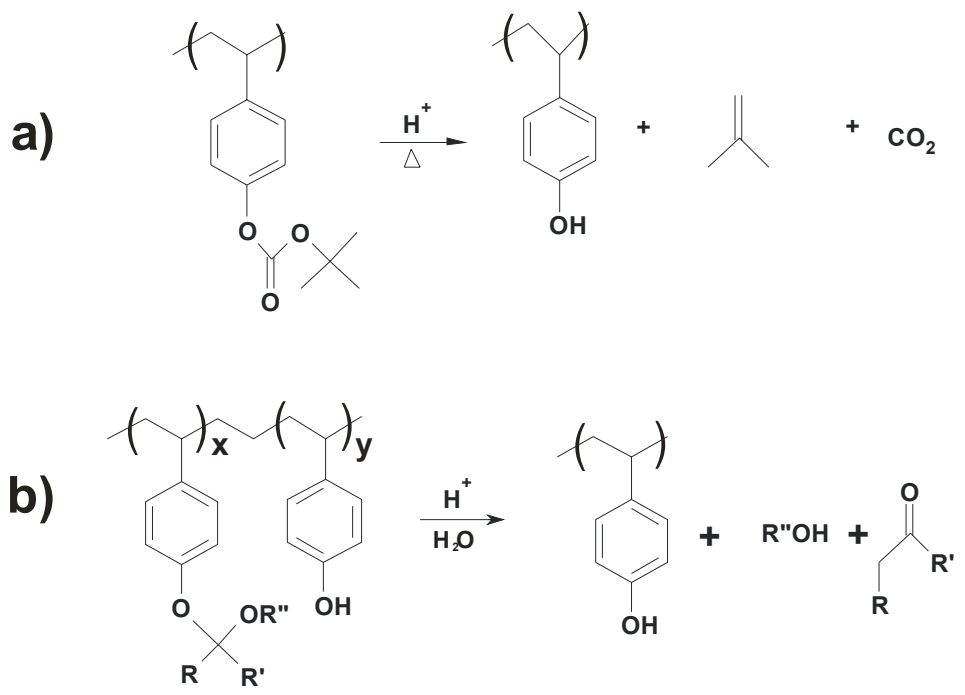

Figure 5.1: Deprotection reactions of polymer systems studied: a) Poly(t-butoyxylcarbonylstyrene) (tBOC) b) Ketal-protected Poly(hydroxystyrene) (KRS-XE)

with a photoacid generator (PAG). Exposure to UV radiation forms the acid, which reacts with the tBOC in the presence of heat and is converted to polyhydroxystyrene (PHOST). The tBOC film is initially relatively dry, but as the polymer is modified it becomes more hydrophilic and rapidly absorbs water. The amount of water absorbed by the photoresist depends on the local humidity. Burns et al.[9] have found that an increase in the humidity will slow the deprotection reaction. This result was unexpected. They hypothesize a "pH leveling" effect in which water reacts with photogenerated acid, decreasing the strength of the acid and lowering the reaction rate. This work provides an additional, complementary explanation.

The chemistry for the KRS-XE system is different.[9,13] The initial exposure occurs in vacuum, while the post exposure processing takes place in a clean room where the humidity is carefully controlled. As shown in Figure 5.1b, a stoichiometric amount of water is required for the solubility switching reaction. The polymer is initially hydrophilic and absorbs the water needed for the deprotection. The activation energy is low, so a post-exposure bake is unnecessary. Burns et al. found that increased humidity in the local environment increases the reaction rate.[9] Like tBOC, the KRS-XE deprotection reaction results in the polymer PHOST. However, the resulting films are not identical, because the composition and quality of the film depends on the processing methods used. Also, the percentage of the polymer that is converted may be different in each case.

Fourier-Transform Infrared (FTIR) spectroscopy has produced insights into the structure of water in polymer films.[4,7,14-19] The vibrational spectrum can be measured in situ at a variety of humidities and provides details about the water-polymer

interactions and hydrogen bonding. In this investigation, the molecular information obtained contributes to the understanding of transport through the polymer, which ultimately helps explain the deprotection reaction kinetics.

5.2 Materials

Polymer solutions were prepared using a previously described method[9] and spun onto 25 mm sapphire wafers. The resulting tBOC photoresist film is 990 nm thick. The modified tBOC, or PHOST sample, was prepared by exposing a tBOC film to a 100 mJ/cm^2 dose of 257 nm ultraviolet light. The wafer was then baked at 100 °C for 90 seconds. The thickness of the resulting film is approximately 635 nm.

The KRS-XE photoresist was also spun onto 25 mm sapphire wafers, but to a thickness of 370 nm. To prepare the modified polymer sample, the resist was exposed to a dose of 100 mJ/cm^2 of ultraviolet light. After 5 minutes of exposure to clean room conditions with controlled humidity, the thickness was 335 nm.

5.3 FTIR Instrument

Figure 5.2 shows the apparatus used for the experiments. It consists of a modified Bruker Optics IFS 66v/s Fourier Transform Infrared (FTIR) spectrometer with a tungsten IR source and a liquid nitrogen cooled MCT (HgCdTe) detector. Both the sample and instrument chambers can be pumped down to 2.0 kPa. The sample chamber is isolated by vacuum flanges with sapphire windows to allow the passing of the infrared radiation. Gas inlets and outlets were added to the faceplate of the sample chamber to allow the sample environment to be humidity controlled. Dry

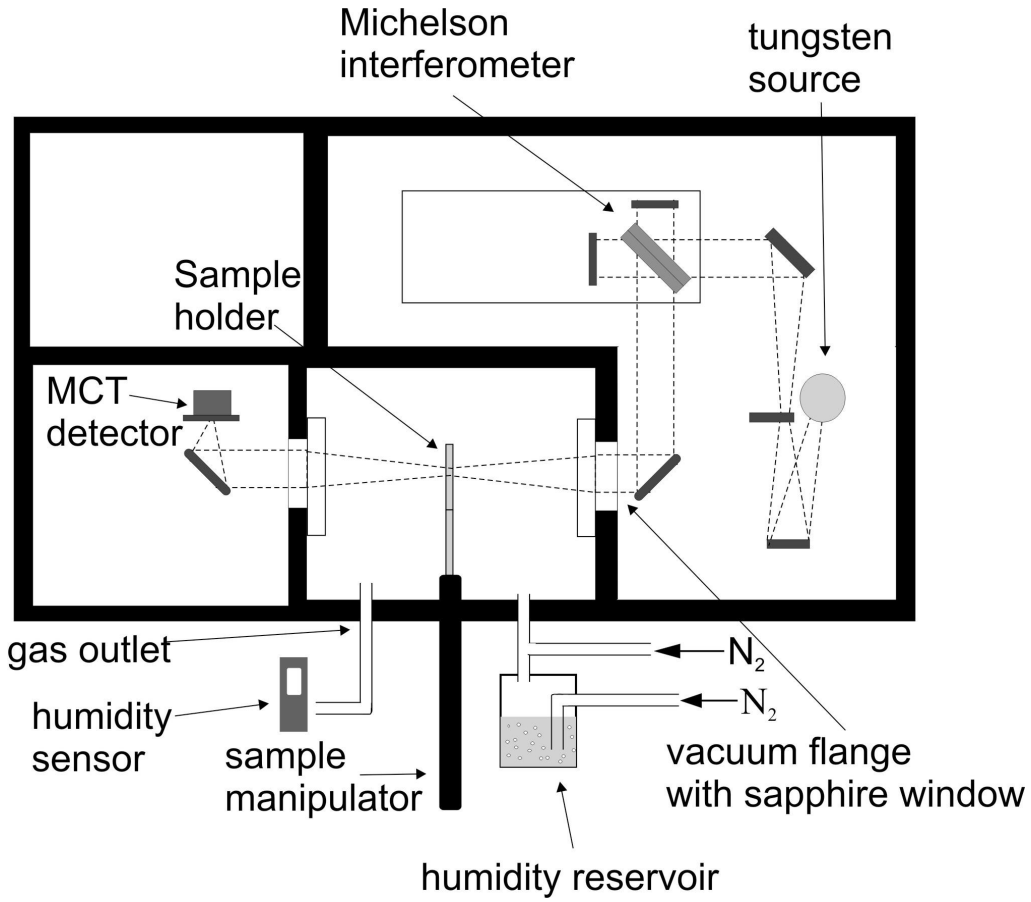

Figure 5.2: Schematic diagram of FTIR spectrometer apparatus.

nitrogen is used to purge the sample. The nitrogen can be passed through a reservoir containing water to produce wet nitrogen. Mixing different ratios of wet nitrogen and dry nitrogen produces the variety of humidities used in this work, which are recorded by a thermohygrometer at the gas outlet.

Samples are loaded onto a holder with mounting positions for two samples. An external manipulator can move samples into the IR beam, as well as move them out of the way to allow for a background scan. For the experiments performed here, the two samples mounted at the same time are the modified and unmodified polymers for either the tBOC or the KRS-XE system. The background scan is taken immediately before or after the sample scan in order to best match the humidity conditions and allow for elimination of the gas phase water features in the spectrum. The final spectra, which show only the absorbance of the water sorbed into the polymer, are obtained through the following subtraction:

$$A = \log\left(\frac{I_0}{I}\right) - \log\left(\frac{I_0^{'}}{I^{'}}\right), \tag{5.1}$$

where I_0 is the background spectrum under humid conditions, I is the spectrum of the sample in humid conditions, $I_0^{'}$ is the background spectrum in dry conditions, and $I^{'}$ is the spectrum of the sample in dry conditions.

5.4 Results and Discussion - tBOC system

Spectra of water sorbed in the modified tBOC polymer were obtained at 10%, 21%, 37%, 67% and 79%, all ± 2%, relative humidity (RH). Figure 5.3a shows the OH stretching region of these spectra, which is the most sensitive region to hydrogen

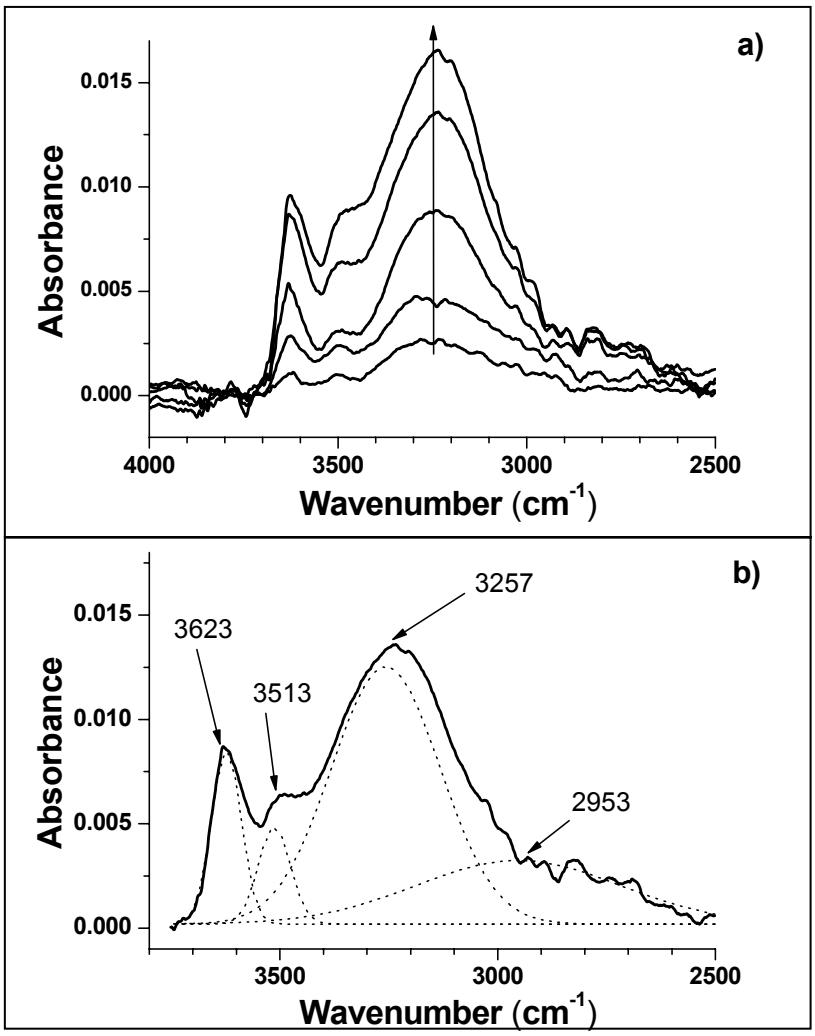

Figure 5.3: Spectra of water absorbed by the modified tBOC system. a) Black lines show spectra taken in modified polymer at 10, 21, 37, 67 and 79% RH. The arrow points in the direction of increasing humidity. b) Deconvoluted spectrum of OH stretching band at 67% RH. Four sub-bands, which represent four different water environments, are shown by dotted lines. The sub-band with a peak at 2953 cm^{-1} represents strongly-bound water molecules, 3257 cm^{-1} is medium-bound, 3513 cm^{-1} is weakly-bound, and 3623 cm^{-1} shows free water molecules.

bonding (H-bonding), with the arrow pointing in the direction of increasing humidity. The band can be deconvoluted into distinct sub-bands within the OH stretching band, which reflect different types of water molecular environments.[4,14,17,18,20] This type of analysis was performed on our sorbed water spectra. We chose four sub-bands and designated them strongly-bound, medium-bound, weakly-bound and free water. The results for modified tBOC are shown in Figure 5.3b.

The lowest frequency band is commonly attributed to the most strongly bound water molecules.[4,7,14,17-21] This peak at 2953 cm^{-1} is due to water molecules H-bonded onto specific polar sites along the polymer network. In the tBOC photoresist system, the OH group formed during the deprotection would be a good candidate for a strong H-bonding site. The strongly-bound peak is usually the broadest, due to heterogeneity of the bonding sites. The largest sub-band, found at 3257 $cm,^{-1}$ corresponds to medium-strength hydrogen bonds. These water molecules are still associated with the polymer chains, but they are not as tightly hydrogen-bonded as the strongly bound ones. In the case of modified tBOC, we believe the medium and strongly-bound bands are larger because of the hydrophilicity of the polymer. The band at 3513 cm^{-1} shows weakly-bonded water molecules, and the highest frequency peak at 3623 cm^{-1} is characteristic of free or unassociated water. These less-bound water molecules can be found in the pores formed by spaces between the polymer chains that make up the hole free volume. The bands are narrower, and because the water molecules are relatively isolated, there is less heterogeneous broadening. Water molecules may also form clusters in these spaces.

The fraction of each type of water is calculated by integrating the indicated sub-band and dividing by the area of the total OH stretching band from 2500 – 3750 cm^{-1}. However, it is not very straightforward to convert these fractions into actual amounts of water molecules. The molar absorptivity significantly increases with the degree of hydrogen bonding, so the cross section would be different for each sub-band.[7,14,17] Therefore, we look only at the change in each fraction with humidity to see how the interaction inside the polymer network is affected when more water is present. The fraction of each type of water present depends on various chemical and physical properties of the polymer, such as structure, cross-linking, molecular weight, pore size and density.[4,14,16,19,22]

The intensity of all four sub-bands, and therefore the amount of each type of water, increases with local humidity. However, the fraction of each of the four sub-bands changes with humidity in a different way, as clearly illustrated in Figure 5.4. Error bars represent one standard deviation from multiple measurements. The deviations are due to the reproducibility of the experiment, particularly because of drift in the humidity conditions. The accuracy of the spectral fit also plays a role.

The amounts of free and weakly bound water molecules increase more rapidly than the medium and strongly-bound water. This is manifested by an increase in the fraction of these subbands with increasing humidity, as seen in Figure 5.4. The fraction of medium-bound water remains fairly constant with humidity, and the fraction of strongly-bound water decreases.

Similar behavior has been observed in other polymers and can be explained by the following considerations.[3,7,8,14,17,18,23] Enthalpy mandates that at the lower

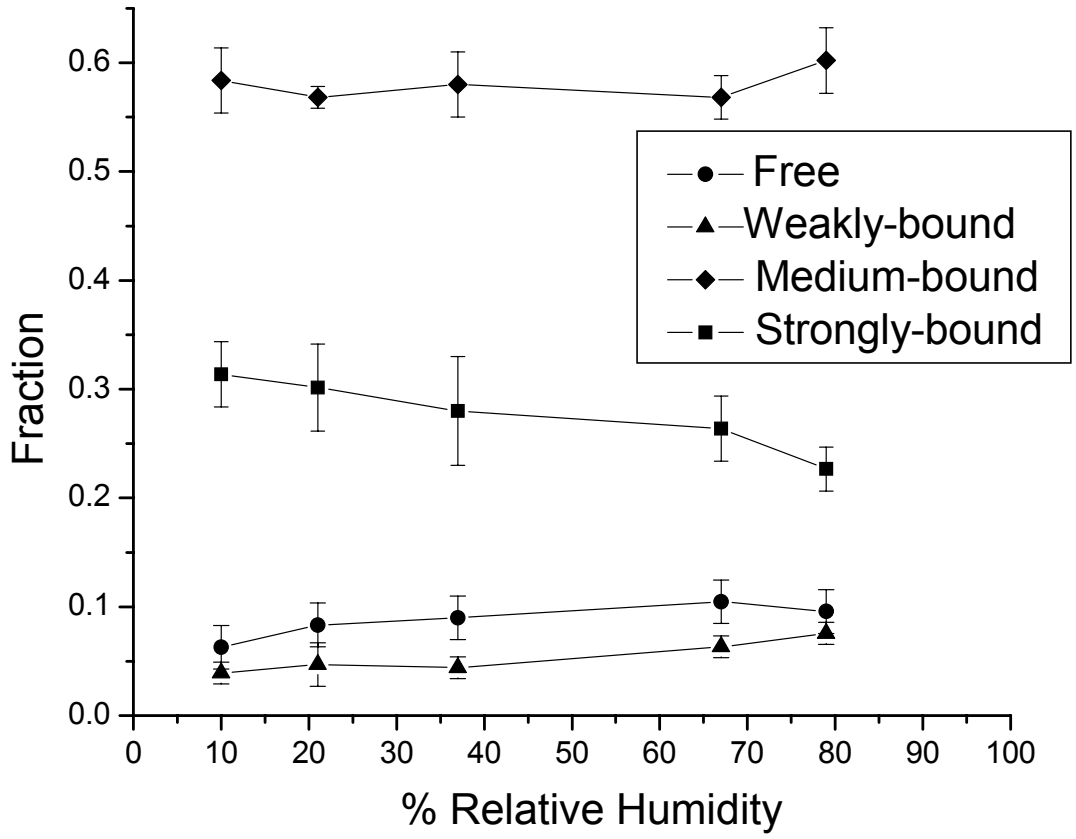

Figure 5.4: Fraction of total OH stretching band vs. relative humidity for the four sub-bands representing strongly-bound (■), medium-bound (◆), weakly-bound (▲) and free (●) water molecules in the modified tBOC polymer sample of Figure 5.3.

humidities, when there is less water available, the absorbed water molecules would be more strongly bound. Water hydrogen bonds to polar sites along the polymer chains. As the sites for water association begin to saturate, the water molecules increasingly tend towards locations in the pores formed by spaces between polymer chains and begin to come together to form dimers and larger clusters.

When water forms clusters in polymer chains, the rates of transport of water and other species in the film can be decreased.[8,17,23,24] Berger et al.[3] found that in the case of PHOST, diffusion is impeded when there is one water molecule present for every two OH sites in the polymer. This is when the hydrogen bonding to hydrophilic sites is saturated enough that water molecules begin to cluster together. The clustering of water molecules may also serve to slow the diffusion of the photoacid species. Interaction with water could decrease the mobility of the large acid counter ion and limit transport to active sites.[25] Therefore, in addition to the dilution of the acid by the water[9], this limiting of transport within the polymer may be an additional cause for the slowed reaction rate with increasing humidity reported by Burns, et al.

Similar experiments were carried out on unmodified tBOC films. The tBOC is hydrophobic and has been reported to take up less than one fourth as much water as PHOST, the modified polymer.[9] In our experiments, it was difficult to measure the spectra because of the small amounts of water present and the low signal-to-noise ratio caused by error in the subtraction of the gas phase water signal.[26] Therefore, we were not able to carry out an analysis of the different water environments on this polymer. We believe that the water molecules would be less strongly-bound than the

waters in the modified polymer because of the lack of hydrophilic sites on the polymer chain of unmodified tBOC.

5.5 Results and Discussion - KRS-XE

Spectra of the water in the KRS-XE system, measured at 12%, 21%, 41%, and 51% (all ± 2%) relative humidity, are shown in Figure 5.5a. In this system, the original polymer needs to absorb water so that it is available as reactant in the deprotection reaction. After the reaction is carried out, the polymer is slightly more hydrophilic and holds more water. This is illustrated in Figure 5.5a. The adjacent solid and dotted lines are spectra of the unmodified and modified polymers at the same humidity, and the arrow points in the direction of increasing humidity. The absorbance is higher for the modified polymer, denoting a greater amount of water present. The shape of the band is similar to the shape of the water band in the modified tBOC, as expected because of the similarity of the chemical structures of these polymers.

Figure 5.5b was constructed in a similar fashion to Figure 5.4 and illustrates the changing shape of the water band with humidity. The KRS-XE system follows a pattern similar to the tBOC system, in that the fractions of free and weakly bound water seem to increase as the medium and strongly-bound water molecule fractions decrease. For the unmodified polymer, there is a big change from 12%RH to 21%RH, and then the fractions stay fairly constant with humidity. This is an interesting point because Burns et al. found that the deprotection reaction rate

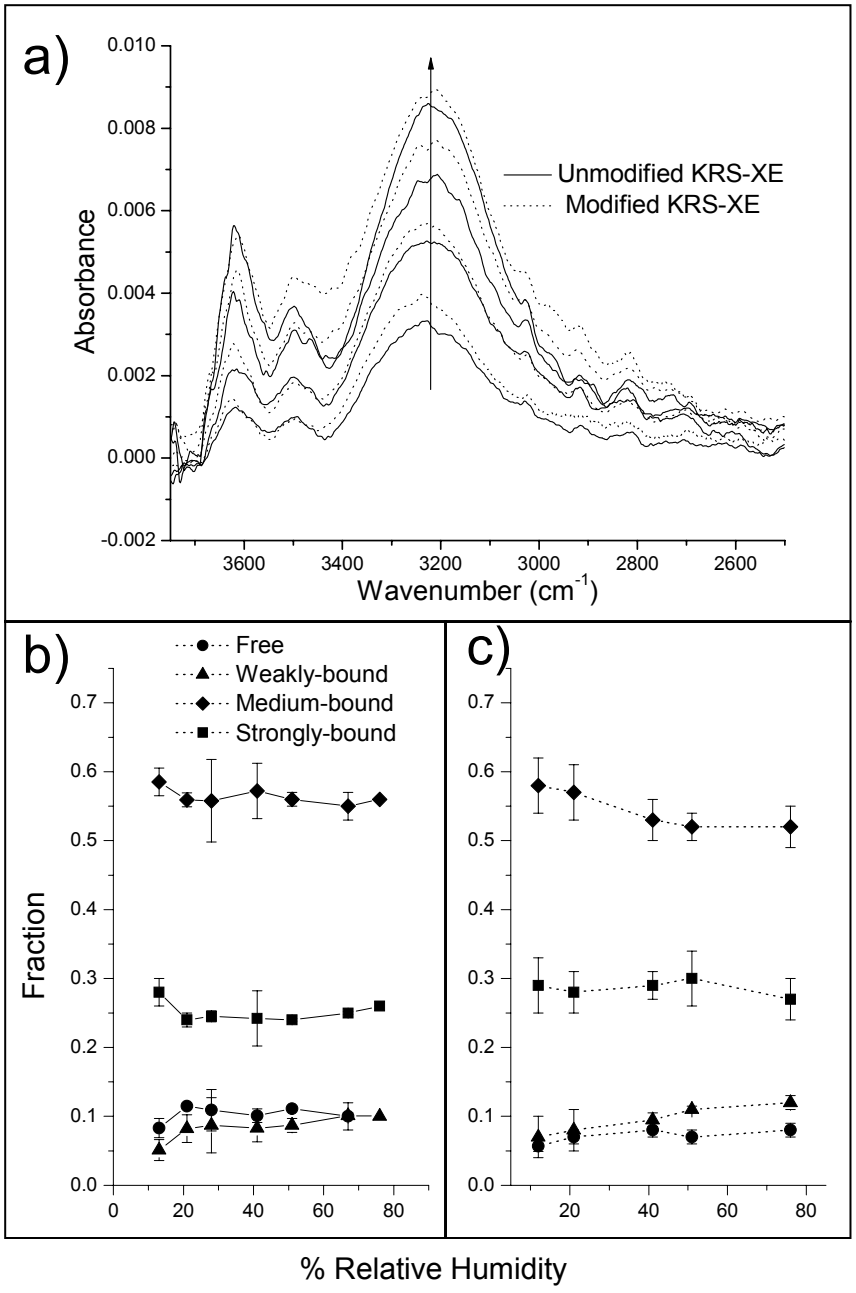

Figure 5.5: Results of KRS-XE experiments. a) Spectra of absorbed water taken at 12%, 21%, 41% and 51% relative humidity. Solid lines show spectra of the unmodified polymer; dotted lines show the modified polymer. The arrow points in the direction of increasing humidity. b) Fraction of total OH stretching band vs. relative humidity for the four sub-bands representing strongly-bound (■), medium-bound (◆), weakly-bound (▲)and free (●) water molecules for the unmodified polymer. c) Fraction of total OH stretching band vs. relative humidity for the modified polymer.

increases with humidity until the humidity reaches 25%, and then it stays constant.[9] Because water is a reactant in the deprotection, the leveling off of the reaction rate can occur when there is an excess of water, meaning the polymer becomes the limiting reagent. Transport could also play a role. As with the modified tBOC, at higher humidities the free and weakly-bound water molecule fractions are increasing because the available hydrophilic sites are becoming saturated. Therefore, it is possible that water molecules are clustering, which may slow diffusion of water and/or the acid to available reactive sites.

In the modified KRS-XE polymer, the increase in free and weakly-bound water species and the decrease in strongly-bound species continues with increasing humidity beyond 21%RH. Another interesting aspect of Figure 5.5b is that in the unmodified polymer, the fraction of free water is greater than the fraction of weakly-bound water. The opposite is true of the modified polymer. This is evidence that a subtle change in the polymer structure can change the water-polymer interactions.

5.6 Comparison of Photoresists

Figure 5.6 shows spectra of water sorbed in three different polymer photoresists, poly (methacrylic acid) (PMAA), KRS-XE and PHOST, all taken at 68% humidity. The basic features of the spectra are very similar. All have the same four sub-bands as presented in the previous sections. Therefore, the polymer-water interactions must be very similar.

Figure 5.7 presents the structures of each of these photoresists. The common aspect of their structures is an OH group off the polymer chain. This is additional

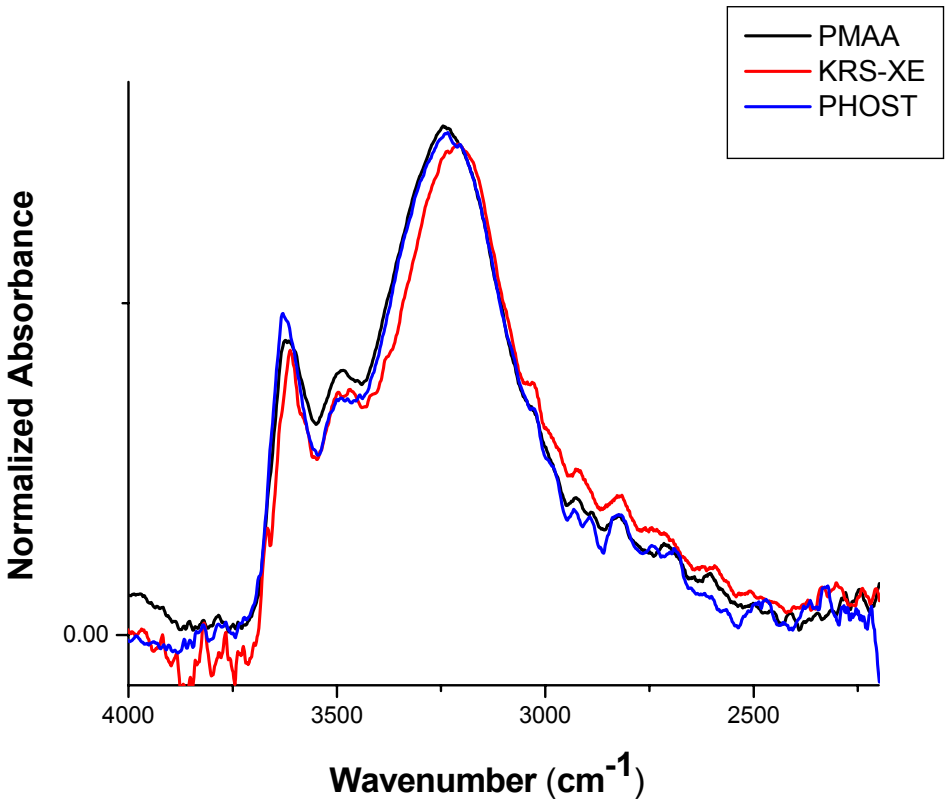

Figure 5.6: FTIR spectra of water sorbed in three different polymers taken at 68% humidity.

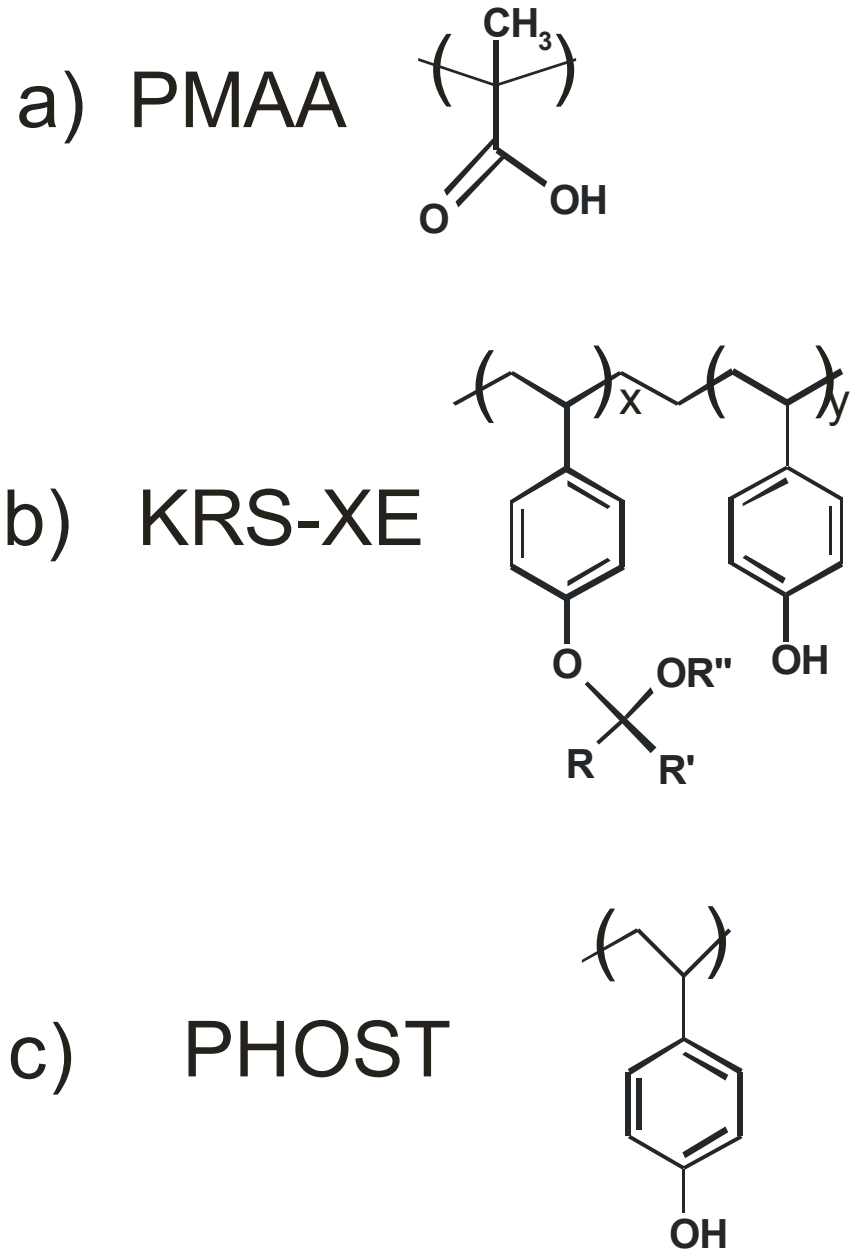

Figure 5.7: Structures of three polymer photoresists.

evidence that it is the polar OH group on the polymer that attracts and binds the water molecules. The KRS-XE water spectrum shows medium and strongly-bound peaks that look slightly shifted from the peaks of the other two polymers. The structure of this polymer has C – O – C bonds that are not present in the other two photoresists. Perhaps they have some influence on the binding of the water molecules.

5.7 Conclusions

This work has provided information regarding the water – polymer interactions in hydrated chemically amplified photoresists. The sorption of water in the polymer films is found to be highly dependent on the humidity of the sample environment. The OH stretching band, found at 2500 – 3750 $cm,^{-1}$ deconvolutes into four sub-bands, which represent four different types of water present in the wet photoresists. These water molecules undergo varying degrees of hydrogen bonding to the polymer chains. The amount of each type of water is humidity dependent, with the fraction of free and weakly-bound water increasing, and the fraction of medium and strongly-bound water decreasing, with increasing humidity. In the case of the tBOC photoresist system, this increase in free and weakly bound water could indicate slowed transport of acid to reaction sites on the polymer, resulting in a decreased deprotection reaction rate. In the case of the unmodified KRS-XE photoresist, similar changes occur at low humidites, but the fractions stay relatively constant with increasing humidity after 21%RH. This mirrors the trend of the deprotection reaction rate with humidity, and it provides additional evidence that the polymer-water

interactions may affect transport and ultimately reaction dynamics within a polymer network.

References for Chapter V

(1) Buchold, R.; Nakladal, A.; Gerlach, G.; Herold, M.; Gauglitz, G.; Sahre, K.; Eichhorn, K. *Thin Solid Films* **1999**, *350*, 178.

(2) Neogi, P. *Diffusion in Polymers*; Marcel Dekker, Inc: New York, 1996.

(3) Berger, C. M.; Henderson, C. L. *Polymer* **2003**, *44*, 2101.

(4) Mura, C.; Yarwood, J.; Swart, R.; Hodge, D. *Polymer* **2001**, *42*, 4141.

(5) Schult, K. A.; Paul, D. R. *Journal of Applied Polymer Science* **1996**, *61*, 1865.

(6) Arce, A.; Fornasiero, F.; Rodriquez, O.; Radke, C. J.; Prausnitz, J. M. *Phys. Chem. Chem. Phys.* **2004**, *6*, 103.

(7) Cotungo, S.; Larobina, D.; Mensitieri, G.; Musto, P.; Ragosta, G. *Polymer* **2001**, *42*, 6431.

(8) Sutandar, P.; Ahn, D. J.; Franses, E. I. *Macromolecules* **1994**, *27*, 7316.

(9) Burns, S. D.; Medeiros, D. R.; Johnson, H. F.; Wallraff, G. M.; Hinsberg, W. D.; Willson, C. G. *Proc SPIE* **2002**, *4690*, 321.

(10) Suga, O.; Yamaguchi, H.; Okazaki, S. *microelectronic engineering* **1991**, *13*, 65.

(11) Shibayama, Y.; Saito, M. *Jap. J. Appl. Phys.* **1990**, *29*, 2152.

(12) Wallraff, G.; Hutchinson, J.; Hinsberg, W.; Houle, F.; Seidel, P.; Johnson, R.; Oldham, W. *J. Vac. Sci. Technol. B* **1994**, *12*, 3857.

(13) Medeiros, D. R.; Aviram, A.; Guarnieri, C. R.; Huang, W.-S.; Kwong, R.; Magg, C. K.; Mahorowala, A. P.; Moreau, W. M.; Petrillo, K. E.; Angelopoulos, M. *IBM J. Res. Dev.* **2001**, *45*, 639.

(14) Sammon, C.; Mura, C.; Yarwood, J.; Everall, N.; Swart, R.; Hodge, D. *J. Phys. Chem. B* **1998**, *102*, 3402.

(15) Maréchal, Y.; Chamel, A. *J. Phys. Chem.* **1996**, *100*, 8551.

(16) Nguyen, Q. T.; Favre, E.; Ping, Z. H.; Néel, J. *J. Membrane Sci.* **1996**, *113*, 137.

(17) Kitano, H.; Ichikawa, K.; Fukuda, M.; Mochizuki, A.; Tanaka, M. *J. Colloid Interface Sci.* **2001**, *242*, 133.

(18) Ping, Z. H.; Nguyen, Q. T.; Chen, S. M.; Zhou, J. Q.; Ding, Y. D. *Polymer* **2001**, *42*, 8461.

(19) Kawagoe, M.; Takeshima, M.; Nomiya, M.; Qiu, J.; Morita, M.; Mizuno, W.; Kitano, H. *Polymer* **1999**, *40*, 1373.

(20) Maeda, Y.; Kitano, H. *Spectrochimica Acta A* **1995**, *51*, 2433.

(21) Ichikawa, K.; Mori, T.; Kitano, H.; Kukuda, M.; Mochizuki, A.; Tanaka, M. *J. Polym. Sci. Part B: Polym Phys* **2001**, *39*, 2175.

(22) Maeda, Y.; Ide, M.; Kitano, H. *J. Mol. Liquids* **1999**, *80*, 149.

(23) Sammon, C.; Deng, C.; Mura, C.; Yarwood, J. *J. Mol. Liquids* **2002**, *101*, 35.

(24) Starkweather, H. W. *Macromolecules* **1975**, *8*, 476.

(25) Wallraff, G. M.; Hinsberg, W. D. *Chem. Rev.* **1999**, *99*, 1801.

(26) Much of the noise comes from the subtraction of the gas phase water. If the local humidity conditions present during the measurement of the I and I_0 spectra are not exactly the same, subtraction noise due to gaseous species is introduced. Performing more averages only gives a greater chance that the local humidity that the sample is exposed to will drift and cause more noise.

Conclusions

Three methods have been used to study water uptake in polymer photoresist films. Infrared Near Field Scanning Optical Microscopy (IR-NSOM) helped determine the regions of the photoresist that absorbed water. Atomic Force Microscopy (AFM) was employed to further understand the water-induced differential swelling of the photoresist pattern and changes in mechanical properties of the polymers. Fourier Transform Infrared (FTIR) spectroscopy measurements were performed to characterize the interactions between the water molecules and the polymer chains in the photoresist. This helped provide an explanation of deprotection reaction kinetics.

An interesting direction for future work would be to combine the microscopy and spectroscopy aspects. Micro-FTIR has been developed by other researchers and currently has a spatial resolution limit of about 10 μm.[1,2] Unfortunately this is not small enough to resolve the features of the photoresists studied in this work, but if the method is improved enough to do so, measurements could provide spatially resolved information on water-polymer interactions in different regions of the patterned polymer.

Work is currently being done to improve the IR-NSOM. Because a large obstacle is the fabrication of a reproducible fiber tip, an improved probe is being investigated. Apertureless NSOM uses an AFM as a base instrument with a metallized commercial Si tip. Infrared radiation illuminates the tip and scatters on to the sample with a small spot size. An optical image of the sample with spatial

resolution better than 30 nm can be obtained. The probe is more reliable and robust, so multiple experiments under a variety of conditions can be obtained, possibly leading to more quantitative information on water sorption in polymers. There is also improved resolution over the fiber-based IR-NSOM. However, it is still a challenge to interpret the optical images, and many researchers are investigating the contrast mechanisms at work.[3-6]

Another method under investigation which shows promise is Scanning Transmission X-ray Microscopy (STXM). This technique boasts chemical selectivity, high spatial resolution, and fast measurements. Investigations on latent images of polymer photoresists have already shown spatial resolution below 50 nm.[7] A goal is to use the technique to monitor acid diffusion during the post-exposure bake. With a few modifications, water diffusion through the film could also be investigated. This method could contribute more quantitative information which could aid in the understanding of photoresist processing and dynamics.

References for Conclusions

(1) Bhargava, R.; Wang, S.-Q.; Koenig, J. L. *Adv Polym Sci* **2003**, *163*, 137.

(2) Kupper, L.; Gulmine, J. V.; R., J. P.; Heise, H. M. *Vibrat. Spect.* **2004**, *34*, 63.

(3) Keilmann, F. *J. Electron Microscpy* **2004**, *53*, 187.

(4) Kim, Z. H.; Liu, B.; Leone, S. R., Nanometer scale optical imaging of epitaxially grown GaN and InN islands using apertureless near-field microscopy (in press).

(5) Stebounova, L.; Akhremitchev, B. B.; Walker, G. C. *Rev. Sci. Inst.* **2003**, *74*, 3670.

(6) Lahrech, A.; Bachelot, R.; Gleyzes, P.; A.C., B. *Optics Lett.* **1996**, *21*, 1315.

(7) Gilles, M. K.; Planques, R.; Muntean, L.; Hinsberg, W. D.; Leone, S. R., Chemical Mapping of Polymer Photoresists by Scanning Transmission X-ray Microscopy (in preparation).

Bibliography

Ablaza, S. L.; Cameron, J. F.; Xu, G.; Yueh, W. J. Vac. Sci. Technol. B 2000, 18, 2543.

Adhikari, B.; Majumdar, S. Prog. Polym. Sci. 2004, 29, 699.

Arce, A.; Fornasiero, F.; Rodriquez, O.; Radke, C. J.; Prausnitz, J. M. Phys. Chem. Chem. Phys. 2004, 6, 103.

Arvanitoyannis, I. S. J.M.S. - Rev. Macromol. Chem. Phys. 1999, C39, 205.

Ash, E. A.; Nicholls, G. Nature 1972, 237, 510.

Bar, G.; Delineau, L.; Brandsch, R.; Ganter, M.; Whangbo, M.-H. Surface Science 2000, 457, L404.

Barbara, P. F.; Adams, D. M.; O'Connor, D. B. Annu. Rev. Mater. Sci. 1999, 29, 433.

Bedoya, M.; Orellana, G.; Morenio-Bondi, M. C. Helvetica Chimica Acta 2001, 84, 2628.

Berger, C. M.; Henderson, C. L. Polymer 2003, 44, 2101.

Betzig, E.; Trautman, J. K.; Harris, T. D. Science 1991, 251, 1468.

Betzig, E.; Chichester, R. J. Science 1993, 262, 1422.

Bhargava, R.; Wang, S.-Q.; Koenig, J. L. Adv Polym Sci 2003, 163, 137.

Brannon-Pepas, L. Polymers in Controlled Drug Delivery; Medical Plastics and Biomaterials, 1997; Vol. 2004.

Brunner, R.; Marti, O.; Hollricher, O. J. Appl. Phys. 1999, 86, 7100.

Buchold, R.; Nakladal, A.; Gerlach, G.; Sahre, K.; Eichhorn, K.-J. Thin Solid Films 1998, 312, 232.

Buchold, R.; Nakladal, A.; Gerlach, G.; Herold, M.; Gauglitz, G.; Sahre, K.; Eichhorn, K.-J. Thin Solid Films 1999, 350, 178.

Burns, A. R.; Carpick, R. W. Appl. Phys. Lett. 2001, 78, 317.

Burns, S. D.; Medeiros, D. R.; Johnson, H. F.; Wallraff, G. M.; Hinsberg, W. D.; Willson, C. G. Proc SPIE 2002, 4690, 321.

Chen, X.; Davies, M. C.; Roberts, C. J.; Tendler, S. J. B.; Williams, P. M.; Davies, J.; Dawkes, A. C.; Edwards, J. C. Ultramicroscopy 1998, 75, 171.

Chen, W.-L.; Shull, K. R. Macromolecules 1999, 32, 136.

Chin, J. W.; Nguyen, T.; Aouadi, K. J. Appl. Polym. Sci. 1998, 71, 483.

Chirife, J.; Buera, M. D. Crit. Rev. in Food Sci. and Nutr. 1996, 36, 465.

Chuang, Y.-H.; Wang, C.-J.; Pan, C.-L. Appl. Phys. Lett. 1996, 69, 3312.

Colchero, J.; Storch, A.; Luna, M.; Gòmez Herrero, J.; Barò, A. M. Langmuir 1998, 14, 2230.

Costa-Fernandez, J. M.; Sanz-Medel, A. Analytica Chimica Acta 2000, 407, 61.

Cotungo, S.; Larobina, D.; Mensitieri, G.; Musto, P.; Ragosta, G. Polymer 2001, 42, 6431.

Cricenti, A. J. Alloys Cmpds 2001, 328, 2.

Croffie, E.; Cheng, M.; Neureuther, A. J. Vac. Sci. Technol. B 1999, 17, 3339.

Cross, G. H.; Ren, Y.; Swann, M. J. Analyst 2000, 125, 2173.

Czaderna, A. W.; Thomas, T. M. J. Vac. Sci. Technol. A 1987, 5, 2412.

Davy, S.; Spajer, M.; Courjon, D. Appl. Phys. Lett. 1998, 73, 2594.

Dean, K.; Kishkovich, O. SPIE, Advances in Resist Technology and Processing 2000.

Deisingh, A. K.; Stone, D. C.; Thompson, M. Int. J. Food Sci. Technol. 2004, 39, 587.

Dentinger, P. M.; Lu, B.; Taylor, J. W.; Bukofsky, S. J.; Feke, G., D.; Hessman, D.; Grober, R. D. J. Vac. Sci. Technol. B 1998, 16, 3767.

Dragnea, B., personal communication.

Dragnea, B.; Preusser, J.; Schade, W.; Leone, S. R.; Hinsberg, W. D. J. Appl. Phys. 1999, 86, 2795.

Dragnea, B.; Preusser, J.; Szarko, J. M.; McDonough, L. A.; Leone, S. R.; Hinsberg, W. D. Appl. Surf. Sci 2001, 175-176, 783.

Dragnea, B.; Preusser, J.; Szarko, J. M.; Leone, S. R.; Hinsberg, W. D. J. Vac. Sci. Technol. B 2001, 19, 142.

Dragnea, B.; Leone, S. R. Int. Rev. Phys. Chem. 2001, 20, 59.

Dragnea, B.; Leone, S. R. Int. Rev. Phys. Chem. 2001, 20, 59.

Dufrene, Y. F. Micros. and Anal. (The Americas) 2003, 62, 13.

Dunn, R. C. Chem. Rev. 1999, 99, 2891.

Durig, U.; Pohl, D. W.; Rohner, F. J. J. Appl. Phys. 1986, 59, 3318.

Eastman, T.; Zhu, D.-M. Langmuir 1996, 12, 2859.

Elbs, H.; Fukunaga, K.; Stadler, R.; Sauer, G.; Magerle, R.; Krausch, G. Macromolecules 1999, 32, 1204.

Feng, R.; Farris, R. J. J. Micromech. Microeng. 2003, 13, 80.

Frechet, J. M.; Ito, H.; Willson, C. G. Proc. Microcirucuit. Eng. 1982, 82, 260.

Garcia, R.; San Paulo, A. Ultramicroscopy 2000, 82, 79.

Garcìa-Parajò, M. F.; Veerman, J.-A.; van Noort, S. J. T.; de Grooth, B. G.; van Hulst, N. F. Bioimaging 1998, 6, 43.

Gilles, M. K.; Planques, R.; Muntean, L.; Hinsberg, W. D.; Leone, S. R., Chemical Mapping of Polymer Photoresists by Scanning Transmission X-ray Microscopy (in preparation).

Golander, C. G.; Rutland, M. W.; Cho, D. L.; Johansson, A.; Ringblom, H.; Jonsson, S.; Yasuda, H. K. J. Appl. Polym. Sci. 1993, 49, 39.

Gray, M. H.; Hsu, J. W. P. Rev. Sci. Inst. 1999, 70, 3355.

Gray, M. H.; Hsu, J. W. P. Appl. Phys. Lett. 2000, 76, 1294.

Han, H.; Seo, J.; Ree, M.; Pyo, S. M.; Gryte, C. C. Polymer 1998, 39, 2963.

Harvard, J. M.; Shim, S.-Y.; Frechet, J. M.; Lin, Q.; Medeiros, D. R.; Willson, C. G.; Byers, J. D. Chem. Mater. 1999, 11, 719.

Hecht, B.; Sick, B.; Wild, U. P.; Deckert, V.; Zenobi, R.; Martin, O. J. F.; Pohl, D. W. J. Chem. Phys 2000, 112, 7761.

Hong, M. K.; Jeung, A. G.; Dokholyan, N. V.; Smith, T. I.; Schwettman, H. A.; Huie, P.; Erramilli, S. Nuc. Inst. Mths. Phys. Res. 1998, 144, 246.

Houle, F. A.; Hinsberg, W. D.; Morrison, M.; Sanchez, I.; Wallraff, G.; Larson, C.; Hoffnagle, J. J. Vac. Sci. Technol. B 2000, 18, 1874.

Houle, F. A.; Hinsberg, W. D.; Sanchez, I. J. Vac. Sci. Technol. B 2004, 22, 747.

Hudlet, S.; Aubert, S.; Bruyant, A.; Bachelot, R.; Adam, P. M.; Bijeon, J. L.; Lerondel, G.; Royer, P.; Stashkevich, A. A. Optics Comm. 2004, 236, 447.

Hutcheon, G. A.; Messiou, C.; Wyre, R. M.; Davies, M. C.; Downes, S. Biomaterials 2001, 22, 667.

Ichikawa, K.; Mori, T.; Kitano, H.; Kukuda, M.; Mochizuki, A.; Tanaka, M. J. Polym. Sci. Part B: Polym Phys 2001, 39, 2175.

Isaacson, M.; Cline, J. A.; Barshatzky, H. J. Vac. Sci. Technol. B 1991, 9, 3103.

Ito, H.; Willson, C. G. Polym. Eng. Sci 1982, 23, 1021.

Jabbari, E.; Peppas, N. A. Macromolecules 1993, 26, 2175.

Jachowicz, J.; Yao, K. J. Cosm. Sci. 2001, 52, 281.

Karrai, K.; Grober, R. D. Appl. Phys. Lett. 1995, 66, 1842.

Kawagoe, M.; Takeshima, M.; Nomiya, M.; Qiu, J.; Morita, M.; Mizuno, W.; Kitano, H. Polymer 1999, 40, 1373.

Keilmann, F. Vibrational Spectroscopy 2002, 29, 109.

Keilmann, F. J. Electron Microscpy 2004, 53, 187.

Kim, Z. H., personal communication.

Kitano, H.; Ichikawa, K.; Fukuda, M.; Mochizuki, A.; Tanaka, M. J. Colloid Interface Sci. 2001, 242, 133.

Knoll, B.; Keilmann, F. Appl. Phys. A 1998, 66, 477.

Kondratowicz, B.; Narayanawamy, R.; Persaud, K. C. Sensors and Actuators B 2001, 74, 138.

Kopp-Marsaudon, S.; Leclere, P.; Dubourg, F.; Lazzaroni, R.; Aimè, J. P. Langmuir 2000, 16, 8432.

Kupper, L.; Gulmine, J. V.; R., J. P.; Heise, H. M. Vibrat. Spect. 2004, 34, 63.

Kusano, H.; Kimura, S.; Kitagawa, M.; Kobayashi, H. Thin Solid Films 1997, 295, 53.

La Rosa, A. H.; Yakobson, B. I.; Hallen, H. D. Appl. Phys. Lett. 1997, 70, 1656.

Lahrech, A.; Bachelot, R.; Gleyzes, P.; A.C., B. Optics Lett. 1996, 21, 1315.

Lange, J.; Wyser, Y. Packag. Technol. Sci. 2003, 16, 149.

Lapshin, D. A.; Letokhov, V. S.; Shubeita, G. T.; Sekatskii, S. K.; Dietler, G. Ultramicroscopy 2004, 99.

Leclere, P.; Dubourg, F.; Kopp-Marsaudon, S.; Bredas, J. L.; Lazzaroni, R.; Aimè, J. P. Appl. Surf. Sci. 2002, 188, 524.

CRC Handbook Of Chemistry and Physics; 84 ed.; Lide, D. R., Ed.; CRC Press, 2003.

Lin, E. K.; Soles, C. L.; Goldfarb, D. L.; Trinique, B. C.; Burns, S. D.; Jones, R. L.; Lenhart, J. L.; Angelopoulos, M.; Willson, C. G.; Satija, S. K.; Wu, W.-l. Science 2002, 297, 372.

Lin, B. J. J. Microlith. Microfab. 2004, 3, 377.

Linossier, I.; Gaillard, F.; Romand, M.; Feller, J. F.; Sci., J. A. P. J. Appl. Polym. Sci. 1997, 66, 2465.

Liu, M.; Wu, P.; Ding, Y. D.; Li, S. Phys. Chem. Chem. Phys. 2003, 5, 1848.

MacDonald, S. A.; Clecak, N. J.; Wendt, H. R.; Willson, C. G.; Snyder, C. D.; Knors, C. J.; Deyoe, N. B.; Maltabes, J. G.; Morrow, J. R.; McGuire, A. E.; Holmes, S. J. Proc. SPIE 1991, 1466, 2.

MacDonald, S. A.; Cleacak, N. J.; Wendt, H. R.; Willson, C. G.; Snyder, C. D.; Knors, C. J.; Deyoe, N. B.; Maltabes, J. G.; Morrow, J. R.; McGuire, A. E.; Holmes, S. J. Proc. SPIE 1991, 1466, 2.

Maeda, Y.; Kitano, H. Spectrochimica Acta A 1995, 51, 2433.

Maeda, Y.; Ide, M.; Kitano, H. J. Mol. Liquids 1999, 80, 149.

Maggi, L.; Segale, L.; Torre, M. L.; Ochoa Machiste, E.; Conte, U. Biomaterials 2002, 23, 1113.

Magonov, S., N.; Reneker, D. H. Annu. Rev. Mater. Sci. 1997, 27, 175.

Marais, S.; Hirata, Y.; Langevin, D.; Chappey, C.; Nguyen, T. Q.; Metayer, M. Mat. Res. Innovat. 2002, 6, 79.

Maréchal, Y.; Chamel, A. J. Phys. Chem. 1996, 100, 8551.

Matsuguchi, M.; Sadaoka, Y.; Shinmoto, M.; Sakai, Y. Bull. Chem. Soc. of Jpn. 1994, 67, 46.

Maxwell, J. M.; Huson, M. G. Rev. Sci Instr. 2002, 73, 3520.

Medeiros, D. R.; Aviram, A.; Guarnieri, C. R.; Huang, W.-S.; Kwong, R.; Magg, C. K.; Mahorowala, A. P.; Moreau, W. M.; Petrillo, K. E.; Angelopoulos, M. IBM J. Res. Dev. 2001, 45, 639.

Michaels, C. A.; Richter, L. J.; Cavanagh, R. R.; Stranick, S. J. Proc. SPIE 2000, 4098, 102

Michaels, C. A.; Gu, X.; Chase, B.; Stranick, S. J. Appl. Spectrosc. 2004, 58, 257.

Mikhaylova, Y.; Pigorsch, E.; Grundke, K.; Eichhorn, K.; B/, V. Macromol. Sym. 2004, 210, 271.

Mura, C.; Yarwood, J.; Swart, R.; Hodge, D. Polymer 2001, 42, 4141.

Nakazawa, K.; Shiobara, E.; Asano, M.; Sato, Y.; Tanaka, S.; Oonishi, Y. Jpn. J. Appl. Phys. 1999, 38, 1569.

Neogi, P. Diffusion in Polymers; Marcel Dekker, Inc: New York, 1996.

Nguyen, Q. T.; Favre, E.; Ping, Z. H.; Néel, J. J. Membrane Sci. 1996, 113, 137.

Nogueira, P.; Ramirez, C.; Torres, A.; Abad, M. J.; Cano, J.; Lopez, J.; Lopez-Bueno, I.; Barral, L. J. Appl. Polym. Sci. 2000, 80, 71.

Ocola, L. E.; Cerrina, F.; May, T. J. Vac. Sci. Technol. B 1997, 15, 2545.

Okuzaki, H.; Funasaka, K. Macromolecules 2000, 33, 8307.

Opdahl, A.; Hoffer, S.; Mailhot, B.; Somorjai, G. A. The Chemical Record 2001, 1, 101.

Padmanaban, M.; Endo, H.; Yoshio, I.; Kinoshita, Y.; Kudo, T.; Masuda, S.; Nakajima, Y. Proc SPIE 1992, 1672, 141.

Padmanaban, M.; Endo, H.; Inoguchi, Y.; Kinoshita, Y.; Kudo, T.; Masuda, S.; Nakajima, Y.; Pawlowski, G. Proc. SPIE 1992, 1672, 141.

Park, K. Superporous Hydrogels for Pharmaceutical &Other applications; Akina, Inc, 2004; Vol. 2004.

Patri, A. K.; Majoros, I. J.; Barker, J., James R. Curr. Opin. Chem. Biol. 2002, 6, 466.

Perera, D. Y. Progress in Organic Coatings 2002, 44, 55.

Ping, Z. H.; Nguyen, Q. T.; Chen, S. M.; Zhou, J. Q.; Ding, Y. D. Polymer 2001, 42, 8461.

Pohl, D. W.; Denk, W.; Lanz, M.; Rohner, F. J. J. Appl. Phys. 1984, 44, 651.

Polonski, V. V.; Yamamoto, Y.; White, J. D.; Kourogi, M.; Ohtsu, M. Jpn. J. Appl. Phys. 1999, 38, L826.

Pradas, M. M.; Ribelles, J. L. G.; Aroca, A. S.; Ferrer, G. G.; Anton, J. S.; Pissis, P. Colloid Polym. Sci. 2001, 279, 323.

Preusser, J., personal communication.

Rahmelow, K.; Hubner, W. Applied Spectroscopy 1997, 51, 160.

Ramon, O.; Kesselman, E.; Berkovici, R.; Cohen, Y.; Paz, Y. J. Polym. Sci. Part B: Polym Phys 2001, 39, 1665.

Ratner, B. D.; Tsukruk, V. V. Scanning Probe Microscopy of Polymers; American Chemical Society: Washington, DC, 1996; Vol. 694.

Reichmanis, E.; Nalamasu, O. Science 2002, 297, 349.

Sahlin, J. J.; Peppas, N. A. J. Appl. Polym. Sci. 1997, 63, 103.

Sahoo, P. B.; Vyas, R.; Wadhwa, M.; Verma, S. Bull. Mater. Sci. 2002, 25, 553.

Sammon, C.; Mura, C.; Yarwood, J.; Everall, N.; Swart, R.; Hodge, D. J. Phys. Chem. B 1998, 102, 3402.

Sammon, C.; Deng, C.; Mura, C.; Yarwood, J. J. Mol. Liquids 2002, 101, 35.

Sangaj, N. S.; Malshe, V. C. Progress in Organic Coatings 2004, 50, 28.

Schaller, R. D.; Saykally, R. J. Langmuir 2001, 17, 2055.

Schaller, R. D.; Johnson, J. C.; Wilson, K. R.; Lee, L. F.; Haber, L. H.; Saykally, R. J. J. Phys. Chem. B 2002, 106.

Schult, K. A.; Paul, D. R. Journal of Applied Polymer Science 1996, 61, 1865.

Sheiko, S. S. Adv. Polym. Sci. 2000, 151, 61.

Shen, Y.; Wu, P. J. Phys. Chem. B 2003, 107, 4224.

Shibayama, Y.; Saito, M. Jap. J. Appl. Phys. 1990, 29, 2152.

Starkweather, H. W. Macromolecules 1975, 8, 476.

Stebounova, L.; Akhremitchev, B. B.; Walker, G. C. Rev. Sci. Inst. 2003, 74, 3670.

Stewart, M. D.; Tran, H. V.; Schmid, G. M.; Stachowiak, T. B.; Becker, D. J.; Willson, C. G. J. Vac. Sci. Technol. B 2002, 20, 2946.

Stranick, S. J.; Chase, B.; Michaels, C. A. Abstracts of ACS 2001, 221, 173.

Suga, O.; Yamaguchi, H.; Okazaki, S. Microelec. Engin. 1991, 13, 65.

Sutandar, P.; Ahn, D. J.; Franses, E. I. Macromolecules 1994, 27, 7316.

Synge, E. Philos. Mag. 1928, 6, 356.

Tang, Y.; Lu, J. R.; Lewis, A. L.; Vick, T. A.; Stratford, P. W. Macromolecules 2002, 35, 3955.

Toomey, R.; Freidank, D.; Ruhe, J. Macromolecules 2004, 37, 882.

Turner, D. T. Polymer 1982, 23, 197.

Valaskovic, G. A.; Holton, M.; Morrison, G. H. Applied Optics 1995, 34, 1215.

van der Wel, G. K.; Adan, O. C. G. Progress in Organic Coatings 1999, 37, 1.

van Hulst, N. F.; Veerman, J.-A.; Garcìa-Parajò, M. F.; Kulpers, L. K. J. Chem. Phys 2000, 112, 7799.

Vogt, B. D.; Soles, C. L.; Jones, R. L.; Wang, C.-Y.; Lin, E. K.; Wu, W.-l.; Satija, S. K. Langmuir 2004, 20, 5285.

Wallraff, G.; Hutchinson, J.; Hinsberg, W.; Houle, F.; Seidel, P.; Johnson, R.; Oldham, W. J. Vac. Sci. Technol. B 1994, 12, 3857.

Wallraff, G. M.; Hinsberg, W. D. Chem. Rev. 1999, 99, 1801.

Weber, A. Z.; Newman, J. J. Electrochem. Soc. 2004, 151, A311.

Wei, P. K.; Fann, W. S. J. Appl. Phys. 2000, 87, 2561.

Yarwood, J.; Sammon, C.; Mura, C.; Pereira, M. J. Mol. Liq. 1999, 80, 93.

Zitzler, L.; Herminghaus, S.; Mugele, F. Phys. Rev. B. 20